Functional phenotypes of macrophages and their role in influenza A virus induced lung injury and repair

Inaugural Dissertation Submitted to the
Faculty of Medicine, Justus Liebig University Giessen
in partial fulfillment of the requirements for the
Doctor in Philosophy (PhD)

By

Balachandar Selvakumar
Born in Villupuram, India

Giessen, 2016

From the Department of Internal Medicine II
Director: Prof. Dr. Werner Seeger
Faculty of Medicine of the Justus Liebig University Giessen

First Supervisor and Committee Member: Prof. Dr. S. Herold
Second Supervisor and Committee Member: Prof. Dr. H.J. Thiel
Committee Members:
Prof. Dr. Friedemann Weber
Prof. Dr. Hans Jürgen Thiel
Prof. Dr. Susanne Herold
Date of Doctoral Defense: 11.05.2016

Table of contents

1. Introduction

1.1 Pulmonary physiology and microanatomy

The lungs form a delicate interface between host and environment, exchanging inhaled atmospheric oxygen and metabolism derived carbon dioxide. The distal lung therefore comprises large surface area of >80m^2 directly exposed to pro-inflammatory material (> 10,800l of gas volume/day), which renders the alveolar-capillary barrier an important site for initial pathogen-host interactions (1, 2). The alveoli are very closely associated with a network of capillaries and the distance of the alveolar space to the vascular compartment is <1µm, allowing rapid exchange of gases by passive diffusion along concentration gradients.

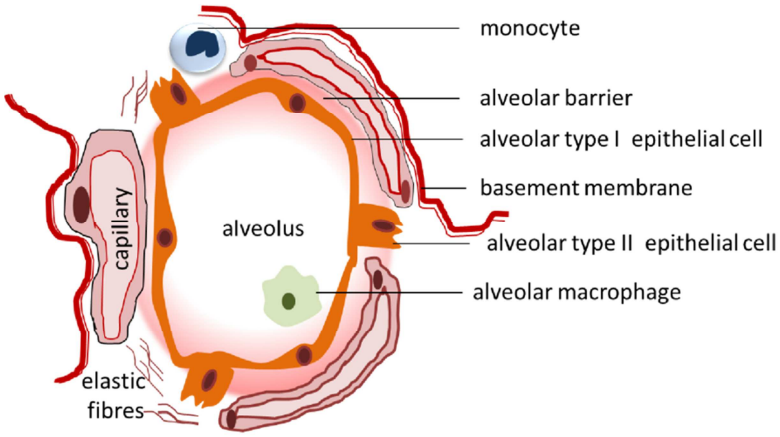

Figure 1-1 Microanatomy of the alveolus. The thin squamous type 1 alveolar epithelial cell (AEC I) in the alveolus and the endothelium of the pulmonary microvasculature are separated by the basement membrane form an ultra-thin alveolar capillary blood-gas barrier. The rounded alveolar epithelial type 2 cells (AEC II) are critical for surfactant production and can serve as a source of AEC I restoration after lung damage. Alveolar macrophages are resident in the alveolar space and maintain alveolar homeostasis by processing surfactant and scavenging foreign particles and cellular debris. Further macrophage subsets are recruited from the circulating monocyte pool upon inflammatory injury of the alveolus.

The proximal airways of the murine lung are lined by cuboidal club cells that secret mucus, thus preventing desiccation of the airway but also trapping incoming agents, and by ciliated cells that help to push the trapped foreign agents out of the lung along with the mucus. The human airway contains only a rare club cell population and consists of mucus secreting goblet cells together with ciliated cells. The microanatomy of the distal lung compartment consists of alveoli (Fig.1-1) the surface of which is covered by the alveolar epithelium which provides the initial barrier to environmental influences. Lung-resident macrophages in the alveoli clear particles and debris that reach the distal lung. Alveolar macrophages also secrete soluble mediators that contribute to the maintenance of homeostasis, including enzymes, cytokines, chemokines, arachidonic acid derivatives and

glycoproteins such as fibronectin (3). The alveolar surface is lined to 97% by type I alveolar epithelial cells (AEC I) which provide a thin surface for optimal gas diffusion (4). They form the alveolar capillary blood-gas barrier together with pulmonary microvascular endothelial cells. Due to their large surface, AEC I are sensitive to damage by e.g. inflammatory or mechanical stress. The type II alveolar epithelial cells (AEC II) cover 3% of alveolar surfaces and secrete pulmonary surfactant which is essential for reducing the alveolar surface tension thus preventing alveolar collapse during exhalation (5). They have proliferative potential and serve as precursors for type I cells during repair after lung injury.

1.2 Pulmonary homeostasis and response to infection

In general, most humans do not develop chronic inflammation of the lung irrespective of the continuous exposure to the atmospheric toxins, pollutant, irritants, etc., which indicates that protective mechanisms are effective to ensure lung homeostasis. The immune system at the mucosal surface involves multiple layers of innate and adaptive immune processes that together with the physical barrier contribute to maintain lung integrity. Special anatomical features of the lung mucosa prevent access of the inspired luminal contents to the sub-epithelium. In addition, the epithelium orchestrates the initial responses to both infectious and noninfectious stimuli in the lung (6). Moreover, AEC II play a role in recognition of pathogens and initiation of innate immune responses (7). Both AEC I and AEC II are well-polarized and tightly interconnected cells, thus providing a structural and functional barrier tightly regulating alveolar fluid homeostasis as well as transport of proteins and solutes in the lung (8). In the alveolar epithelium, these tight junctions are formed by E-cadherin and proteins of the catenin family (8, 9). The tight junctions are apically located multiprotein complexes consisting of claudins, occludins and scaffolding proteins such as zona-occludins protein 1 (ZO-1). Tight junctions (TJ) are essential for limiting para-cellular transport and as well as for maintenance of cell polarity (10). The alveolar mononuclear phagocyte system is a major part of the front line defense in the lung. Resident alveolar macrophages (rAM) originate from fetal liver monocytes that initially colonize the lung during embryonic development (11). Under steady-state conditions, the rAM is a long-lived cell and remains sessile in close connection to the alveolar epithelial cells (12-16). Its task is to elicit immediate innate immune responses towards invading pathogens, but at the same time remain relatively inactive towards innocuous stimuli (17). The rAM inflammatory response is dampened by a number of blocking inhibitory molecules such as epithelial expressed CD200, SIRPα (signal-regulatory protein alpha), MARCO

(macrophage receptor with collagenous structure) and surfactant proteins A and D, and also by macrophage autocrine anti-inflammatory signaling elicited by TGF-β (transforming growth factor beta) and IL-10 (interleukin-10) (17, 18–23). During infection the loss of epithelial regulatory ligands, presence of necrotic cells and signaling by diverse pattern recognition receptors (PRR) (24, 25) like toll-like receptors (TLR) (26, 27), nucleotide oligomerization domain (NOD)-like receptors (28, 29), intracellular helicases like retinoic acid inducible gene I (RIG-I) (30, 31) and protein kinase R (PKR) (32, 33) lead to production of a range of inflammatory cytokines and chemokines (e.g. CCL2, CX_3CR1, tumor necrosis factor-alpha (TNF)-α, TGF-β) which further promote the innate immune response. This leads to recruitment of polymorphonuclear leukocytes (PMNs), exudate macrophages (ExMa) and lymphocytes to the alveolar compartment (24, 34, 35).

1.3 Acute Respiratory distress syndrome/ acute lung injury

Acute lung injury (ALI) and its extreme form, the acute respiratory distress syndrome (ARDS) are syndromes of acute respiratory failure with substantial morbidity and mortality (36, 37). In 1967, Ashbaugh and colleagues (38) first used the term ´adult respiratory distress syndrome´ (ARDS) to describe a group of 12 critically ill patients with acute respiratory failure. After different definitions had been proposed for a decades, in 1994 the American-European consensus conference committee recommended the definition which was globally accepted but had limitations (39–43). Recently, a definition known as “Berlin Definition” published in 2013 was created by a consensus panel of experts who convened in 2011 (an initiative of the European Society of Intensive Care Medicine endorsed by the American Thoracic Society and the Society of Critical Care Medicine). This definition includes acute onset, the presence of bilateral opacities on chest radiographs consistent with pulmonary edema and a value of the PaO_2/FiO_2 (arterial oxygen tension/inhaled oxygen fraction) ratio of below 300 mmHg (44). The disease is categorized by the degree of hypoxemia as mild (PaO_2/FiO_2 ratio between 300 and 200 mmHg), moderate PaO_2/FiO_2 ratio between 200 and 100 mmHg) or severe (PaO_2/FiO_2 ratio below 100 mmHg). Patients with ARDS require urgent admission to critical care units for advanced life support and utilize considerable health care resources. ARDS can develop as a result of direct injury to the lungs, such as viral or bacterial pneumonia, aspiration of gastric contents, or smoke or toxic gas inhalation. Alternatively, ARDS can occur indirectly during the course of systemic inflammation, such as during sepsis, after polytrauma or following transfusion called TRALI (45). The mortality rate of ARDS is 27-

45% with multi-organ failure as the most common cause of death (46, 44). Fatality risk depends on the nature of the underlying disorder (36, 47) and is influenced by age and race. Younger patients have lower mortality rates and Afro-Americans or Hispanics have increased risk of death when compared to Caucasians (36, 47). To date, no pharmacological treatment options are available for the therapy ARDS. Therefore, there is an urgent medical need for the development of novel therapies to further improve clinical outcomes (48).

1.3.1 Pathology of ARDS/ALI

ARDS/ALI is an acute inflammatory disorder that disrupts the lung epithelial and endothelial barriers with influx of edema fluid as well as of various inflammatory cells and mediators (Fig. 1-2). The alveolar endo/epithelial barrier is composed of adjacent layers of the alveolar epithelium and the microvascular endothelium only separated by the basement membrane. Maintaining the integrity of this barrier is crucial for liquid homeostasis and effective gas exchange in the lung. Cellular characteristics of ALI include functional and structural loss of epithelial integrity and disruption of the basement membrane which lead to the efflux of protein-rich fluid into the distal airspaces of the lung (49). This is accompanied by an excessive extravasation of neutrophils and inflammatory monocytes releasing various pro-inflammatory mediators (45, 50). Elevated plasma levels of interleukin (IL)-6, 8, and TNF-α were found to be markers for mortality prediction (51, 52). In addition, lower plasma levels of protein C and higher plasma levels of plasminogen activator inhibitor-1 were strong independent predictors of mortality, as well as for ventilator-free days and organ failure (53). Excessive and prolonged activation of neutrophils and monocytes in the alveolar space contributes to basement membrane destruction and increased membrane permeability. Neutrophils release elastase which in turn degrades epithelial junctional proteins, possesses pro-apoptotic properties, and thus damages the alveolar epithelium (54-58). In consequence, this uncontrolled feed-forward mechanisms result in barrier dysfunction that eventually leads to respiratory failure (45). In some animal models of ARDS, neutrophil depletion was shown to be protective (59- 62), however, even in the absence of circulating neutrophils, ALI can occur (63). Bone marrow derived monocytes recruited during injury (termed exudate macrophages) are an important source of pro-inflammatory mediators and thus may contribute to barrier disruption. CCR2-/- animals which lack monocyte/macrophage recruitment during lung infection,

were shown to maintain barrier integrity after influenza virus (IV) induced ALI (64) in contrast to wild type animals.

Under homeostasis, type I and type II alveolar epithelial cells (AEC) form tight junctions with each other to maintain epithelial barrier integrity. During the acute phase of pneumonia-associated lung injury, infected or injured AEC lose tight junction integrity and partially undergo apoptosis that leads to increased permeability and in severe cases eventually to a denuded basement membrane (Fig. 1-2) (45, 49). Recently, it has also been reported that alveolar edema fluid from ALI patients down regulated the expression of ion transport genes that are involved in fluid reabsorption when added to primary cultures of human alveolar epithelial type II cells (65). Patients who survive the acute stage of ARDS enter a proliferative response phase, which is characterized by the presence of hyperplastic alveolar epithelial type II (AECII) cells and fibroblasts. The AECII migrate along alveolar septa and proliferate in order to reconstitute junctional epithelial integrity (66). The effort of epithelial repair undertaken during the proliferative phase may result in complete restoration of lung function. However, proper re-epithelialization is frequently prolonged and even disturbed which can result in progression to the fibrotic phase of ARDS/ALI (45). In this case, the alveolar space is filled with proliferating fibroblasts, abnormal amounts of extracellular matrix and new blood vessels, collectively described as fibrosing alveolitis (67, 68).

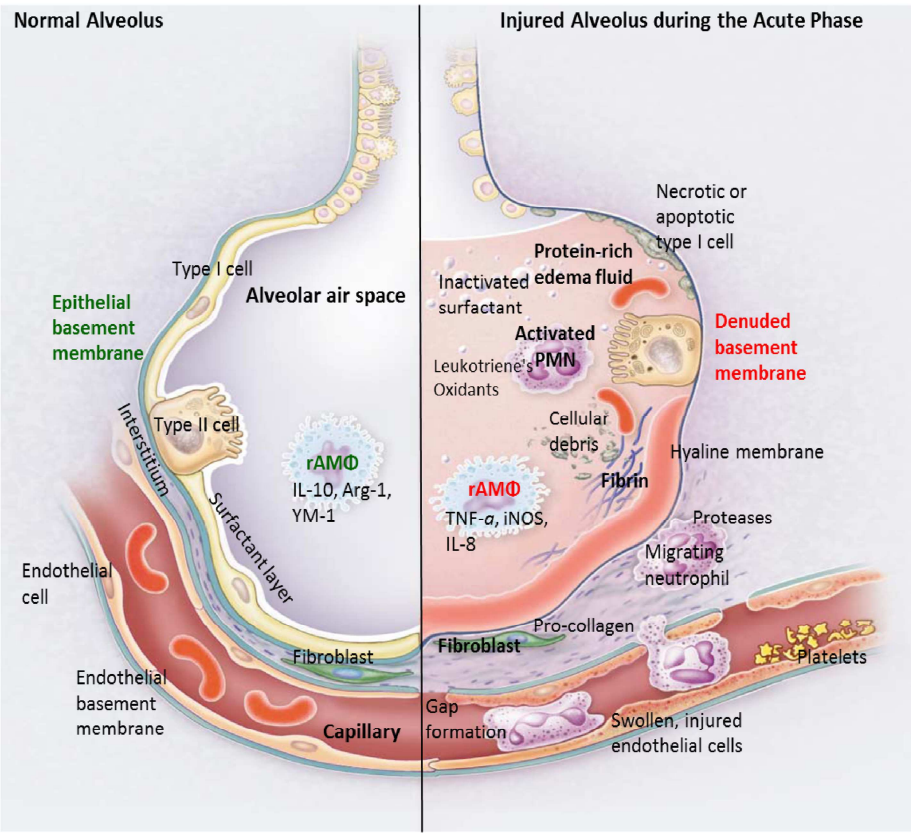

Figure 1-2 Schematic overview of alveolar compartment in homeostasis (left side) and during acute phase of ARDS (right side). The left-hand side depicts the healthy alveolus with an intact epithelial barrier consisting of type I and type II epithelial cells. The right side shows the injured alveolus with leukocytes and red blood cells intravasated into the alveolar airspace. Disruption of the endothelial and epithelial barrier leads to edema formation, inflammatory activation of alveolar macrophages, and infiltration of additional leukocytes which drives further damage of alveoli. *Adapted from Matthay and Zimmerman 2005 (50)*

1.4 Influenza A Virus

1.4.1 Structure

Influenza A viruses (IAV) are classified together with influenza B, influenza C and *Thogoto virus* as *orthomyxoviridae.* They are characterized by a single stranded, negative oriented and segmented RNA genome. The structure of IAV (Fig. 1-3) consists of a host cell-derived lipid coated bi-layer membrane. The genera can be differentiated by the molecular and serological characteristics of the viral matrix und nucleoproteins and have different amounts of gene segments (69), of which IAV possess eight. IAV are further separated into subtypes by antigenic characteristics displayed by their hemagglutinin (HA) and neuraminidase (NA) proteins, of which we know 18 and 11 subtypes, respectively, found circulating in wild birds and waterfowl (70), as well as a unique HA-NA combination found recently in bats (H17N10 and H18N11) (71). IAV are named by genus, host species (if not human), place of isolation, number of the isolate, year of isolation and its subtype (for example: A/Puerto Rico/8/34 (H1N1) - PR8). IAV form pleomorph particles of 80-120nm diameter. Inside, the viral RNA is complexed with the viral nucleoprotein (NP) and the polymerase complex, generating the viral ribonucleoprotein (RNP). The viral RNA consists of 13.6 kilobase (kb) which encode 11 viral proteins: non-strucutral (NS) proteins NS1 and NS2 which are important for regulation of host innate immune responses and export of viral RNA from the nucleus, respectively, matrix proteins M1 and M2, NA, NP, HA and the polymerase subunits PA, PB1 and PB2 (72-75).

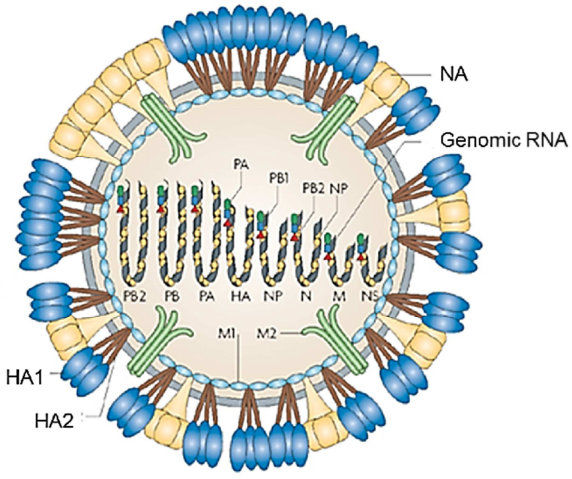

Figure 1-3 Structure of influenza A virus. Three viral proteins are exposed on the outside of virus particles: haemagglutinin (HA, which forms trimers), neuraminidase (NA) (which forms tetramers) and M2 (which forms tetramers that make up ion-channels). Upon proteolytic cleavage, HA0 (not shown) is processed to HA1 and HA2. The influenza virus matrix protein M1 associates inside the viral membrane, and the viral genome consists of eight negative-strand RNA segments and is packaged into the particle as a ribonucleoprotein in complex with nucleocapsid protein (NP) and the viral polymerases PA, PB1 and PB2. On average, the number of HIV-1 envelope glycoprotein spikes is thought to be considerably lower than the number of HA molecules per influenza A virion. *Adapted from Karlsson Hedestam GB et al 2008 (76).*

1.4.2 Epidemiology

IAV cause morbidity and mortality worldwide in animals and human beings and continue to impose a major burden on healthcare systems (77). IAV infection may also lead to severe respiratory disease and admission to the intensive care unit (78). IAV are transmitted by respiratory droplets and primarily infect the epithelium of the proximal as well as distal respiratory tract which results in a primary viral pneumonia causing severe damage to the alveolar compartment and acute respiratory distress syndrome (ARDS) (79- 81). Often, additional secondary super-infections with *Streptococcus pneumonia*, *Staphylococcus aureus* and *Haemophilus influenzae* worsen outcome substantially (82, 83). The genetic re-assortment is an important way to promote the evolution of new IAV subtypes. Novel re-assortment of virus in animal reservoirs may generate pandemic IAV strains in humans. In history, several human pandemic influenza viruses were assembled by genetic re-assortment between avian, human and swine influenza viruses. In 2009, pandemic (H1N1) 2009 (pdm/09 H1N1) influenza virus composed of two swine influenza virus genes, one avian and one human influenza virus gene, highlighted the crucial role of genetic re-assortment in generation of novel pandemic IAV strains.

1.4.3 Host-Virus Interactions

Replication of IAV in a host cell greatly impacts on cellular function and structure. In the lung, IAV infection can activate epithelial cells and alveolar macrophages, leading to release of various cytokines and chemokines. These large amounts of pro-inflammatory mediators further impact on the functional integrity of the alveolar epithelium. IAV directly affect tight junction stability, through the action of NS1. Its carboxyl terminus domain contains a PDZ-ligand binding motif that can interact with host factors scribble and Dlg1 (Disks large homolog 1), leading to tight junction disruption accompanied by lower trans-epithelial resistance (TER) and higher protein diffusion rates of the epithelial cell layer (84). M2 expression leads to enhanced levels of reactive oxygen species (ROS) formation and subsequent protein kinase C (PKC) activation (85). The cellular recognition of pathogen-/danger-associated molecular patterns (PAMPs/ DAMPs) by diverse pattern

recognition receptors (PRRs) induces the activation of inflammatory, anti-viral signal cascades. Detection of uncapped 5´-triphosphorylated RNA by RIG-I (RNA helicases retinoic acid inducible gene-I) and subsequent interaction with MAVS (mitochondria associated antiviral signaling protein), TRIM25 (Tripartite motif-containing protein 25) and IPS-1 (Interferon-beta Promoter Stimulator-1) leads to an IRF-3 and IRF-7 (interferon regulatory factor)-dependent transcription and translation of type I interferons (IFN) (30, 86). Furthermore, recognition of viral patterns by protein kinase R (PKR) activates NF-κB (nuclear factor 'kappa-light-chain-enhancer' of activated B-cells) translocation to the nucleus and transcriptional activation of pro-inflammatory, pro-apoptotic and anti-viral gene clusters (87, 88). The RIG-I, PKR, NLRP3 (NOD-like receptor family, pyrin domain containing 3) inflammasome and endosomally located TLR3 and TLR7 (89- 92) contribute to sensing IAV infection. Activation of NLRP3 induces caspase-1 dependent release of pro-inflammatory IL-1β and IL-18 (93), whereas TLR3/TLR7 act via IRF-3, IRF-7 and NF-κB, again triggering the induction of the IFN and pro-inflammatory cytokine responses (94). In addition to the epithelial response, IAV infection induces release of pro-inflammatory mediators by alveolar macrophages that amplify lung injury after IAV-infection (95- 98). In particular, exuberant production of IFN and IFN-dependent TNF-related apoptosis-inducing ligand (TRAIL) has been demonstrated to promote epithelial barrier failure and lung tissue injury, to hamper resolution of inflammation and to increase mortality (64, 79, 99-101).

1.5 Current treatment of ARDS and therapeutic perspectives

ARDS is the leading cause of death in critical care, with mortality rates of 40 to 60%. Currently, the only non-pharmacologically treatment with proven efficacy is the use of lung-protective mechanical ventilation with low-tidal-volume ventilation (6 ml/kg of ideal body weight) and maintaining a plateau pressure of 30 cm of water or less, together with appropriate fluid management. This strategy has been proven to effectively reduce mortality in ARDS clinical trials by reducing lung injury and down regulating pro-inflammatory cytokines (102, 103). Despite ongoing intensive research efforts over four decades, there are no pharmacologic therapies available till now (103). Several pharmacological treatment trials with e.g. corticosteroids, beta-adrenergic agonists, anticoagulants, vasodilators, anti-oxidants, immune-modulating agents such as IL-10, and surfactant failed to show an overall improvement in mortality during clinical trials (104), irrespective of their experimental/preclinical success (105-110). In addition, various pharmacologic agents such as ketoconazole, pentoxifylline, and *N*-acetylcysteine (NAC)

have been investigated for the reduction of pulmonary damage in ALI/ARDS. But none of these therapies has demonstrated a reduction in mortality (107, 111). Treatments with recombinant human activated protein C (112) or HMG-CoA reductase inhibitors (statins) were found to significantly reduce mortality in some subgroups of patients (113-115) but recombinant human activated protein C was associated with an increased risk of bleeding (112, 116). Novel therapeutic approaches have shown promising results in animal models. For example, bone marrow derived mesenchymal stem cells (MSCs) were found to possess anti-inflammatory properties both *in vitro* and *in vivo* (117). Endothelial progenitors, embryonic and induced pluripotent stem cells are at an earlier stage in the translational process, but offer the hope of directly replacing injured lung tissue (118). In another cell therapy study, macrophages were used as vehicles to deliver keratinocyte growth factor (KGF) expression to injured lungs (119). In future, experimental therapies could include cells or cell derived pharmacological compounds to enhance edema clearance, stimulate repair pathways, inhibit pro-inflammatory transcription factors, and target inflammatory cytokines.

1.6 Macrophages

Since Elie Metchnikoff first described the macrophage as phagocyte in 1882 this cell type has been reported to reside in almost every part of the body as large, tissue resident myeloid cell characterized by the presence of pseudopodia and phagocytic granules and by distinct functional profiles. As central part of the innate immune system they have a crucial host defense function but also contribute to the maintenance of tissue homeostasis through the clearance of apoptotic and damaged cells. Macrophages also play an essential role during organogenesis in embryonic development, where they are highly concentrated at sites of high cell death, such as developing limb buds (120). These tissue re-modeling functions are found to be conserved in the adult life thereby supporting wound healing and tissue repair/remodeling processes after infection and injury. Macrophages are also known to acquire tissue-specific phenotypes and functions in different organs (Fig. 1-4). For example, liver macrophages (Kupffer cells) remove toxins, lung macrophages (alveolar & interstitial) are highly equipped with clearance machineries to eliminate inhaled environmental particles, bone macrophages (osteoclasts) are essential for bone re-modeling, placenta macrophages (Hofbauer cell) are involved in preventing the transmission of pathogens from the mother to the fetus and renal macrophages (intra-glomerular mesangial cells) play a role in filtration, structural support, and phagocytosis of debris in the glomerulus. Although they exert tissue specific functions, all of these tissue

macrophages also release common soluble mediators including enzymes, cytokines, chemokines, arachidonic acid derivatives and glycoproteins such as fibronectin, that contribute to maintenance of homeostasis and tissue repair (121,122).

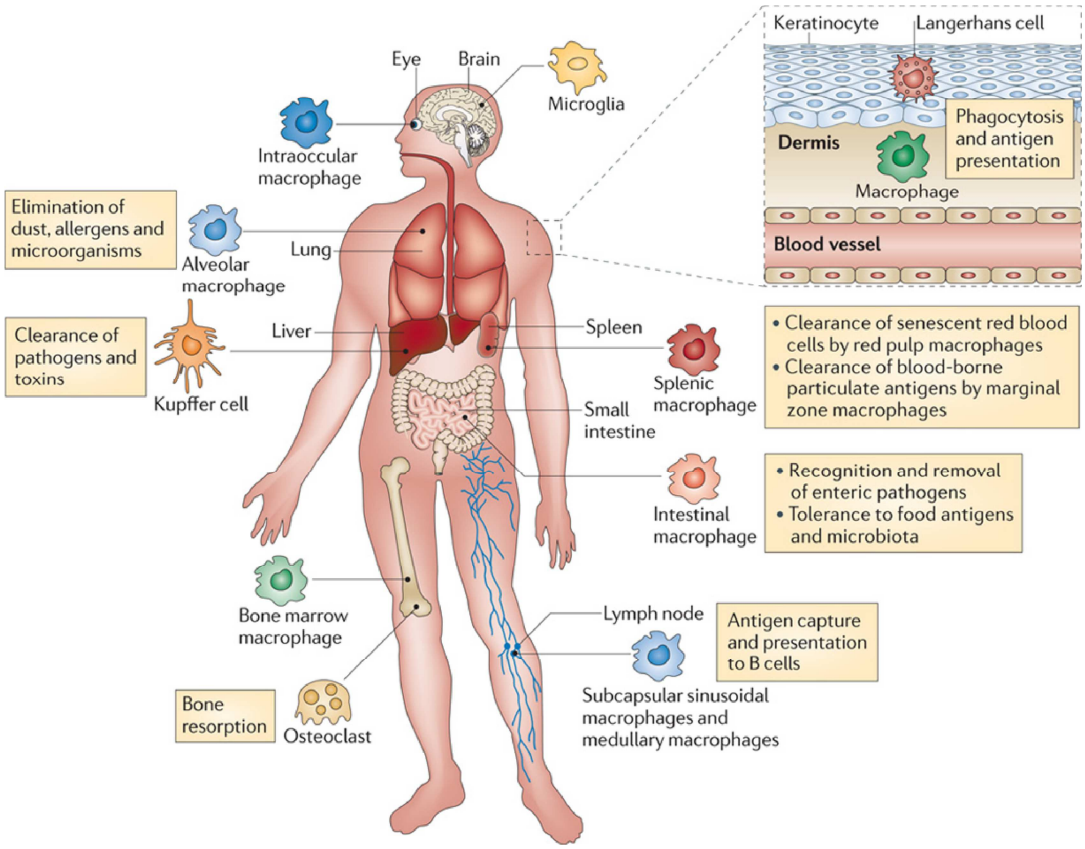

Figure 1-4 Macrophages in different tissues. Mononuclear phagocytes are generated from committed haematopoietic stem cells located in the bone marrow. Macrophage precursors are released into the circulation as monocytes and quickly migrate into nearly all tissues of the body, where they differentiate into mature macrophages. Macrophages are found in every organ and in different tissues where they have specialized functions. *Adapted from Murray PJ and Wynn TA 2011 (123).*

1.6.1 Macrophage origin, differentiation and development

Ontogeny and differentiation of tissue macrophages are briefly summarized in Fig. 1-5. Macrophages may originate at the prenatal stage from the yolk sac and fetal liver, and during the postnatal stage from the bone marrow (124, 125). Alveolar macrophages belong to the tissue macrophage type shown to arise from embryonic progenitors that seed the organ and mature locally before and shortly after birth and are maintained by proliferative self-renewal throughout life, largely independent of replenishment by blood monocytes in the steady state (126, 127). However, during inflammation, blood monocytes are recruited from bone marrow to inflamed lung tissue where they give rise to exudate macrophage (ExMa) populations. Under these conditions, the macrophage composition of the lung reflects a dynamic balance of recruited and tissue-resident macrophages. These cells with

distinct ontogenetic and proliferative histories are exposed to regional signals in inflamed lung tissue, but their distinct responses and further programming is largely unresolved.

Tissue resident macrophages originate from both yolk sac and fetal liver in pre-natal stage, while during inflammation/injury, ExMa originate from bone marrow (128). These ExMa infiltrate to inflamed tissues via chemokine/chemokine receptor axis CCL2/CCR2 dependent way not occurring in CCR2-deficient mice (129, 130). After extravasation, these ExMa are exposed to the respective organ microenvironment, correspondingly adapt their functional repertoire and may differentiate into organ-specific resident macrophages if these are depleted by inflammatory stimuli or infection (131).

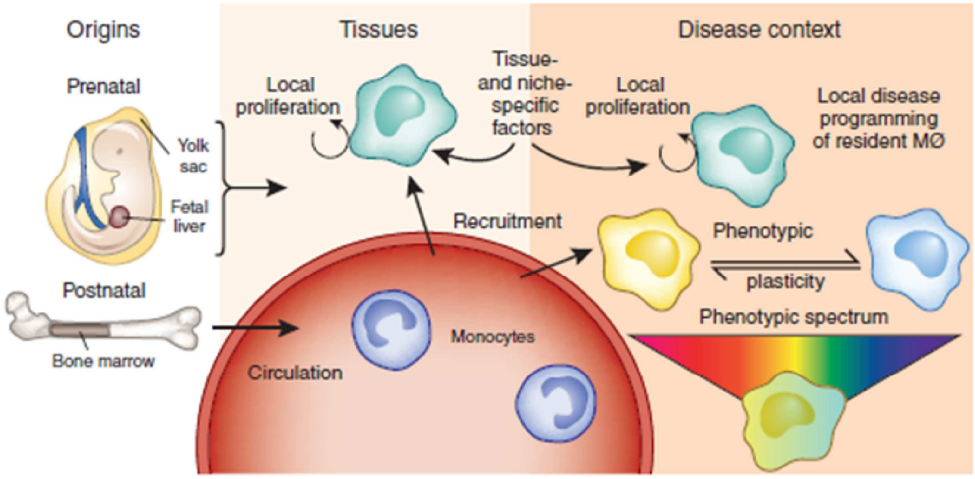

Figure 1-5 Macrophage origin, differentiation and plasticity. Macrophages may originate both at the prenatal stage from the yolk sac and fetal liver, and during the postnatal stage from the bone marrow. In specific tissue contexts, macrophages are programmed by local factors. Here they may be both long-lived self-renewing cells or replenished from the blood monocyte pool. The macrophage activation states in tissues can be loosely equated to macrophages in disease tissues, but they are heterogeneous in origin and phenotypically plastic, with variable contributions to disease progression. MØ, macrophage. *Adapted from Liddiard and Taylor 2015 (128)*

In mice, two blood monocyte subsets have been distinguished based on differential expression of Ly6C (or Gr-1) and CX_3CR1 (132). Monocytes that express high levels of Ly6C and intermediate levels of CX_3CR1 as well as high levels of CCR2 are termed $Ly6C^{hi}$ monocytes. They are also known as inflammatory monocytes due to their ability to migrate to sites of inflammation and to produce pro-inflammatory cytokines during infection or tissue damage (132, 129, 133, and 134). The second major monocyte subset in mice characterized by low expression of Ly6C, high expression of CX_3CR1 and low expression of CCR2 is termed $Ly6C^{low}$ patrolling monocytes, acting to maintain capillary integrity (135). After extravasation, $Ly6C^{hi}$ monocytes differentiate into ExMa and monocyte-derived dendritic cells (Mo-DC).

It also been shown that ExMa can complement the prenatally established macrophage compartment, especially under conditions of severe depletion of the rAM population (such as irradiation and infection). Thus, depending on the organ and its inflammatory history, rAM may have a chimeric origin, being derived from both yolk sac/fetal liver as well as by bone marrow monocytes, (125, 136). Despite their longevity and self-renewing property during homeostasis (137), rAM were shown to be depleted in severe inflammatory conditions, e.g. influenza A infection (138). This depleted pool of rAM is replenished during later stages of injury/infection by either self-renewal of $CD11c^{hi}CD11b^{-}$ rAM or differentiation of lung recruited $CD11c^{low}CD11b^{hi}$ ExMa derived from circulating blood $Ly6C^{hi}$ monocytes (139).

1.6.2 Macrophage activation

Diverse terms have been applied to describe macrophage activation and polarization first studied *in vitro* where a stimulus such as cytokines or toll-like receptor (TLR) agonists were observed to produce distinct patterns of gene and protein expression (140). This led to a widespread use of different definitions of macrophage activation, combining terms such as M1 (classical) and M2 (alternative) activation. The origins of these terms was first coined in the early 1990s when differential effects of IL-4 compared to IFN-γ and/or lipopolysaccharide (LPS) on macrophage gene expression were described (141,142). IL- 4 was described to induce alternative activation compared to the effects of IFN-γ. After several years once again, Mills proposed the M1–M2 terminology (143). This concept originated from the differential arginine metabolism between macrophages from C57BL/6 and Balb/c mice, an effect which was correlated with differences between Th1 and Th2 cell responses in the same strains. Mills and colleagues further proposed that the M1–M2 dichotomy was an intrinsic property of macrophages associated with transitions from inflammation to healing that would occur in the absence of an adaptive immune response and arose early in evolution (144). A third set of nomenclature expanded the M1–M2 definitions to account for different activation scenarios (M2a, M2b etc), balanced by the idea that activation exists on a spectrum and cannot easily be binned into defined groups (145-149). A fourth definition refers to macrophages grown in GM-CSF-1 as M1 and CSF-1 as M2 (150). Notably, significant differences have been documented in the transcriptomes of macrophage populations primarily generated with the use of CSF-1 or GM-CSF, without and with exogenous perturbation (151) but no substantial evidence exists. Although the M1/M2 macrophage polarization concept was originally deduced from *in vitro* experiments and may reflect only a small part of the plasticity of macrophage

function *in vivo*, it is considered as a valid starting point to characterize the dynamics of macrophage function.

1.6.2.1 Classically activated M1 macrophages

Inflammatory monocytes (GR-1^{hi}/MHCII^{low}/CD11c^{low}/CD11b^{hi}C/CCR2^{hi}/CX_3CR1^{low}) enter the site of infection and recognize PAMPs that triggers via Toll-Like-Receptors (TLR's) and other PRR inflammatory signaling cascades. This leads to the priming of macrophages by IFN-γ via IFN-γ receptor (152, 153) controlled by transcription factors such as STAT1, STAT3, IRF3, IRF5 and IRF7 (154,155). If primed macrophages subsequently encounter an appropriate stimulus, such as bacterial LPS or other pro-inflammatory cytokines and chemokines (156) in the local micro-environment they get shaped to a classically activated (CAM) or M1 phenotype (Fig. 1-6). Upon acquiring the CAM (M1) phenotype, further pro-inflammatory mediators such as IL-1 β, IL-6, TNF-α (157-159) and chemokines like IL-8/CXCL8, IP-10/CXCL10, MIP-1 alpha/CCL3, MIP-1 beta/CCL4, and RANTES/CCL5 (160) are released. This leads to increased recruitment of inflammatory leucocytes such as monocytes and neutrophils, which are known to exaggerate the inflammatory response. In addition, CAM (M1) generate increased levels of nitric oxide (NO) from L-arginine via inducible nitric oxide synthase (iNOS or NOS2) which causes DNA damage and is essential for the elimination of intracellular pathogens (161). Moreover, CAM (M1) have the ability to upregulate the expression of MHC class II and co-stimulatory molecules such as CD40, CD80 and CD86 which allows them to act as antigen presenting cells (APC) (162). These pro-inflammatory properties of CAM (M1) are important for host defense but when uncontrolled they cause significant host tissue damage by exaggerated leukocyte infiltration as well as by tissue flooding with inflammatory mediators, pro-apoptotic factors and matrix degrading proteases. In addition, CAM (M1) release proteolytic enzymes including MMP-1, -2, -7, -9, and -12, which degrade collagen, elastin, fibronectin, and other ECM components (163, 164). TNF-α also contributes to the pro-apoptotic activity of the CAM (M1) (165, 166) through Fas Ligand/TNFSF6 secretion (165).

1.6.2.2 Alternatively activated M1 macrophage

In vitro studies have demonstrated that T helper cell type 2 (TH2) derived cytokines such as IL4 or IL13 are the key triggers for macrophages to polarize to an alternatively activated macrophage (AAM) or M2 phenotype (Fig. 1-6). This mechanism was found to be controlled by transcription factors like IRF4, STAT6 and PPAR-γ (167, 168). AAM are characterized by their high phagocyte activity and high expression of CD206 (mannose

receptor), FIZZ1 and Ym-1 (158). In contrast to CAM (M1), AAM (M2) secret various immune-modulatory cytokines and chemokines like IL10, TGF-β, and CCL17, CCL18, CCL22 and CCL24 (169-171). Further, AAM (M2) are known to be poor scavengers of reactive oxygen and nitrogen species. Instead they have been shown to express high levels of arginase-1 (172). Pro-angiogenic factors like vascular endothelial growth factor (VEGF) (173) and platelet-derived growth factor (PDGF) secreted by AAM (M2) has been shown to be involved in tissue remodelling (174,175). AAM (M2) are commonly found during parasitic infection, allergy and in repair phase after tissue damage (158).

Well balanced M1 versus M2 macrophage polarization *in vivo* contribute to maintainance of host homeostasis as well as to achieving pathogen elimination and tissue recovery during disease. However, tissue specific mechanisms that regulate M1 and M2 phenotype in different organs *in vivo* are largely unknown.

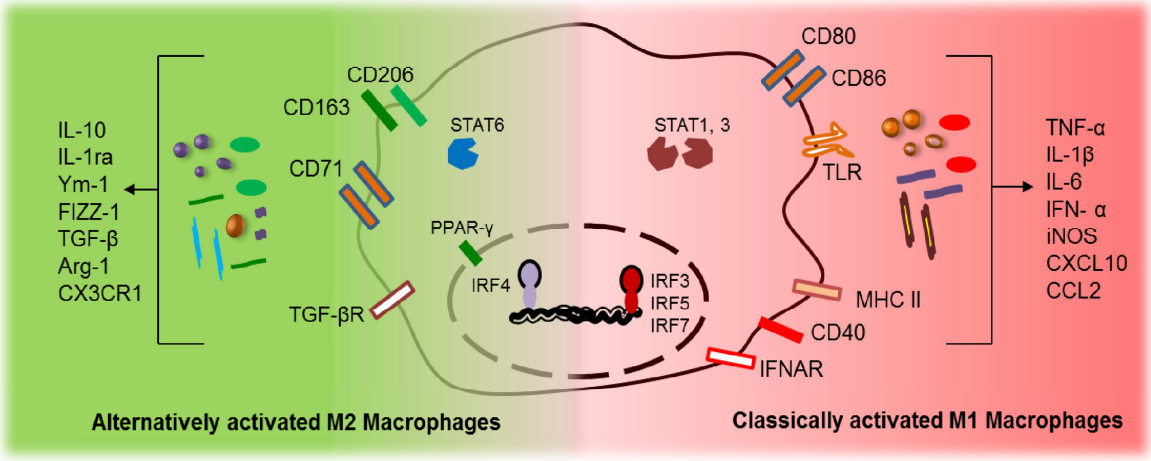

Figure 1-6 Macrophage activation phenotypes. Macrophages are activated either classically (M1 phenotype) or alternatively (M2 phenotype). M2 polarized macrophages express high levels of CD206, CD71 and TGF-βR while M1 express high levels of CD40, CD80, and CD86 on the cell surface. STAT1, 3 are highly activated in M1 phenotype and STAT6 in M2 phenotype. Interferon regulatory factors (IRF) 3, 5, 7 are active in M1phenotype while IRF4 in M2 phenotype. The cytokines and chemokines like TNF-α, IL-1β, IL-6, iNOS, CXCL10, CCL2 are in high levels in M1 phenotype and IL-10,IL-1ra, Ym-1, FIZZ-1, Arg-1, CX_3CR1 are highly expressed by M2 phenotype.

1.6.3 Regulators of macrophage activation

Macrophages can be activated to acquire either M1 or M2 phenotypes, based on micro-environmental signals. The M1 macrophages are highly pro-inflammatory and help in defending host against pathogens. In contrast, the M2 macrophage highly expresses growth factors (GF's) and anti-inflammatory mediators that promote in tissue repair and remodeling after injury. An unbalanced M1 vs M2 polarization could impair host defense or lead to the significant host tissue damage (176-180). Therefore, a tight regulation of macrophage activation and deactivation is required. M1 polarized macrophages recognize

TLR ligands via extracellular leucine rich repeat (LRR) elements which by conformational change brings intracellular Toll and IL1 receptor (TIR) domains together. Thereafter, the MyD88 adaptor molecule is recruited to the TIR domain, which in turn recruits IL1 receptor associated kinase (IRAK) 4 (181). IRAK4 causes phosphorylation of IRAK1, which then binds TNF receptor activated factor-6 (TRAF6). The IRAK1-TRAF6 complex then dissociates from MyD88 and activates TGFβ-activated kinase 1 (TAK1) and TAK1 binding protein 2 (TAB2). This leads to the phosphorylation of the inhibitory κB (IKK) complex which in turn phosphorylates IκB, causing the release of NF-κB from inhibition and the activation of IFN regulatory factors (IRFs), especially IRF7 and IRF5. NF-κB then translocates to the nucleus and induces the transcription of pro-inflammatory cytokines, chemokines and co-stimulatory molecules. MyD88 independent TLR3 pathway recruits TIR-domain containing adaptor protein inducing IFNβ (TRIF) that induces the expression of the transcription factor IRF3, leading to the production of type I IFN. TLR4 signals via MyD88 or TRIF dependent routes, causing activation of the TRIF-related adaptor molecule (TRAM), which in turn leads to activation of IRF3 and NF-κB. These pathways integrate to generate massive pro-inflammatory waves. In contrast to M1 macrophages, M2 macrophages have in-built negative feedback loops that terminate TLR signaling. For example, LPS stimulation of M2 macrophages has been reported to induce MyD88s, a splice variant of the MyD88 protein that lacks the domain necessary to interact with IRAK4, thus preventing TLR signaling (182). Similarly, IRAK-M is a TLR-inducible molecule that inhibits the dissociation of IRAK1-IRAK4 complexes from MyD88, thereby preventing further signaling (183). In addition to regulation of TLR signalling, macrophages express further inhibitory receptors that control their activation. Many of these inhibitory receptors are paired with structurally related receptors involved in activation, such as those belonging to the immunoglobulin domain superfamily and the C-type lectin family (184). Within the immunoglobulin superfamily, these include signal regulatory proteins (SIRP), triggering receptors expressed by myeloid cells (TREM) and the CD200 receptor (CD200R) family. TREM-1 is a potent amplifier of pro-inflammatory responses in monocytes, macrophages and some granulocytes (185), whereas TREM-2 has been shown to attenuate macrophage activation. In an *in vivo* study, TREM2 KO mice showed enhanced pro-inflammatory cytokine release in response to TLR stimulation (186). Recently, it has been shown that M2 macrophages produce soluble TREM2 (sTREM2) that supports macrophage pool preservation after inflammatory insults (187).

1.7 Pulmonary Macrophages in ALI/ARDS

Resident lung macrophages are crucial for maintaining tissue homeostasis and are actively kept silent in steady state conditions (126, 188). Disruption of tissue homeostasis by infection or inflammation results in macrophages activation with phenotypic and functional modifications (189). Under these conditions resident pulmonary macrophages are critically involved in lung host defense as sentinels for pathogens and through initiation and control of innate and adaptive immune responses. To respond to threatening changes of their environment resident macrophages possess various PRRs such as TLRs, NLRs and retinoic acid inducible-I (RIG-I)-like receptors (190), as well as the scavenger receptors such as CD163, CD36, MARCO, mannose receptor (CD206) (191). In addition, macrophages express Fc and complement receptors that allow them to recognize and engulf opsonized foreign particles (190,191). At the site of infection/inflammation, macrophages are exposed to various inflammatory signals sensed by the above mentioned receptors which induce macrophage activation crucial for their host defense functions. During influenza virus infection, the main antiviral functions of resident alveolar macrophages are considered phagocytosis of viral particles and release of a plethora of inflammatory cytokines and chemokines to initiate and drive the immune response (192, 193). Resident alveolar macrophages (rAM) may either phagocytose collectin-opsonized viruses or virus-bearing apoptotic cells, thereby contributing to IV clearance even when they are not themselves infected (194, 195). Depletion of resident alveolar macrophages prior to infection resulted in higher viral load, increased mortality, and decreased type I IFN production (196). Cytokines released by activated rAM stimulate neighboring alveolar cells to produce chemokines which in turn mediate the recruitment of neutrophils, and later on, further MonPh populations as well as lymphocytes (197, 198).

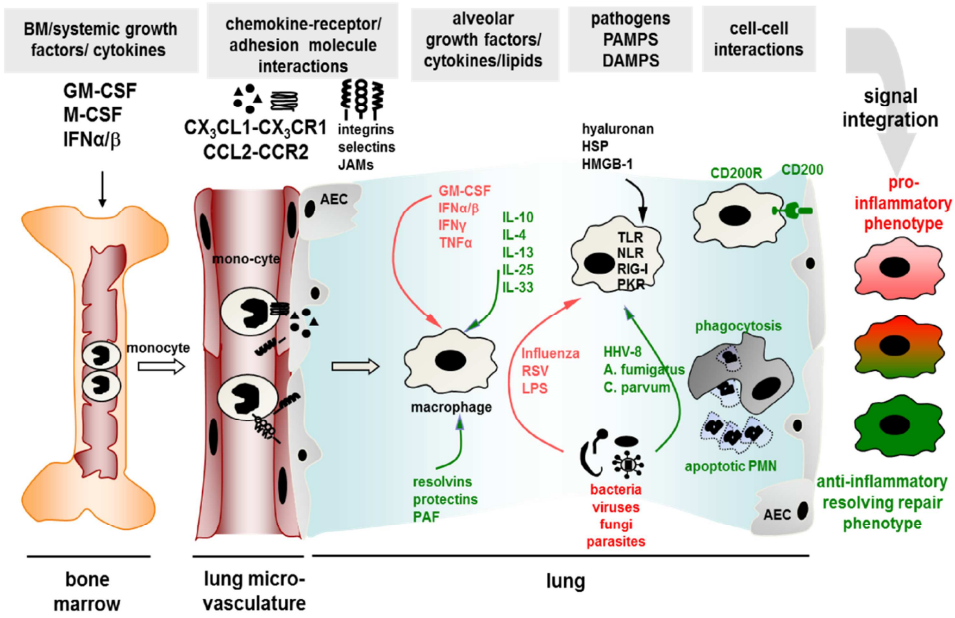

Figure 1-7 Macrophage activation and polarization. Different extracellular signals are integrated to shape pulmonary macrophage phenotypes during lung inflammation**.** Growth factors such as GM-CSF, M-CSF, or type I interferons (IFN) drive differentiation and activation of macrophage progenitors or lineage precursors, Macrophages obtain signals from chemokines or cellular adhesion molecules upon transendo/epithelial recruitment to the alveoli. Macrophages receive signals from cytokines like GM-CSF and interferons integrate to drive towards M1 phenotype or IL-4, IL-13, IL-25, or IL-33 drive towards M2 phenotype. Pathogens, PAMPs, or DAMPs deliver signals via TLR, NLR, or other pattern recognition receptors. Cell–cell communications during phagocytosis of apoptotic neutrophils (PMN) or via CD200–CD200R interaction with AEC add on these signals and may support an anti-inflammatory macrophage phenotype. JAMs, junctional adhesion molecules; HSP, heat shock proteins; HMGB-1, high mobility group box-1; S. pn. *Streptococcus pneumoniae;* K. pn., *Klebsiella pneumoniae*; AEC, alveolar epithelial cells. *Adapted from Herold et al 2011 (24).*

As outlined above, resident alveolar macrophages form the first line of defense towards infectious challenge in the lung, but pathogen elimination and restoration of homeostasis following infection and tissue damage additionally requires the coordinated mobilization of two circulating MonPh subsets defined according to lineage marker (GR-1) and chemokine receptor expression, namely the GR-1^{low}/$CCR2^{low}$/CX_3CR1^{hi} and the GR-1^{hi}/$CCR2^{hi}$/CX_3CR1^{low} peripheral blood monocytes (PB-Mo). GR-1^{low}/$CCR2^{low}$/CX_3CR1^{hi} PB-Mo patrols the resting vasculature, populate normal or inflammatory sites CX_3CR1-dependently and participate in resolution of inflammation and tissue repair (132, 199). GR-1^{hi}/$CCR2^{hi}$/CX_3CR1^{low} PB-Mo are predominantly inflammatory and migrate to injured and infected sites. CCR2 and its major ligand, CCL2 (also known as MCP-1) are evidently important in both emigration of these cells from the bone marrow into the blood stream and their immigration into inflamed tissues. During immigration to the inflamed lung, and upon contact with the local inflammatory milieu GR-1^{low}/$CD11b^{low-hi}$/$CD11c^{hi}$/$MHCII^{low}$/$SiglecF^{hi}$ (ExMa) recruited from the circulating $Ly6c^{hi}$ monocyte pool receive a variety of signals depending on the type of infection and on the state of tissue inflammation. It also has been shown that, the activated macrophages in response to injury

can undergo differentiation into two broad but distinct subsets of macrophages that are categorized as either classically activated (CAM or M1) and alternatively activated (AAM or M2) macrophages (Fig. 1-7). The emerging concept of macrophage plasticity is largely based on the effects of cytokines on monocytes observed *in vitro*. In such experiments, GM-CSF was found to induce an M1-like phenotype in macrophages, a process which was mediated by the transcription factor IRF-5, whereas M2 macrophages showed IRF-4 activation (200). Recently, a critical role for type I IFN/IFNAR signalling in differentiation of PB-Mo towards defined lung macrophage phenotypes was demonstrated in an influenza pneumonia mouse model (201).

As a key component of the inflammatory response that determines tissue destruction or recovery, increasing evidence suggests that macrophages do not remain committed to a single activation state. They may regress to a resting state and can subsequently be reactivated in a different direction, as recently demonstrated (202). Following phagocytosis of apoptotic cells, classically activated M1 macrophages may revert to an M2 activated state. These results suggest that macrophages are phenotypically polarized by the microenvironment to mount specific functional profiles (203), and this process depends on activation of distinct transcriptional programs. However, the heterogeneity of macrophages in the lung, their diverse role in lung inflammation and tissue remodeling, and the coordinated activation and programming by other inflammatory and parenchymal cells are not fully understood. In particular, the cell specific tasks of macrophage subsets and their progeny within the lung microenvironment during bacterial and viral infection are largely unknown. Therefore, a more precise knowledge of the molecular signals co-ordinating spatial and temporal macrophage differentiation and fine tuning of the functional response in infection that resolves the division of labor between the various macrophage subsets are needed to develop clinically useful intervention strategies. Analysis of the molecular basis of signal integration during macrophage polarization opens the perspective for interventional approaches to polarize/repolarize macrophage phenotypes for therapeutic purposes to target host defense, termination of inflammation and tissue repair in the time course of bacterial or viral infections.

2. Hypothesis and aims of the study

As discussed in the previous sections, during inflammation such as influenza-induced lung injury the macrophage composition of the lung reflects a dynamic balance of recruited and tissue-resident macrophages. These macrophage populations with distinct ontogenetic histories are exposed to various regional signals in the inflamed lung tissue, but their distinct response and further functional programming remained unresolved. Therefore, the central goal of the current study was to develop a flow-cytometry based protocol to characterize macrophage activation profiles separately for resident and recruited lung macrophages during early and late phases of influenza virus pneumonia. Hypothesizing that macrophage phenotypes differ at early vs. late infection states, further goals were to characterize the gene expression profile/transcriptome of these different macrophage subtypes in detail and to further investigate their functional capacities in vivo by adoptive cell transfer experiments. Finally, this project aimed at identifying crucial effector molecules for distinct macrophage subtype functions defined by the outlined approach in the course of IAV induced lung injury.

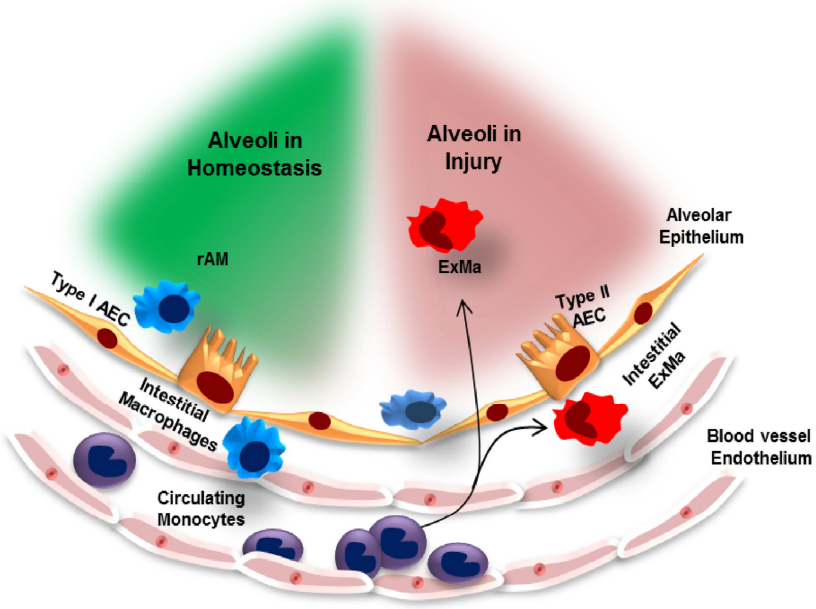

Figure 2-1 Composition of lung macrophages in homeostasis and during injury. In steady state, resident alveolar (rAM) and interstitial macrophages derived from precursors of fetal liver origin are a central part of the distal airway organotypic milieu. During inflammation, exudate macrophages (ExMa) originating from bone marrow migrate via blood stream into the inflamed lung tissue. These, resident and recruited lung macrophages with different ontogenetic and migration histories are exposed to dynamically changing regional signals which impact on their functional profile.

3. Materials and Methods

3.1. Materials

3.1.1 Mice

C57BL/6 wildtype (wt) mice, B6.SJL-Ptprc^{a} mice expressing the CD45.1 alloantigen (Ly5.1 PTP) on circulating leukocytes (with C57BL/6 genetic background) were purchased from Charles River Laboratories. CCR2-/- mice were generated as described previously and backcrossed to the C57BL/6 background (204). Mice were bred under specific pathogen-free conditions and were used between 8 and 12 weeks of age, unless specified otherwise.

3.1.2 Influenza A virus (PR8) propagation

Influenza virus A/Puerto Rico/8/34 (H1N1) (PR8) was propagated on canine epithelial MDCK II cells. Cells were passaged in a T75-cell culture flask at a ratio of 1:3 a day prior to infection to achieve an 85-90% confluency of the cells at the time point of infection. Cells were washed with PBS and infected with a multiplicity of infection (MOI) of 0.001. The virus dilution was prepared in MDCK II infection media (MDCK medium as described above but supplemented with 0.2% BSA instead of FCS). Cells were inoculated with 5ml virus dilution for 1h at 37°C and 5% CO_2, were then washed and further incubated with 10ml infection medium. Cell culture supernatants containing virus particles released from the infected cells were harvested after 72hrs and centrifuged at 3000rpm at 4°C for 30min. Supernatants were stored as aliquots at -80°C.

3.2 Reagents

Table-1 Chemicals and consumables

Chemical and consumables	company
Ampicillin	Sigma-Aldrich, GER
Atropin	B.Braun, GER
BSA (bovine serum albumin)	Sigma-Aldrich, GER
Cell culture flasks 75cm^2	Greiner, GER
Cell culture plates, single- and multi-well	Greiner, GER
Cell scaper, 28cm and 40cm handle	Greiner, GER

Cell strainer filters 40, 70 and 100µm	BD Biosciences, USA
Cell nylon filters 20µM	Merck Millipore, GER
Dispase	Corning Life Sciences, USA
Dispase II	Böhringer, GER
DNase	Serva, GER
DNase	Serva, GER
DMEM	Gibco Carlsbad, USA
dNTP's (desoxynucleoside triphosphate)	Thermo Scientific, USA
Dithiothreitol (DTT)	Thermo Scientific, USA
EDTA (Ethylenediaminetetraacetic acid)	Roth, GER
Ethanol	Sigma-Aldrich, GER
FITC tagged albumin	Sigma-Aldrich Chemie GmbH, GER
GentleMACS C tubes	Miltenyi Biotec, GER
Haematoxylin, eosin	Bayer AG, GER
MLV-RT	Life Technologies, USA
L-Glutamin [200mM]	Gibco BRL, GER
FCS (fetal calf serum)	Life Technologies, USA
HEPES	Merck Millipore, GER
Magnesium sulfate	Sigma-Aldrich, GER
PBS	Life Technologies, USA
PBS^{++} (containing MgCl)	PAN-Biotech, GER
Parafilm	American National, USA
Paraformaldehyde (PFA)	Merck, GER
Penicillin/Streptomycin [5000 U/ml]	Gibco BRL, GER
Polystyrene tubes, 15ml and 50ml	Greiner, GER
Polystyrene round-bottom tubes 5ml	BD Biosciences, USA
Ketaminhydrochloride (Ketavet)	Pharmaci & Upjohn, USA
Paraformaldehyde (PFA)	Merck, GER
Methanol	Roth, GER

Sandoglobulin	Novartis, CH
Saponine	Merck Millipore, GER
Annexin V binding buffer	BD Pharmingen, GER
7-AAD	BioLegend, GER
SYBR Green I	Life Technologies, USA
Reaction tubes 0.5ml and 1.5ml	Eppendorf, GER
Syringe 1ml, 10ml and 20ml	B.Braun, GER
Transwell permeable supports	Corning Life Sciences, USA
Trypsin-EDTA	Merck Millipore, GER
Trypsin-TPCK	Worthington Biochemical, USA
RNase	Serva, GER
Trypsin-TPCK	Worthington Biochemical, USA
RNase	Serva, GER
DNase	Serva, GER
recombinant mouse Plet1	Cusad, GER
RPMI	Life Technologies Carlsbad, USA
RNeasy Kit	Qiagen, GER

Table-2 Buffers and compositions

Buffer/medium	**composition**
FACS	PBS, 5% FBS, 1% EDTA 0.1% NaN3 sodium azide
MACS	PBS, 5% FBS, 1% EDTA
Mu AEC medium	DMEM, 10%FCS, 1% Penicillin/Streptomycin, 1% L- Glutamine, 2.5% HEPES
Mu AM medium	RPMI, 2%FCS, 1% Penicillin/Streptomycin, 1% L- Glutamine, 2.5% HEPES
PBS-EDTA	2mM EDTA in PBS

Table-3 Antibodies

The following anti-mouse mAbs were used in flow cytometry analysis. * Antibodies used in plet1 protein validation experiments (Table-3).

Antibodies	Dillution	Company
CD11c FITC	1:20	Miltenyi Biotec, GER
Siglec-F PE	1:50	Miltenyi Biotec, GER
CD45-APC-Cy7/FITC	1:100	BD Pharmingen, GER
CD45.1-FITC	1:100	BD Pharmingen, GER
CD45.2-APC-Cy7	1:100	BioLegend, GER
GR1-PE-Cy7	1:100	BioLegend, GER
CD11c-FITC/ PE-Cy5.5	1:20	Biolegend, GER
SiglecF-PE/Pacific blue	1:50	BD Pharmingen, GER
CD11b-Pacific blue/ BV421	1:50	Biolegend, GER
MHCII-FITC/ PE-CF594	1:100	BD Pharmingen, GER
CD206-APC	1:20	Biolegend, GER
CD40-Pe-Cy5	1:50	Biolegend, GER
CD326- APC-Cy7	1:100	BioLegend, GER
CD31-FITC	1:50	BD Pharmingen, GER
CD24-Pe-Cy7	1:50	BioLegend, GER
CD49f-Pacific blue	1:50	BioLegend, GER
annexin V-Alexa Fluor 647	1:20	Invitrogen, GER
anti-influenza NP-FITC	1:50	abcam, USA
Ki67-PE	1:10	BD Pharmingen, GER
*Plet1	20μg/ng	R&D Systems, Inc., GER
Active-caspase3	1:50	R&D Systems, Inc., GER
ZO-1 / TJP1	1:200	Life technologies, GER
APC Rat IgG2a,k Isotype	1:500	BioLegend, GER
Pe-Cy5 Rat IgG2a,k Isotype	1:500	BioLegend, GER
*Rat IgG1 Isotype Control	20μg	R&D Systems, Inc., GER

PE Mouse IgG1,k Isotype control	1:500	BD Pharmingen, GER
Alexa Fluor 488 goat anti-rabbit IgG	1:400	Invitrogen, GER

Table- 4 RT-PCR primers

Genes	***Primers***	
	Forward (5'-3')	***Reverse (5'-3')***
β-Actin	accctaaggccaaccgtga	cagaggcatacagggacagca
Mu FIZZ-1	tcctgccctgctgggatgac	ggcagtggtccagtcaacga
Mu IFN-γ	gccacggcacagtcattgaaagc	caccatccttttgccagttcctcca
Mu IL1-β	tacctgtggccttgggcctcaa	gcttgggatccacactctccagct
Mu IRF4	tgacgtttggcccacgaggc	ggttcctgtcacctggcaaccatt
Mu Mrc1	gggacgtttcggtggactgtgg	ccgcctttcgtcctggcatgt
Mu Klf4	ctgcgaactcacacaggcgaga	agcgggcgaatttccaccca
Mu iNOS	ttggaggccttgtgtcagccct	aaggcagcgggcacatgcaa
Mu Arg1	accacagtctggcagttggaagc	agagctggttgtcaggggagtgt
Mu Ym-1	gcactgacaggctttgcggt	aagcttccaacgccttcccg
Mu IL-10	ggcagagaagcatggcccagaa	aatcgatgacagcgcctcagcc
Mu IL-1ra	tgcctgatcactctggccatca	tgtctccttctactgtacaccctgc
Mu TNF	cggtccccaaagggatgagaagt	acgacgtgggctacaggctt
Mu CD206	atggattgccctgaacagca	tgtaccgcaccctccatcta
Mu CD40	gtttaaagtcccggatg ga	ctcaaggctatgctgtctgt
Mu CD86	ttacggaagcacccacgatg	ctccacggaaacagaatctga
Mu CD80	tggcccgagtataagaaccg	tatgtgccccggtctgaa
Mu PPAR-G	ttgctgtggggatgtctcac	aacagcttctccttctcggc
Mu Bax	gctggacactggacttcctc	gaggccttcccagccac
Mu Bcl2	ctgagtacctgaaccggcat	agttccacaaaggcatcccag
Mu Trem2	cccgaggagtcatcgagtttc	cacaggatgaaacctgcctgga
Mu Cldn1	cgacattagtggccacagca	tggccaaattcatacctggca
ZO-1	gcttctcttgctggccctaa	gggagcctgtagagcgtttt

Mu Ocln	tctttccttaggcgacagcg	agataagcgaacctgccgag
Mu Cdh1	aacccaagcacgtatcaggg	gagtgttgggggcatcatca
Mu EpCam	tgctccaaactggcgtctaa	ttgttctggatcgccccttc
Mu PDGF-a	agaggtccaggtgaggttaga	acctcacatctgtctcctcctc
Mu PDGF-b	ctgctagcgtctggtca	catcaaaggagcggatggag
Mu PDGF-c	aattgtgcctgttgtctcca	tat gcaatcccttgactcca
Mu EGF	tcgttgttagcaccatccctc	ggcacaaccaggcaaaggat
Mu FGF 7	catgcttccacctcgtctgt	cagttcacactcgtagccgt
Mu FGF 10	gctcccaggagaggacaaaaa	catccaccaacagcgttttct
Mu IGF 2	tcggtttgcatacccgcag	gggatccccattggtacctgg
Mu Vopp1	cttcggacggtcctcgc	tcagtgcactccactagcag
Mu Ccpg1	caattcaagaagcgcccagc	tgaaaagacgggttctggct
Mu VEGF-b	ccctggaagaacacagccaa	agaggatcctggggctgtc
Mu Notch1	caactgccagaaccttgtgc	tggtactgcgtgttggtctg
Mu Plet1	tcctcatcgtcgtcaatcgc	tgaggctgagggttgtacttg
Mu IRF7	accgtgtttacgaggaaccc	gctgcgctcggtgagag
Mu CcnD1	tcaagtgtgacccggactgc	ccttggggtcgacgttctg

3.3 Methods

3.3.1 Influenza A virus titration

To determine the amount of virus particles capable of multicycle replication (plaque forming units, pfu), MDCK II cells were seeded in 6-well plates one day prior to infection to achieve a confluency of 85-90% at the time point of infection. Cells were washed with PBS and infected with 333µl of subsequent 1:10 dilutions of the virus stock in PBS/0.2%BSA, covering a range of dilutions from $1:10^3$ to $1:10^9$. Virus dilutions were inoculated at 37°C 5% CO_2 for 1h, cells were then washed and covered with 1.5ml Avicel medium (2xMEM, 1% Penicillin/Streptomycin, 0.1% NaHCO3, 0.2% BSA, 2µg/ml Trypsin-TPCK, 1.25% Avicel). Due to its high viscosity, Avicel prevents viral spread through the cell culture by diffusion of viral particles in the surrounding media and only allows virus spread from cell to cell. Cells were incubated for further 48h at 37°C 5% CO_2 to allow formation of plaques caused by local cell death of infected MDCK II cells. After

this incubation, cells were fixed with 4% PFA for 20min at 4°C followed by permeabilization by 0.3% Triton-X-100 for 15min at RT. Blocking of unspecific antigenic epitopes was performed using Normal Horse Serum (NHS) diluted 1:100 in PBS/ 0.2% BSA. Plaques were visualized by immunohistochemical staining with anti-Influenza NP antibody diluted 1:100 in PBS/10% NHS/0,05% Tween 80 for 1h at RT followed by a Horse raddish peroxidase (HRP)-marked secondary anti-mouse antibody diluted 1:200 for 1h at RT. Addition of TrueBlue, an HRP-substrate yielding a blue colour after enzymatic progressing, allowed counting of plaques per well.
The titer of the virus stock was calculated by:

number of plaques per well*dilution^{-1}*1ml/333µl = pfu/ml

3.3.2 In vivo infection protocol

Mice were pre-administred with Atropin (application 0.05mg/kg; diluted in 0.9% sterile NaCl to 0.05mg/ml and applied subcutaneously at 0.02ml per 20g body weight) and anesthesized with Xylazine hydrochloride (application 16mg/kg; diluted in 0.09% sterile NaCl to 3.33mg/ml) and Ketamine hydrochloride (application 100mg/kg; diluted in 0.09% sterile NaCl plus 3.33mg/ml Xylazine hydrochloride to a concentration of 25mg/ml) applied intraperitoneally at 0.2ml per 20g body weight. Mice were kept on a heating pad to minimize loss of body temperature. Achieved anesthesia was verified by pinching of the tip of the tail. Mice were then fixed at the upper teeth and hindlegs in supine position on an intubation stand, and an endotracheal tube was inserted orally, passing the vocal chords into the trachea. Using a Hamilton syringe, mice were inoculated with 250pfu (plaque forming units) of PR8 or diluted in 70µl sterile PBS$^{-/-}$. Control groups were inoculated with 70µl of sterile PBS without additives. Infected mice were monitored 1-3 times per day.

3.3.3 Isolation of alveolar macrophages by magnetic assisted cell sorting (MACS)

Mice were sacrificed by cervical dislocation and the trachea was exposed to insert a 21-gauge cannula via a small incision. Mice were then lavaged with 10x 500µl PBS/ 2mM EDTA. Bronchoalveolar lavage fluid (BALF) was stored on ice until further processing. Cells in BALF were pelleted by centrifugation at 1400rpm for 10min at 4°C and resuspended in MACS buffer (Phosphate-buffered saline (PBS), 2% calf serum, 1 mM EDTA). These cells were pelleted and incubated with mouse Fc-blocking reagent for 10mins at 4°C. Then the cells were stained with fluorescein isothiocyanate (FITC)-

conjugated anti-CD11c antibody followed by magnetic labelling with Anti-FITC MultiSort MicroBeads. Following positive selection, the magnetic particles are removed from the cells by using the MultiSort Release reagent according to the manufacturer instructions. The CD11c positive cell populations were then stained with phycoerythrin (PE) conjugated anti-SiglecF antibody followed by magnetic labelling with anti-PE MultiSort MicroBeads. Finally the double positive (CD11c and SiglecF) cells were magnetically isolated to obtain the total alveolar macrophage population.

3.3.4 Preparation of BALF and lung homogenates for flow cytometry

Mice were sacrificed by exsanguination. BALF were collected and cells were pelleted as described above in section 3.2.3, then resuspended in FACS buffer (PBS, 5-10% FBS, 0.1% NaN3 sodium azide) and stored on ice for flow cytometry analysis. Lavaged lungs were perfused with sterile PBS via right heart ventricle puncture. The lungs are filled slowly with 800-1500µL of dispase using a 21-gauge cannula via a small incision into trachea and tied with a suture thread to avoid the leakage of dispase. The lungs were then removed, after carefully dissecting out the heart and incubated for 40 min at room temperature in dispase. The lungs are then subjected to a MACS tissue dissociator and filtered using 100µm and then 40µm filters. Obtained cells were pelleted by centrifugation at 800rpm for 8min at 4°C, re-suspended in 1ml PBS, counted and adjusted to 10^7cells/ml and stored on ice for flow cytometry analysis.

3.3.5 Flow cytometry analysis of alveolar and interstitial macrophages

$1–5\times10^5$ cells were resuspended in FACS buffer and stained directly after isolation from BAL or preparation of single cell suspensions from lung tissue in 96-well plates and incubated with 10µl Sandoglobulin® to block Fc-receptors. Cells were then incubated with the respective antibodies for 20min at 4°C or resuspended in annexin V staining buffer (10 mM HEPES, 140 mM NaCl and 2.5 mM $CaCl_2$) to analyse apoptosis. The rest of the cells were fixed in 1%PFA/PBS for later analysis. Flow cytometric analysis was performed using a BD LSRFortesa flow cytometer (BD Biosciences, Heidelberg, Germany) and FACS Diva Software.

3.3.6 Purification of M1 and M2ExMa by fluorescence activated cell sorting (FACS)

Wild type mice were infected with 250pfu of PR8 and lavaged to obtain BALF (as described in 3.2.3) on D7, D10, D14 and D21pi. The BALF was then centrifuged at 1400rpm for 10min at 4°C and the pelleted cells were blocked with 10µl Sandoglobulin® and incubated with a mixture of antibodies (CD45, Gr-1, CD11b, SiglecF, CD11c, CD206 and CD40) in 250µl MACS-buffer (PBS, 7.4% EDTA, 0.5% FCS pH 7,2) for 20min at 4°C. The cells were washed to remove unbound antibodies and resuspended in 3ml of MACS-buffer. 7-AAD (1:10) was added to each sample, 10min before sorting. M1 ExMa's ($CD40^{hi}$ $CD206^{low}$ $CD11b^{+}$ $CD11c^{+}$ $SiglecF^{low}$) from D7, D10, D14pi and M2 ExMa's ($CD206^{hi}$ $CD40^{low}$ $CD11b^{+}$ $CD11c^{+}$ $SiglecF^{low}$) from D21, D10, D14pi were then flow sorted into alveolar macrophage medium using a BD FACSAria™ III Cell Sorter. The purities of sorted M1 and M2ExMa were assessed by flow cytometry analysis which showed a purity ≥ 90% in all samples. Sorted M1 and M2ExMa were centrifuged at 1400rpm for 10min at 4°C and pellets were resuspended in 350µL of RLT buffer and stored at -80°C for RNA isolation.

3.3.7 Adoptive transfer

For adoptive transfer of M1 and M2ExMa, the cells were sorted from D7pi or D21pi as described in 3.2.6. 50.000 sorted cells of M1 and M2ExMa were resuspended in 60µl sterile $PBS^{-/-}$ only or together with anti-Plet1 antibody or IgG isotype and transferred orotracheally to PR8-infected CCR2-deficient mice on D3pi. Thereafter the effects of the adoptive cells transfers with respect to inflammation and alveolar barrier protection were analyzed at D7pi.

3.3.8 Generation of bone marrow chimeric mice

Bone marrow (BM) cells were isolated under sterile conditions from the tibias and femurs of wt C57BL/6 donor mice (expressing the CD45.2 alloantigen) as previously described and transferred to CD45.1 alloantigen-expressing recipient mice which had received total body irradiation (6 Gy) [76]. To assess BM engraftment the proportion of donor CD45.2-expressing leukocytes in blood, BALF and lung homogenate was analyzed by flow cytometry. Two weeks after transplantation, regularly >90% of circulating leukocytes were of donor type (CD45.2) whereas >90% lung-resident myeloid cells were of recipient type (CD45.1) determined by FACS analyses of the proportions of CD45.1 vs. CD45.2 cells.

Chimeric mice were housed under specific pathogen free conditions for 14 days before PR/8 infection.

3.3.9 Administration of recombinant Plet1 in vivo

Mice were prepared as described in 3.2.2. Using a Hamilton syringe, recombinant murine plet1 (R&D Systems, 5µg in 50 µl PBS) was orotracheally delivered to infected mice on D3pi. Control groups were inoculated with 50µl of sterile PBS. Treated mice were monitored 1-3 times per day.

3.3.10 FITC albumin alveolar leakage

Alveolar leakage was analyzed by the lung permeability assay with i.v. injection of FITC-labeled albumin (Sigma-Aldrich, Taufkirchen, GER) and detection of FITC-fluorescence in serum and BALF, as previously described (64) or by determination of total protein concentrations in BALF by a commercially available spectrophotometric assay (BCA assay, Biorad, München, Germany).

3.3.11 Isolation of primary murine alveolar epithelial cells

Murine alveolar epithelial cells (AEC) were isolated based on the protocol developed by Corti et al (205). Mice were sacrificed by cervical dislocation. The chest cavity was opened and lungs were perfused with sterile HBSS via the right ventricle. To insert dispase into the lung, a small incision was made into the trachea to insert a shortened 21-gauge cannula. This cannula was fixed and 1.5ml of sterile dispase was administered into the lungs to allow enzymatic separation of distal epithelial cells. The lungs and trachea were dissected out, washed in PBS and placed in dispase for 40min at room temperature (RT). The heart, trachea and large airways were removed and the remaining lung tissue was dissected in DMEM/ 2.5% HEPES plus 0.01% DNase in C tubes using the gentle MACS dissociator. (Milteny Biotec). Cells were filtered through 100, 40 and 20µm cell filters, washed, resuspended in DMEM/ 2.5% HEPES and counted. Then cells were incubated with biotinylated anti-mouse CD31, CD16/32 and CD45 antibodies for 30 min at 37°C to remove remaining endothelial and lymphoid cells. Antibody amounts were calculated by following equations:

number cells/1,000,000 *0,9 = µl of CD45 antibody
number cells/1,000,000 *0,675= µl of CD16/32 antibody
number cells/1,000,000 *0,4 = µl of CD31 antibody

After incubation, cells were washed and streptavidin-linked magnetic beads (washed thrice with 1ml PBS) were added for 30 min at room temperature with gentle rocking. Amounts of magnetic beads were calculated by following equation:

number cells/1,000,000 /3*50µl = µl of magnetic beads

After incubation, magnetic separation was performed for 15 min and remaining cells were washed and resuspended in mAEC medium. The purity of freshly isolated mAEC was assessed by flow cytometry for murine EpCAM (staining epithelial cells) and pro-surfactant protein C (staining type II AEC). Cell suspensions with a purity ≥ 90% were used for further experiments. Cell viability was examined by trypan blue staining and was ≥95%. Murine AEC were seeded at a density of 120-150,000 cells/cm^2 and grown for 3 days to confluency prior to use. For analysis of AEC apoptosis, lungs were digested by intratracheal application of Dispase and processed as outlined previously (64).

3.3.12 Influenza A infection of cultured cells

To infect murine alveolar epithelial cells (mAEC) with PR8, the virus stock was diluted in PBS^{++}, 0.2% BSA to the indicated multiplicity of infection (MOI). The final concentration of the inoculum was calculated as follows:

Number of cells/well*MOI*1ml/inoculation volume µl = pfu/ml

The cells were washed with PBS and inoculated with the final virus dilution for 1h at 37°C/ 5% CO_2. Thereafter the virus dilution was removed and replaced by infection medium containing 0.2% BSA instead of FCS. Chemicals were added together with the infection medium at the indicated concentrations. Infected cells were kept at 37°C/ 5%CO_2 throughout the course of infection.

3.3.13 Trans-epithelial resistance

Trans-epithelial resistant (TER) on cell layers of mAEC was determined by changes of the flow of ions across the cell layer in apical and basal cell culture media. mAEC were seeded as described in 3.2.12 in 0,4µm pore size transwell cell culture dishes and cultured until achieving electrochemical resistances of ≥600Ω /cm^2 as measured by Millicell-ERS2 device. Cells were infected with PR8 at MOI 0.5 or mock infected for 1h at 37°C and then supplied with 20ng/ml recombinant (r) murine Plet1 (Cusad, GER) or mock treated. The TER was recorded by Millicell-ERS2 device at 4, 6, 8, 12, 16, 24 and 30hrs of post infection. The recorded values are multiplied with the area of the transwell to obtain the TER value.

3.3.14 RNA isolation

For RNA isolation, cells were washed with PBS and then incubated in 350µl RLT buffer provided by the RNeasy Kit (Qiagen), leading to cell lysis, protein denaturation and thus RNase deactivation. Samples were processed according to the manufacturer's instructions. By adding 350µl of 70% ethanol, RNA was precipitated and then bound to a silica membrane, washed and finally eluted in small volumes. RNA amounts were measured using the spectrophotometer Nanovue Plus (GE Healthcare).

3.3.15 cDNA synthesis

For cDNA synthesis 150- 250ng of isolated RNA plus dH2O in a total volume of 13.5µl were heated up to 70°C for 5min to break up secondary RNA structures and linearize the RNA. Samples were then put on ice for 3-5min. Then 11.5µl of PCR Master Mix were added including a reverse transcriptase needed for transcription of RNA into cDNA according to the manufacturer's instructions. Samples were kept at 37°C for 1h and then heated up to 95°C for 5min to inactivate the reverse transcriptase. All incubation steps were performed in a PeqSTAR thermocycler (Peqlab, Erlangern, GER).

3.3.16 Quantitative real-time polymerase chain reaction (RT-PCR)

RT-PCR was performed with SYBR green in the AB Step one plus Detection System (Applied Bioscience) using the reaction setup provided by the manufacturer's instructions. β-actin expression served as normalization control. Data are presented as ΔCt or fold change ($2^{\Delta\Delta Ct}$) as described (206). The primers used were listed in the table- 4.

3.3.17 Transcriptome analysis by genome array

For genome array of M1 and M2 ExMa, the cells were sorted as described in 3.2.6. The sorted M1 ExMa from D7pi and the M2 ExMa from D7pi and D21pi were re-suspended in RLT buffer and stored at -80°C until RNA isolation and further processing for transcriptome analysis. The isolated RNA was amplified by Ribo-SPIA technology using the Ovation PicoSL WTA v2 kit (NuGen). The amplified cDNA was Cy3-labelled using the Genomic DNA Enzymatic Labeling kit (Agilent). 2µg labelled cDNA was hybridized on SurePrint G3 Mouse GE 8x60K Microarrays (Agilent, Design ID 028005) following the Agilent protocol. Washed slides were dried with acetonitrile and treatment with Agilent dye-stabilization solution. Slides were scanned at a resolution of 2 µm/pixel with an InnoScan 900 instrument. Image analysis was done with Mapix 6.5.0. Further data analysis

was done using R 3.1.0 (207) and the limma package (208) from BioCondurctor. Mean spot signals were quantile-normalized. Log-signals of replicate spots were averaged. Gene set tests were based on rank-sum statistics of the moderated t-values. Pathway definitions were taken from the KEGG database (http://www.kegg.jp) (209, 210).

3.3.18 Cytospin staining

Aliquots of FACS-purified cells (0.5-1x105 cells) were spun onto Polysine TM glass microscope slides (VWR International) at 300 RPM for 6 minutes using a cyto-centrifuge (Shandon, Runcorn, UK). Cells were then allowed to air dry for 10 minutes and then stained using May Gruenwald and Giemsa stain for 5min and 10min, respectively with a thorough distilled water wash at the end of each staining step. Then, slides were allowed to air dry and mounted in DPX mountant (BDH, UK) under glass. Stained cells were assessed for morphology using an Olympus BX41 microscope.

3.3.19 Fixation and preparation of lung tissue for histology

For histological staining of mouse lung tissue, lungs were clipped at the trachea before opening of the chest cavity, then perfused, removed and fixed for 24h in 4% PFA. Lungs were embedded in Parrafin (Leica ASP200S), cut into 3-5µm thick sections and stained with hematoxylin and eosin in the following procedure:

Xylene 5min (twice), 100% ethanol 30sec (twice), 96% ethanol 30sec, 96% ethanol 30sec, 70% ethanol 30sec, 70% ethanol 30sec, hematoxylin 3min, 0.1% HCl 2sec, H_2O 5min, Eosin G solution 3min, H_2O 30sec, 70% ethanol 30sec, 90% ethanol 30sec, 100% ethanol 30sec (twice), xylene 5min (twice). Analysis was performed with a Leica DM 200 microscope.

3.3.20 Fixation of cell cultures for immunofluorescence microscopy

For immunofluorescence microscopy, cells were washed with PBS and then air-dried for 1min at RT. Cells were fixed and permeabilized by a pre-cooled (-20°C) 1:1 acetone/methanol suspension that was left on the cells for 3min at RT. Cells were then washed thrice with PBS/0.3% BSA and blocked with 3% BSA in PBS over night at 4°C.

3.3.21 Statistical analysis

All data are given as mean ± standard deviation. Statistical significance between two groups was estimated using the two-tailed paired or the unpaired student's t-test for paired or unpaired samples, respectively. For comparison of > two groups with each other one-way ANOVA was applied. Significances were calculated with the prism or with MS-xl for windows software program. A value of $p<0.05$ was considered as significant.

4. Results

4.1 Polarization profile of total alveolar macrophages in IAV induced ALI

To evaluate the dynamics of alveolar macrophage polarization during IAV induced ALI, alveolar macrophages were isolated from bronchoalveolar lavages (BAL) obtained from PR8 (250pfu) infected mice at different time points post infection (pi) (D0, D2, D7, D14, D21) by magnetic assisted cell sorting (MACS). The purity of the isolated macrophage population was evaluated by flow cytometric immuno-phenotyping using CD11c and SiglecF as macrophage markers and by morphology in Pappenheim stained cytospins. Both evaluations showed enrichment of the macrophage proportion to > 90 % (Fig. 4-1 A, B).

A.

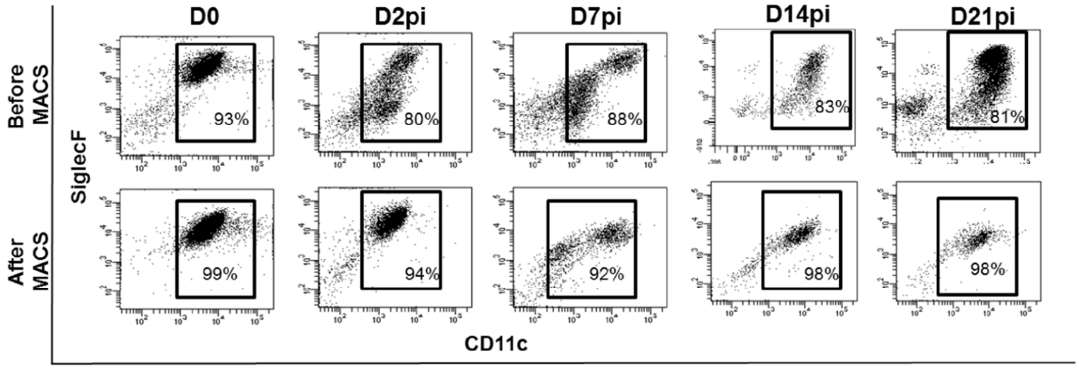

B.

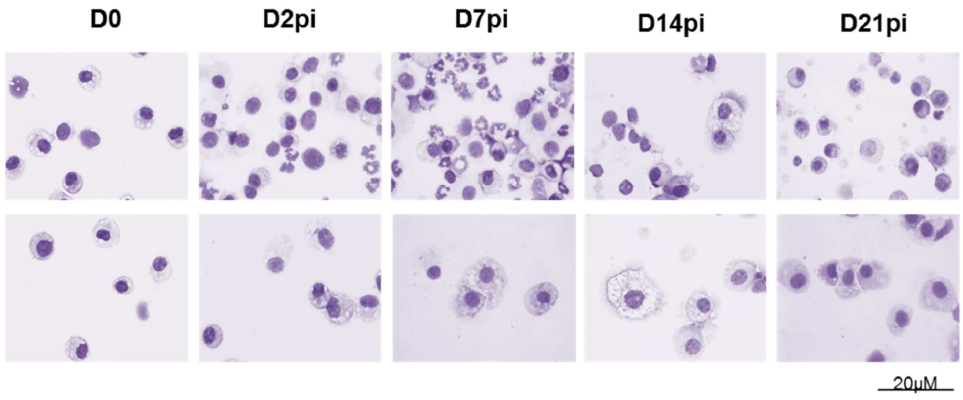

Figure 4-1 Isolation of alveolar macrophages by immuno-magnetic cell sorting from BAL in IAV induced ALI. Bronchoalveolar lavage (BAL) were collected from mice infected with PR8 (250pfu) at D0, D2, D7, D14 and D21 post infection (pi) and alveolar macrophages were enriched using CD11c and SiglecF antibodies tagged magnetic beads by magnetic assisted cell sorting (MACS). **A.** Flow cytometry dot plots show the proportion of alveolar macrophages ($CD11c^{+}$, $SiglecF^{+}$) before and after MACS enrichment **B.** Papenheim staining of cytospins before and after MACS enrichment. Representative experiments for D0, D2, D7, D14 and D21 post infection (pi) days with 4n/each pi time point.

The mRNA expression of prototypic markers for M1 and M2 macrophage polarization in MACS enriched total alveolar macrophages was analyzed by RT-PCR at different time points pi. The gene expression of both M1 and M2 polarization markers was found to be

slightly increased in the early phase of infection and returned to the baseline at later stages of pi (Fig. 4-2) suggested the presence of both M1 and M2 phenotypes during the course of infection.

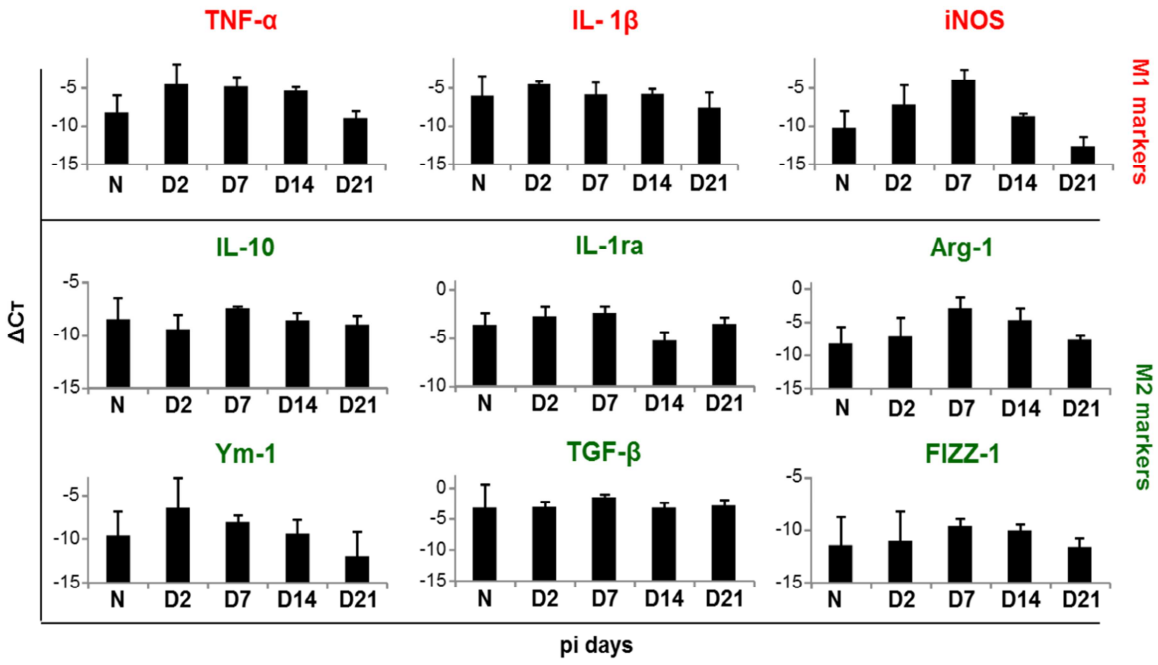

Figure 4-2 mRNA expression levels of prototypic M1 and M2 markers in MACS enriched alveolar macrophages from BAL during IAV induced ALI. MACS enriched alveolar macrophages from bronchoalveolar lavages (BAL) of PR8 infected (250pfu) mice at D0, D2, D7, D14 and D21 post infection (pi) were analyzed for the expression of the prototypic M1 (TNF-α, IL-1β, iNOS) and the M2 markers (IL10, IL-1ra, Arg-1 Ym-1, TGF-β and FIZZ-1) by RT-PCR. The graphs are represented with ΔCT relative expression normalized to β-actin with means ± SD of 3 independent experiments.

4.2 Polarization profile of FACS separated alveolar macrophage subsets in IAV induced ALI

During inflammation such as influenza induced lung injury the macrophage composition of the lung reflects a dynamic balance of recruited and tissue-resident macrophages both exposed to various regional signals in the inflamed lung tissue. To dissect the functional programming of these macrophage populations with distinct ontogenetic histories with respect to M1 vs. M2 profiles, we developed a flow cytometry based protocol to characterize macrophage activation profiles separately for resident and recruited lung macrophages during early and late phases of influenza virus pneumonia. To discriminate rAM and ExMa subsets, a previously established gating strategy was used (Fig. 4-3 A). To screen for phenotypic plasticity of the different macrophage subsets during infection, the expression of prototypic surface markers related to M1 vs. M2 polarization was evaluated on alveolar macrophages isolated from the BAL of PR8 infected mice on D7pi and D21pi by flow cytometry. The prototypic markers CD40 for M1 and CD206 for M2 polarization

were found to be differentially expressed at distinct time points during IAV induced ALI. Additionally, RT-PCR analysis of alveolar macrophages from BAL of PR8 infected mice at D0, D2, D7, D14 and D21 pi days showed increased mRNA expression of CD206 in the early and late phase of infection, whereas CD40 was strongly upregulated during the acute phase of infection (Fig. 4-3 B, C). Therefore, CD206 and CD40 were selected as surrogate markers for potential M1 vs. M2 polarization, respectively and employed to investigate the dynamics of macrophage plasticity separately in rAM and ExMa during IAV induced ALI (Fig. 4-4).

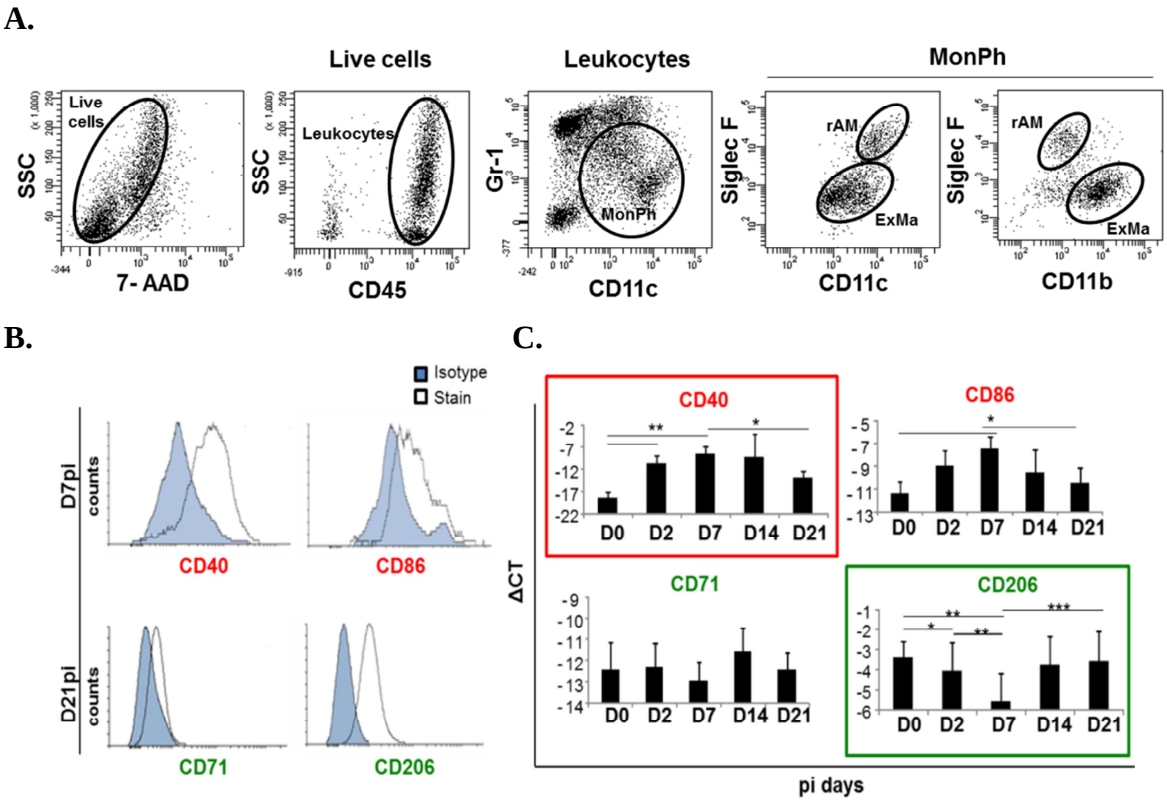

Figure 4-3 Gating strategy to discriminate rAM vs. ExMa and expression of prototypic M1 and M2 markers in alveolar macrophages during IAV induced ALI. A. Representative dot plots of multicolour stained BAL cells obtained on D7pi. The gating strategy was used to differentiate rAM and ExMa. $CD45^{+}$ live cells ($7\text{-}AAD^{-}$) were differentiated according to CD11c and Gr-1 expression, whereby $CD11c^{+}Gr\text{-}1^{low}$ cells represent the mononuclear phagocyte (MonPh) pool. Differentiation of resident alveolar macrophages (rAM) and exudate macrophages (ExMa) was achieved by gating for SiglecF and either CD11c or CD11b. rAM were identified as $SiglecF^{hi}CD11c^{hi}CD11b^{low}$ and ExMa as $SiglecF^{-}CD11c^{low}CD11b^{hi}$. **B.** Flow cytometric analysis showing the surface expression of M2 (CD71, CD206) and M1 markers (CD40, CD86) on alveolar macrophages at D7pi and D21pi respectively from PR8 infected (250pfu) mice. **C.** The bar graphs represent the mRNA expression of M2 markers (CD71, CD206) and M1 markers (CD40, CD86) in alveolar macrophages from bronchoalveolar lavage (BAL) of PR8 infected (250pfu) mice at D0, D2, D7, D14 and D21 post infection (pi) days. The bar graphs are presented as ΔCT relative expression normalized to β-actin with means ± SD of 3 independent experiments. *p<0.05; **p<0.01; ***p<0.001.

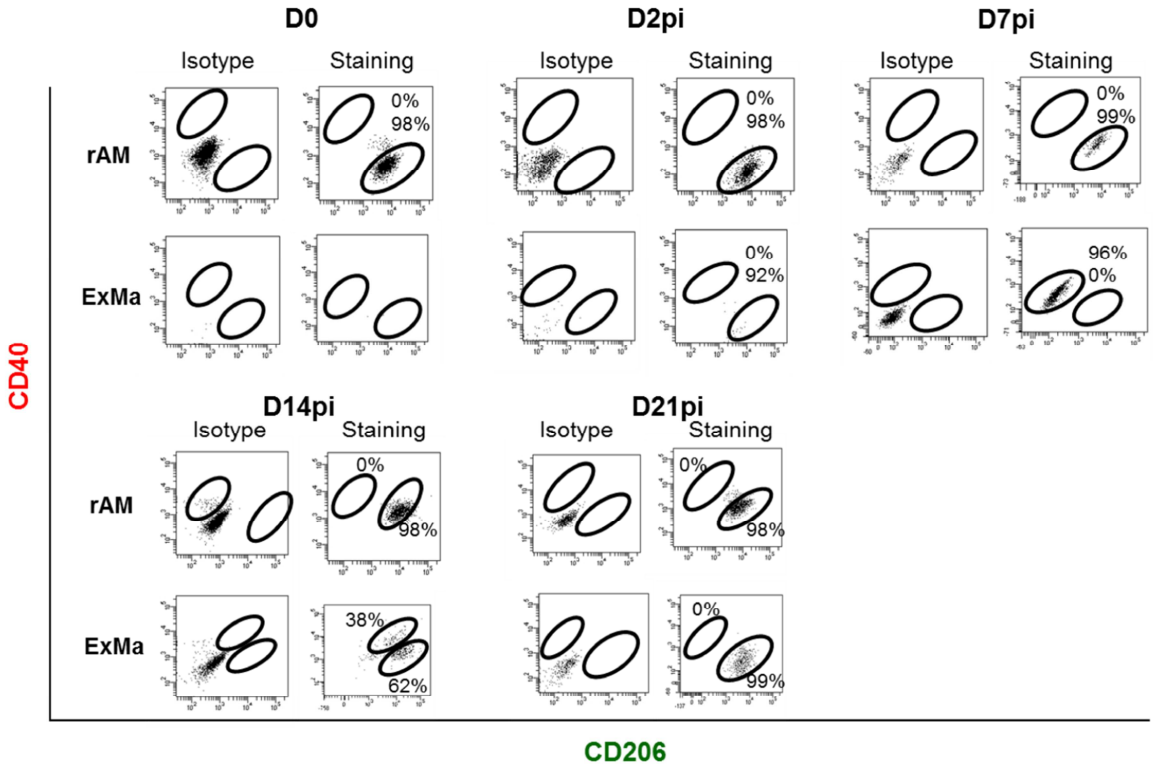

Figure 4-4 Phenotype of alveolar macrophage subsets in IAV induced ALI. Alveolar macrophages from bronchoalveolar lavage (BAL) of PR8 (250pfu) infected mice were analyzed for surface expression of CD40 and CD206 on resident alveolar macrophages (rAM) and exudate macrophages (ExMa). The rAM and ExMa subsets were discriminated by the gating strategy shown in Fig 4-3 A. Surface expression of CD206 and CD40 on both rAM and ExMa were compared to isotype controls at different time points post infection (pi) and shown in representative dot plots. Flow cytometry plots represent the gatings of M1 and M2 phenotype based on CD40 and CD206 expression.

Quantification of CD40 and CD206 expression cells within the rAM and ExMa populations, respectively were analyzed at different time points post PR8 infection and revealed that, ExMa displayed a M1 polarized ($CD40^{hi}$) phenotype in the acute phase of infection at D2 and D7. In the early repair phase (D14pi), both M1 and M2 polarized cells were observed in the ExMa population which completely shifted to a M2 ($CD206^{hi}$) phenotype during the late repair phase (D21pi) of infection. In contrast to this plasticity with respect to CD40 and CD206 expression observed in the ExMa subset, rAM showed constant CD206 expression and lack of CD40 in all phases of IAV infection.

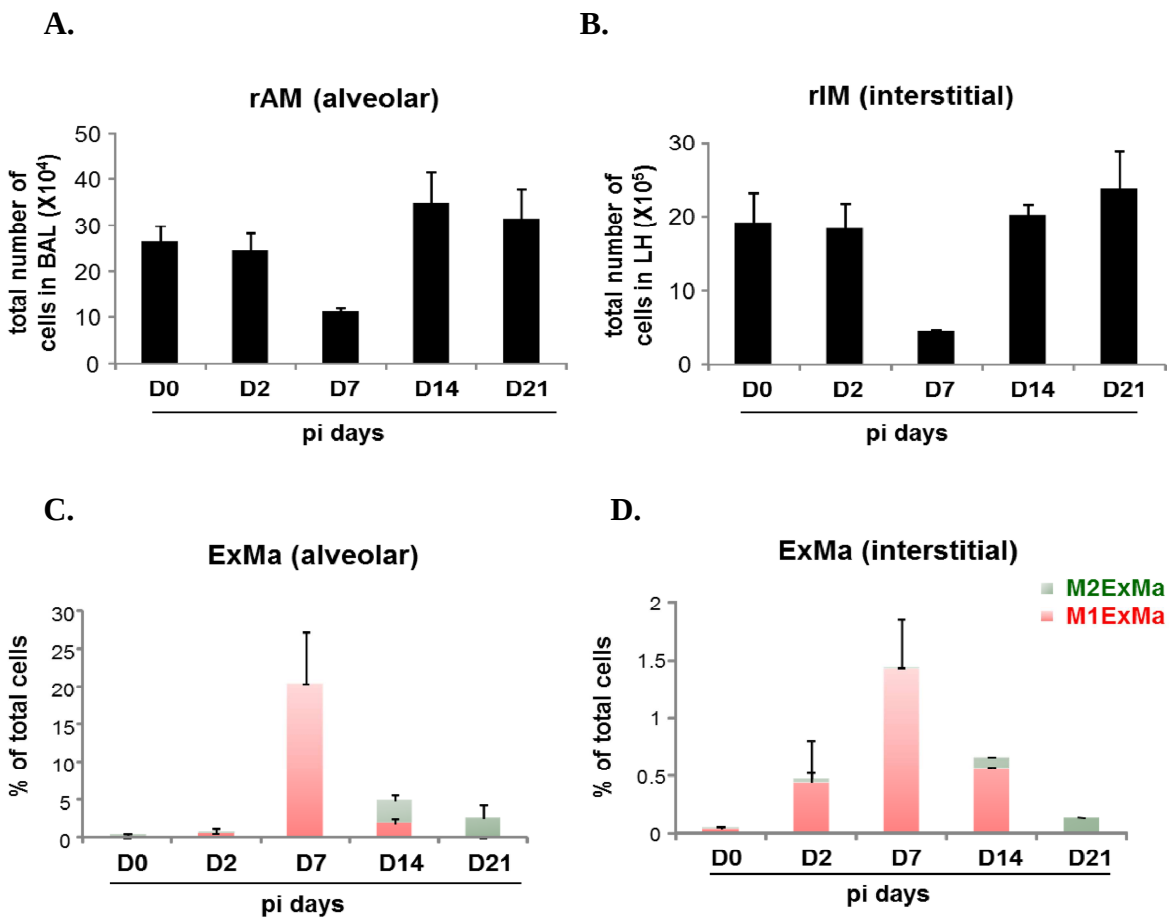

Figure 4-5 Depletion of resident macrophages and plasticity of exudate macrophages during the time course of IAV induced ALI. The total number of **A.** resident alveolar macrophages (rAM) in bronchoalveolar lavage (BAL) and **B.** resident interstitial macrophages (rIM) in lavaged lung homogenates were quantified at D0, D2, D7, D14 and D21 post PR8 infection (250pfu). The percentage of **C.** alveolar exudate macrophages (ExMa- alveolar) from BAL and **D.** lavaged lung homogenates (ExMa- interstitial) was analyzed at D0, D2, D7, D14 and D21 post PR8 infection. The red bars represent the percentage of $CD40^{hi}$ ExMa while the green bars represent the percentage of $CD206^{hi}$ ExMa. Bar graphs show means ± SD of 4n / each time points.

4.3 Gene expression of further prototype markers for M1 and M2 polarization in sorted $CD40^{hi}$ and $CD206^{hi}$ exudate macrophages in IAV induced ALI

To verify the plasticity of ExMa, M1 and M2ExMa from D10pi were flow sorted using the established gating strategy (Fig.4-3 A and 4-4). The mRNA levels of prototypic genes for M1 and M2 polarization were analyzed. RT-PCR quantification revealed a significant increase of IL-1β, iNOS, CD40 in $CD40^{hi}$ ExMa and of Arg-1, FIZZ-1, TGF-β and CD206 in $CD206^{hi}$ ExMa confirming the respective M1 and M2 polarization of $CD40^{hi}$ and $CD206^{hi}$ ExMa.

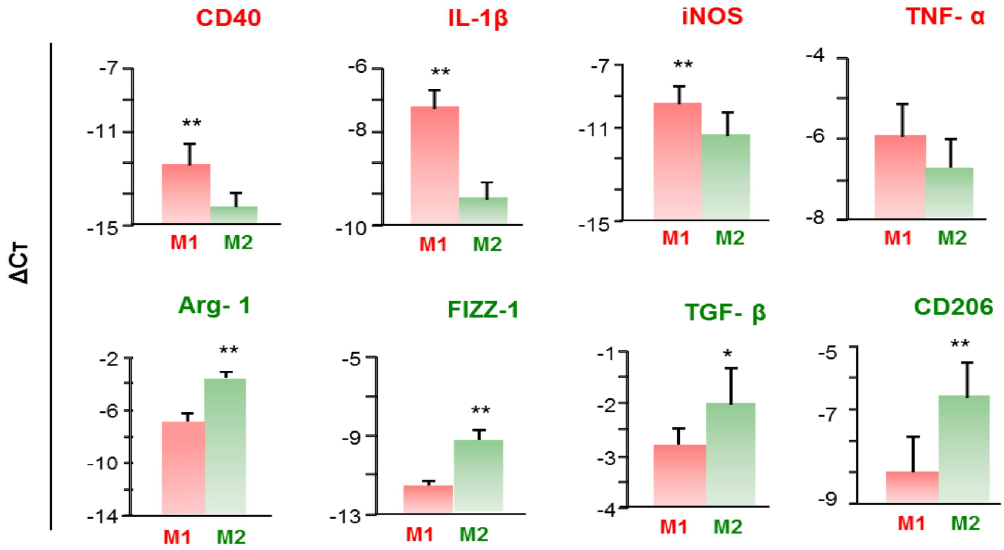

Figure 4-6 Gene expression of prototypic M1 and M2 markers in flow sorted CD40^{hi} and CD206^{hi} ExMa during IAV induced ALI. mRNA levels of prototypic markers for M1 vs. M2 polarization were quantified by RT-PCR in flow sorted CD40^{hi} and CD206^{hi}, exudate macrophages (ExMa) derived from bronchoalveolar lavage (BAL) of PR8 infected (250pfu) mice at D10pi. The green bar represents the CD206^{hi} ExMa and the red bars show the CD40^{hi} ExMa subset. The graphs are presented as ΔCT relative expression to normalized β-actin and represent means ± SD of 3 independent experiments. *p<0.05; **p<0.01; ***p<0.001.

4.4 Relationship between bone marrow derived ExMa and rAM in IAV induced ALI addressed in a chimeric mouse (CD45.1/CD45.2) model

To further investigate the relationship between recruited and resident macrophage populations and particularly the contribution of ExMa in replenishing the depleted rAM pool after IAV infection, bone marrow chimeras of CD45.2 donor mice and irradiated CD45.1 recipient mice were generated. In chimeric animals >90% of circulating blood cells displayed the CD45.2 donor phenotype whereas the rAM population was of recipient (CD45.1) phenotype at 2 week (w) post bone marrow transplantation (BMT). Chimeric mice were infected with PR8 (250pfu) and the proportions of CD45.2 donor vs. CD45.1 recipient cells were flow cytometrically quantified separately in the rAM and in the ExMa fraction at different time points pi (Fig 4-7). Recipient CD45.1 AM were found to be completely replaced by donor type cells starting at D10pi. As expected, bone marrow derived ExMa were found to be of CD45.2 donor type and displayed a CD40^{hi} M1 phenotype in the early phase of infection until D10pi and increasingly a CD206^{hi} M2 phenotype in the late phase of infection. Although a direct transition of donor ExMa into the rAM pool was not formally demonstrated, the increasing emergence of donor type cells in the rAM fraction at late time points and the donor type ExMa present in the alveolar space express a CD206^{hi} M2 phenotype, suggests that CD206^{hi} ExMa might contribute to replace the depleted rAM pool after IAV infection.

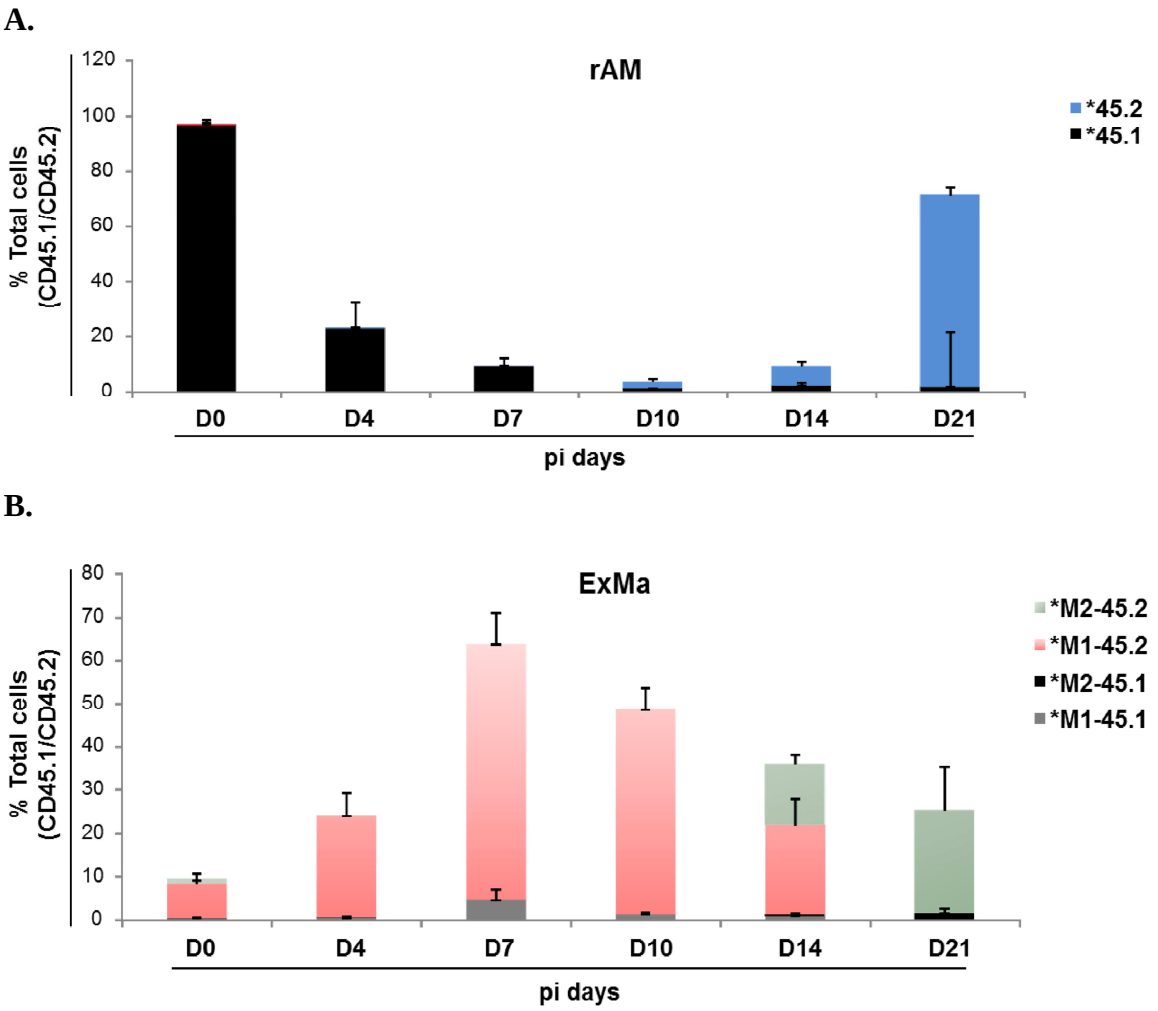

Figure 4-7 M2ExMa replenishes the rAM after IAV infection *in vivo*. Wildtype (wt) donor (CD45.2) bone marrow was transplanted into recipient (CD45.1) mice and infected (*) with PR8 (250pfu). The bronchoalveolar lavage (BAL) was collected from the infected recipient mice at different post infection (pi) time points (D0, D4, D7, D10, D14 and D21) and analyzed for resident alveolar macrophage (rAM) pool and exudate macrophages (ExMa) phenotypes. **A.** Represents the percentage of rAM, the **black** bar represents recipient (CD45.1) and **blue** bar represents the donor (CD45.2) rAM. **B.** Represents the phenotype of ExMa, the **green** bar represents M2 and **red** bar represents M1 phenotype of donor (CD45.2) ExMa, the **grey** bar represents the M1 and **black** bar represents M2 phenotype of recipient (CD45.1) ExMa . Irradiated but uninfected mice were used as controls in all the above mentioned time points in parallel. Bar graphs show means ± SD of 5n/group in all the mentioned time points pi.

4.5 Effect of M1 vs. M2ExMa adoptive transfer on IAV induced ALI in CCR2-/- mice

To investigate the functional capacity of M1 vs. M2ExMa in IAV induced ALI, wt mice with CD45.1 phenotype were infected with PR8 and M1 and M2ExMa were flow sorted from infected animals at D7pi and D21pi, respectively. Flow sorted M1 and M2ExMa (50,000 cells) were transferred orotracheally to IAV infected CCR2-/- mice (defective in CCR2/CCL2 dependent exudate macrophage recruitment) on D3pi. Alveolar macrophage quantification in adoptively transferred (CCR2-/-) mice at D7pi revealed significantly higher rAM numbers in M2ExMa transferred (M2T) mice when compared to the un-transferred (UT) or M1ExMa transferred (M1T) animals. To evaluate whether the increased

rAM numbers in the M2T group was due to increased rAM proliferation the rAM proliferation rate at D7pi was measured after Ki67 staining by flow cytometry. M2T transferred mice showed no significant increase of rAM proliferation compared to UT or M1T animals, indicating that, the increased rAM numbers in M2T animals were not due to increased local rAM proliferation at the analyzed time point but may rather reflect reduced rAM loss in M2T animals.

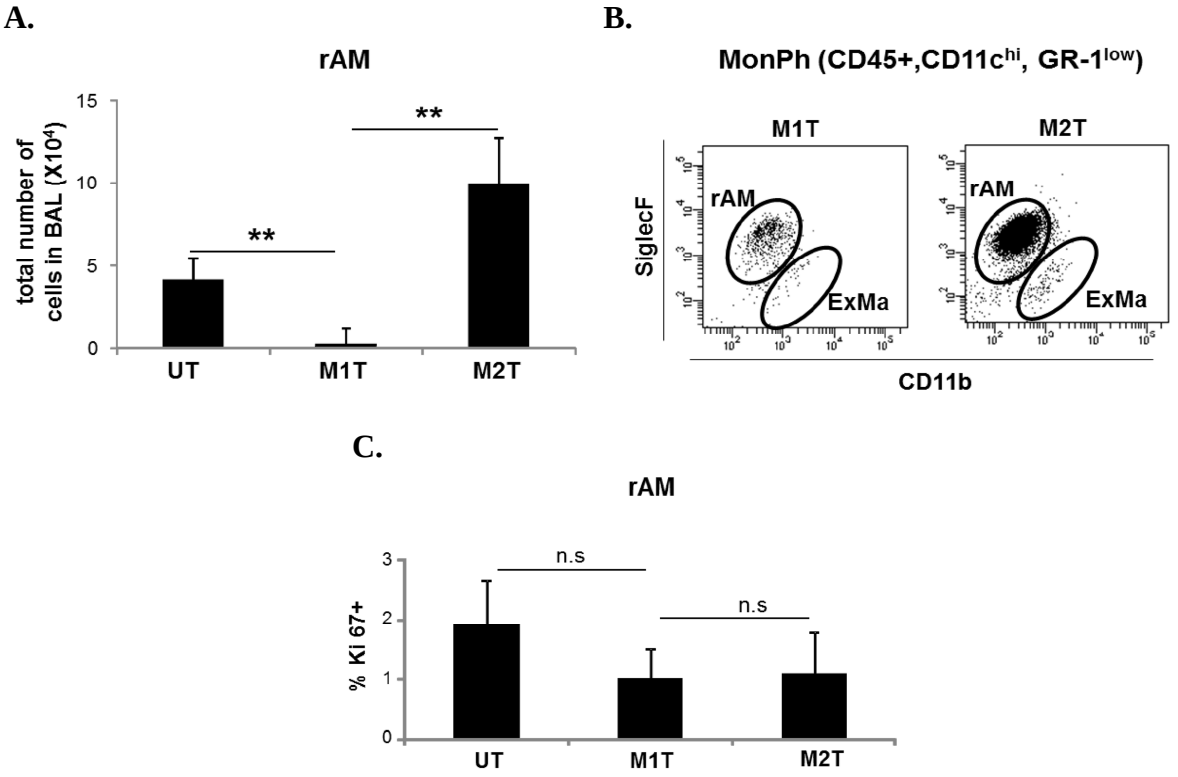

Figure 4-8 Preservation of rAM by adoptively transferred M2ExMa in IAV infected CCR2-/- mice. Flow sorted M1 (obtained at D7pi) and M2 exudate macrophages (ExMa) (obtained at D21pi) from the bronchoalveolar lavage (BAL) of IAV infected wt mice were transferred into IAV infected CCR2-/- mice at D3pi and at D7pi. The resident alveolar macrophages (rAM) population of un-transferred (UT), M1ExMa transferred (M1T) and M2ExMa transferred (M2T) groups was analyzed. **A.** The bar graph represents the absolute numbers of flow cytometrically identified rAM in BAL of M1T, M2T and UT groups. **B.** Represents dot plot of mononuclear phagocytes (MonPh- $CD45^{+}$, $CD11c^{hi}$, $GR\text{-}1^{low}$) gated for rAM ($SiglecF^{hi}$ and $CD11b^{low}$) from M1T and M2T animals showing the preservation of the rAM pool in M2T group**. C.** The bar graph represents the percentage of Ki67 positive rAM in UT, M1T and M2T mice analyzed by flow cytometry. Bar graphs show means ± SD of (A) 10n; (C) 3n in M1T and M2T groups, 4n in all UT groups. *p<0.05; **p<0.01; ***p<0.001.

In addition to the increased rAM numbers, M2T animals showed significantly less barrier FITC-albumin leakage when compared to M1T mice (Fig. 4-9 A). Alveolar leakage in UT CCR2-/- is known to be low due to lack of exudate macrophage recruitment. Moreover, in M2T animals the AEC proliferation rate determined by Ki67 staining was significantly increased when compared to UT or M1T mice (Fig. 4-9 B). These data demonstrate that M2ExMa transfer to CCR2-/- mice attenuates IAV induced ALI compared to M1ExMa

transfer, suggesting a differential functional repertoire of M2ExMa vs. M1ExMa in IAV induced ALI.

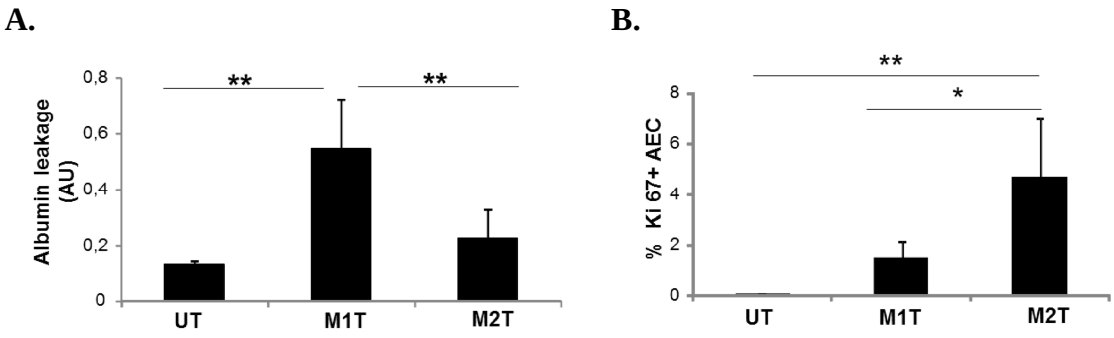

Figure 4-9 Adoptively transferred M2ExMa attenuate alveolar albumin leakage compared to transferred M1ExMa and increased AEC proliferation in IAV infected CCR2-/- mice. Flow sorted M1 (D7pi) and M2 exudate macrophages (ExMa) (obtained from D21pi) from the bronchoalveolar lavage (BAL) of IAV infected wt mice were transferred to IAV infected CCR2-/- mice at D3pi and albumin leakage as well as AEC proliferation were analyzed at D7pi in un-transferred (UT), M1ExMa transferred (M1T) and M2ExMa transferred (M2T) animals. **A.** Alveolar albumin leakage analyzed in UT, M1T and M2T groups at D7pi after intravenous injection of FITC-labeled albumin and depicted as ratio of serum and BALF FITC-fluorescence in arbitrary units (AU). **B.** In lung homogenates of UT, M1T and M2T groups, AEC ($EpCam^+$) proliferation was analyzed by flow cytometry based on the Ki67 expression. Bar graphs show means ± SD of (A) 6n; (B) 10n in M1T and M2T group, 4n in all UT groups. *p<0.05; **p<0.01; ***p<0.001.

4.6 Transcriptome analysis of M1 and M2ExMa in mice with IAV induced ALI

Due to the functional diversity of M1 vs. M2ExMa demonstrated in adoptive transfer experiments, it was speculated that M2ExMa may provide factors and mediators which could be directly or indirectly involved in repair mechanisms. To investigate the gene expression pattern in M1 and M2ExMa and to determine key mediators of M2ExMa that are possibly involved in attenuating IAV induced ALI, a transcriptome analysis was performed on flow sorted M1 and M2ExMa derived from infected wt mice at D7pi and D21pi respectively. The relative gene expression of M2 compared to M1ExMa revealed that, among 3404 total expressed genes, 2291 showed an upregulation and 1113 genes were found to be downregulated. For subsequent analysis, the differentially expressed genes were divided into different categories, based on known phenotypic profiles and biological activities (Fig. 4-10). The genome-array confirmed the dichotomy of M1 and M2ExMa by showing differential expression of prototypic M1 vs M2 markers. In addition, M2ExMa showed increased gene expressions of pro-survival mediators (Fig. 4-10 B) and growth factors (Fig. 4-10 C).

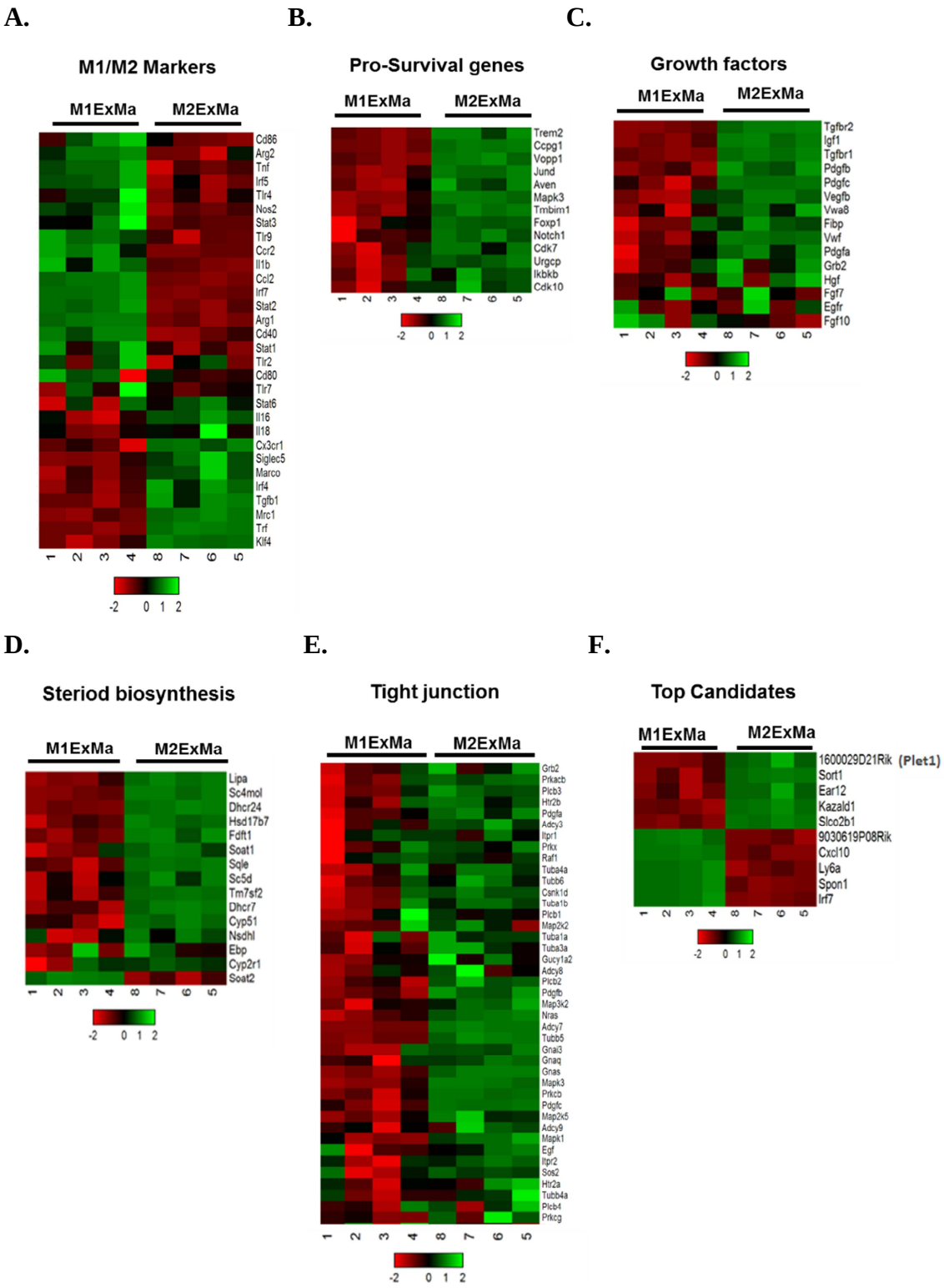

Figure 4-10 Heat maps showing gene expression patterns obtained by transcriptome analysis of M1 and M2ExMa in IAV induced lung injury. Flow sorted M1 (D7pi) and M2 (D21pi) exudate macrophages (ExMa) from bronchoalveolar lavage (BAL) of infected (PR8-250pfu) mice were subjected to transcriptome analysis as described in materials and methods. Heat maps show **A.** differentially expressed prototypic M1 and M2 markers, **B.** pro-survival genes highly expressed in M2ExMa compared to M1ExMa, **C.** growth factors highly expressed in M2ExMa compared to M1ExMa, **D.** molecules involved steroid biosynthesis highly expressed in M2ExMa, **E.** tight junction (TJ) regulating molecules highly expressed of in M2ExMa compared to M1ExMa and **F.** top 5 most highly expressed genes of M1and M2ExMa. The array data was developed from 4n samples of M1ExMa and M2 ExMa.

In addition, genes involved in steroid biosynthesis were also observed to be highly expressed in M2ExMa compared to M1ExMa (Fig. 4-10 D), which could be related to the release one of the initial stimuli (gluco-corticosteroids, prostaglandin E2 (PGE2)) to drive the M2 phenotype. There was a striking increase of genes potentially involved in formation of tight junctions (TJ) during macrophage/epithelium cross talk in M2ExMa compared to M1ExMa (Fig. 4-10 E). Some of the genes differentially expressed showed ≥ 6 fold increase or decrease in gene expression levels in M2ExMa compared with M1ExMa ($P < 0.001$) (Fig. 4-10 F). Among them, the gene (Placenta expressed transcript 1- Plet1) with the highest fold increase of 7.001 compared with M1ExMa *($p < 0.001$)* was selected for further evaluation.

4.7 Validation of highly upregulated genes of pro-survival mediators and growth factors in M1 and M2ExMa from IAV induced ALI

Some of the highly expressed genes on M1 and M2ExMa identified in the transcriptome screen were validated by the RT-PCR in flow sorted M1 and M2ExMa derived from IAV infected mice at D7pi and D21pi respectively. The pro-apoptotic and pro-inflammatory genes like TRAIL, IRF7, BAX and Daxx were found to be upregulated in M1ExMa compared to M2ExMa (Fig. 4-11 A). While PDGF-α, IGF-1 and EGF failed to show a significant increase, other growth factors like PDGF-β, FGF-7 and 10 were found to be significantly increased in M2ExMa compared to the M1ExMa (Fig. 4-11 B). Similarly, pro-survival genes like BCL2, Notch1, CcnD, TREM-2 and Vopp1 showed a significant increase in M2ExMa compared to M1ExMa (Fig. 4-11 C).

A.

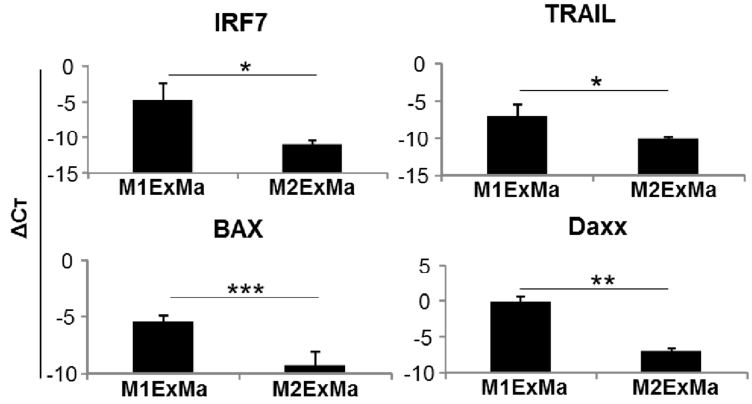

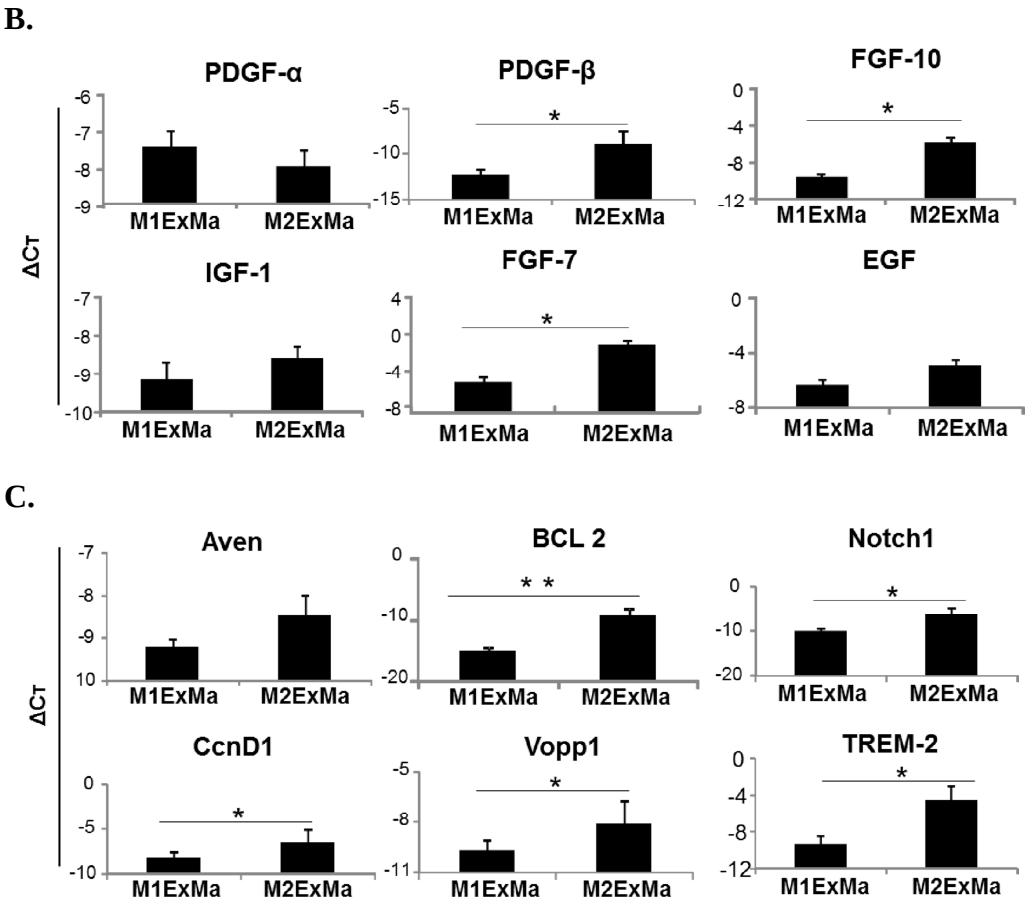

Figure 4-11 mRNA expression of growth factors and pro-survival mediators in flow sorted M1 and M2ExMa. Flow sorted M1 (D7pi) and M2 (D21pi) exudate macrophages (ExMa) from bronchoalveolar lavage (BAL) of infected (PR8-250pfu) mice were processed for RT-PCR analysis. The Bar graph represents the **A.** mRNA expression of highly upregulated genes on M1ExMagrowth factors (PDGF-α, PDGF-β, FGF-10, IGF-1, FGF-7, and EGF) and **B.** pro-survival mediators (Aven, BCL2, Notch1, CcnD1, Vopp1 and TREM-2) in M1 and M2 ExMa. The mRNA analysis on M1 and M2ExMa genes is presented as ΔCT relative expression normalized to β-actin. The Bar graphs represent means ± SD of 3 independent experiments. *p<0.05; **p<0.01; ***p<0.001. PDGF, platelet-derived growth factor; FGF, fibroblast growth factors; IGF, insulin-like growth factor; EGF, epidermal growth factor; Aven, apoptosis, caspase activation inhibitor; BCL, B-cell lymphoma; CcnD, cyclin-D; Vopp, vesicular, overexpressed in cancer, prosurvival protein 1; TREM-2, Triggering receptor expressed on myeloid cells 2; IRF7, Interferon regulatory factor 7; TRAIL, TNF-related apoptosis-inducing ligand; BAX, Bcl-2-associated X protein; Daxx, Death domain-associated protein 6.

When the gene (Plet1) with highest fold increase in the transcriptome screen was validated by RT-PCR in flow sorted M1 and M2ExMa derived from IAV infected mice at D7pi, D14pi and D21pi. M2ExMa were found to express significantly increased Plet1 mRNA levels when compared to M1ExMa (Fig. 4-12)

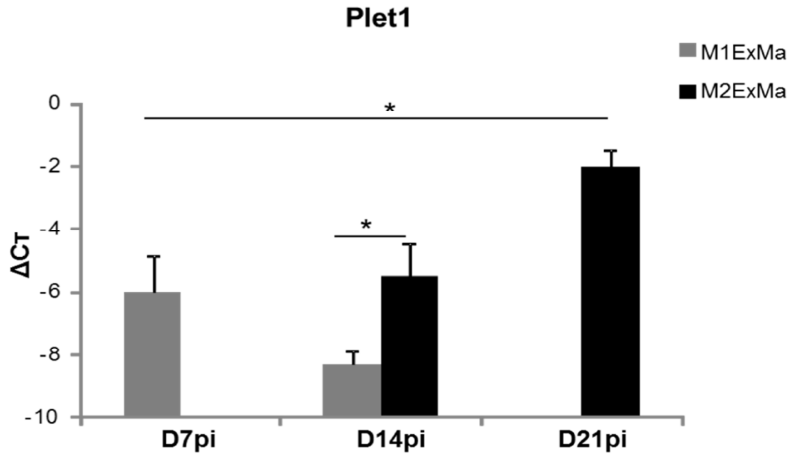

Figure 4-12 High mRNA expression of Plet1 in flow sorted M2ExMa. mRNA expression of Plet1 in flow sorted M1 and M2 exudate macrophages (ExMa) obtained from mice at D7pi, D14pi and D21pi were analyzed by RT-PCR. The mRNA analysis of Plet1 in M1 and M2ExMa was performed with ΔCT relative expression normalized to β-actin. Bar graphs represent means ± SD of 3 independent experiments. *p<0.05; **p<0.01; ***p<0.001.

4.8 Evaluation of the protective effect of M2ExMa derived Plet1 in IAV induced ALI

The genome array screen (Fig 4-10 F) and the upregulation of Plet1 mRNA in M2ExMa confirmed by RT-PCR (4-12) suggested M2ExMa derived Plet1 as a potential candidate for the observed protective effects, when M2ExMa were adoptively transferred (orotracheally) in IAV induced ALI (Fig. 4-8, 4-9). Therefore, to evaluate the protective effect of M2ExMa derived Plet1 in the IAV induced ALI, M2ExMa were flow sorted from IAV infected wt (CD45.1 phenotype) mice at D21pi and adoptively transferred via orotracheal application along with 5µg of anti-Plet1 antibody (M2-ab) or with 5µg IgG isotype control (M2-iso) into IAV infected CCR2-/- mice (45.2 phenotype) at D3pi. The number of rAM was analyzed at D7pi in the M2-ab and M2-iso groups. The results showed significant increased numbers of rAM in the M2-iso group compared to the M2-ab group (Fig. 4-13), which indicates that M2ExMa derived Plet1 is involved in preserving the rAM pool during IAV induced ALI.

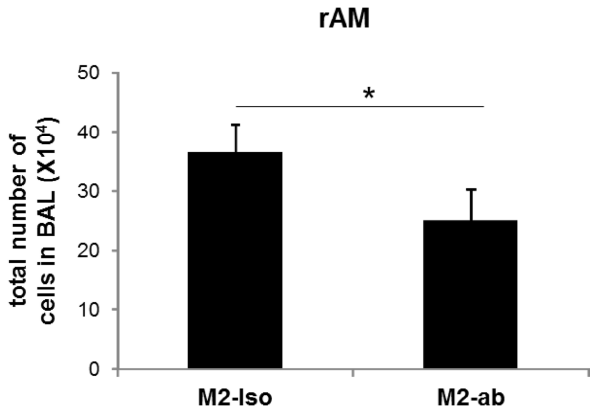

Figure 4-13 Effect of Plet1 inhibition by neutralizing antibody on the rAM pool size after adoptive transfer by of M2ExMa IAV infected CCR2-/- mice. Flow sorted M2 exudate macrophages (ExMa) (obtained from D21pi) from the bronchoalveolar lavage (BAL) of PR8 (250pfu) infected wt mice were transferred along with the anti-Plet1 antibody (M2-ab) or IgG isotype (M2-iso) orotracheally into PR8 (250pfu) infected CCR2-/- mice at D3pi. Bar graphs represent the total number of the resident alveolar macrophages (rAM) in BAL at D7pi of M2-iso and M2-ab groups. Bar graph show means ± SD of 3n in each group.

In addition, alveolar albumin leakage analysis of these mice (M2-iso and M2-ab groups) at D7pi, showed a significant decrease in albumin leakage in the M2-iso group when compared with the M2-ab group (Fig. 4-14). Thus confirming the protective role of M2ExMa derived Plet1 on lung barrier function in the adoptive transfer model

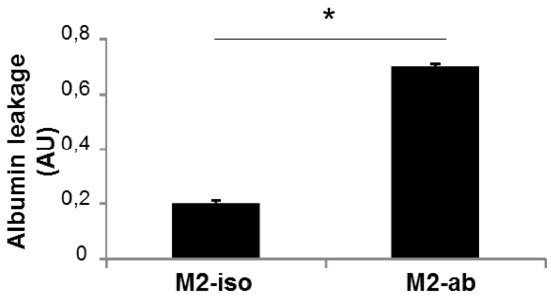

Figure 4-14 Plet1 inhibition by neutralizing antibody abolished the attenuating effect on alveolar albumin leakage of M2ExMa transferred into IAV infected CCR2-/- mice. Alveolar albumin leakage was analyzed in M2-iso and M2-ab groups at D7pi by intravenous injection of FITC-labelled albumin and was depicted as ratio of serum and bronchoalveolar lavage fluid (BALF) FITC- fluorescence in arbitrary units (AU). Bar graphs show means ± SD of minimum 3n each in M2-iso and M2-ab group.

To evaluate the effect of M2ExMa derived Plet1 on TJ proteins of AEC in IAV induced ALI, the lungs were harvested from M2-iso and M2-ab groups and AEC from lungs were flow sorted. The mRNA expression of TJ proteins in the flow sorted AEC (Fig. 4-15 A) from M2-iso and M2-ab groups were analyzed by RT-PCR. The mRNA levels of TJ proteins such as ZO-1, Claudin-1 and Occludin were found to be significantly higher in the M2-iso group compared to the M2-ab group at D7pi of PR8 infection.

A.

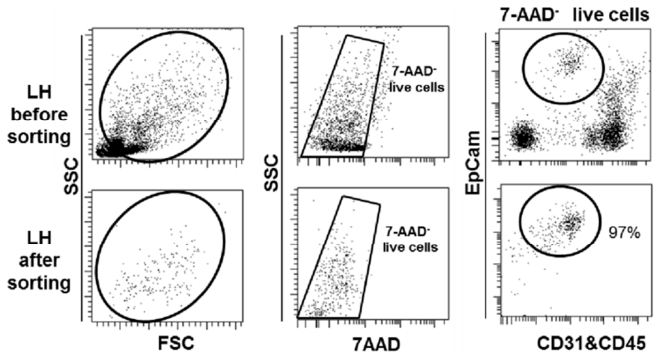

B.

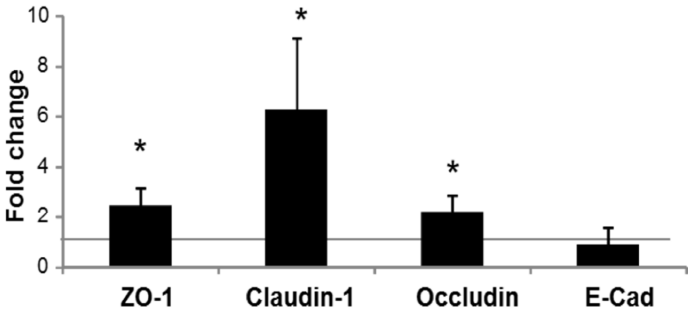

Figure 4-15 Effect of Plet1 inhibition by neutralizing antibody on AEC TJ molecule gene expression after adoptive transfer by of M2ExMa into IAV infected CCR2-/- mice. A. Representative flow cytometry gating for AEC sorting of lung homogenates (LH) of the superior right lobe of mice from M2-iso and M2-ab treated groups. The upper panel (LH before sorting) shows representative dot plots before sorting, the lower panel (LH after sorting) represents dot plots after sorting showing that live cells (7-AAD$^-$) AEC (CD31$^-$, 45$^-$, EpCam$^+$) were sorted with a purity of ≥ 97%. **B.** mRNA expression of ZO-1, E-Cadherin (E-Cad), Occludin and Claudin-1 in AEC derived from the M2-iso vs. M2-ab group. The mRNA analysis of genes encoding TJ proteins were normalized by relative expression normalized to β-actin and are presented as fold change ($2^{\Delta\Delta Ct}$) of the M2-iso to M2-ab group. Bar graphs show means ± SD of minimum 3n each in M2-iso and M2-ab group.

To investigate the effect of M2ExMa derived Plet1 on AEC proliferation and apoptosis, AEC proliferation apoptosis analyzed by Ki67 and annexin V staining were compared in lung homogenates of M2-iso and M2-ab groups. The M2-iso group showed significantly increased Ki67 expressing AEC proportions compared to the M2-ab group (Fig. 4-16 A) whereas the proportion of Annexin V stained AEC was significantly decreased in the M2-iso group (Fig. 4-16 B) indicating that, the M2ExMa derived Plet1 is involved in enhancing the proliferation and attenuating apoptosis of AEC during IAV induced ALI in the adoptive transfer model.

A. **B.**

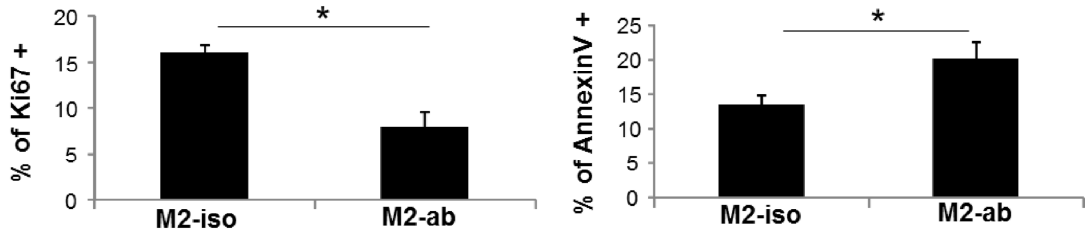

Figure 4-16 Effect of Plet1 inhibition by neutralizing antibody on AEC proliferation and apoptosis after adoptive transfer by of M2ExMa into IAV infected CCR2-/- mice. Lung homogenates from M2-iso and M2-ab groups obtained at D7pi were gated for alveolar epithelial (AEC- EpCam$^+$) by flow cytometry analysis. **A.** Bar graphs represent the percentage of AEC stained for Ki67. **B.** Bar graph represents the percentage of apoptotic AEC based on Annexin V expression. Bar graphs show means ± SD of minimum 3n each in M2-iso and M2-ab group.

To evaluate the role of M2ExMa derived Plet1 in resolving the lung inflammation after IAV induced ALI, the total number of PMNs and lymphocytes in the BAL were analyzed by flow cytometry (Fig. 4-17 A, B). The results showed a significant decrease in the number of both PMNs and lymphocytes in the M2-iso group compared to M2-ab group. Additionally, hematoxylin and eosin (H&E) stained lung sections from M2-iso group showed largely reduced infiltrations in the peri-bronchiolar space compared to the M2-ab group (4-17 C). These results suggest that the M2ExMa derived Plet1 has a role in attenuating inflammatory responses in IAV induced ALI.

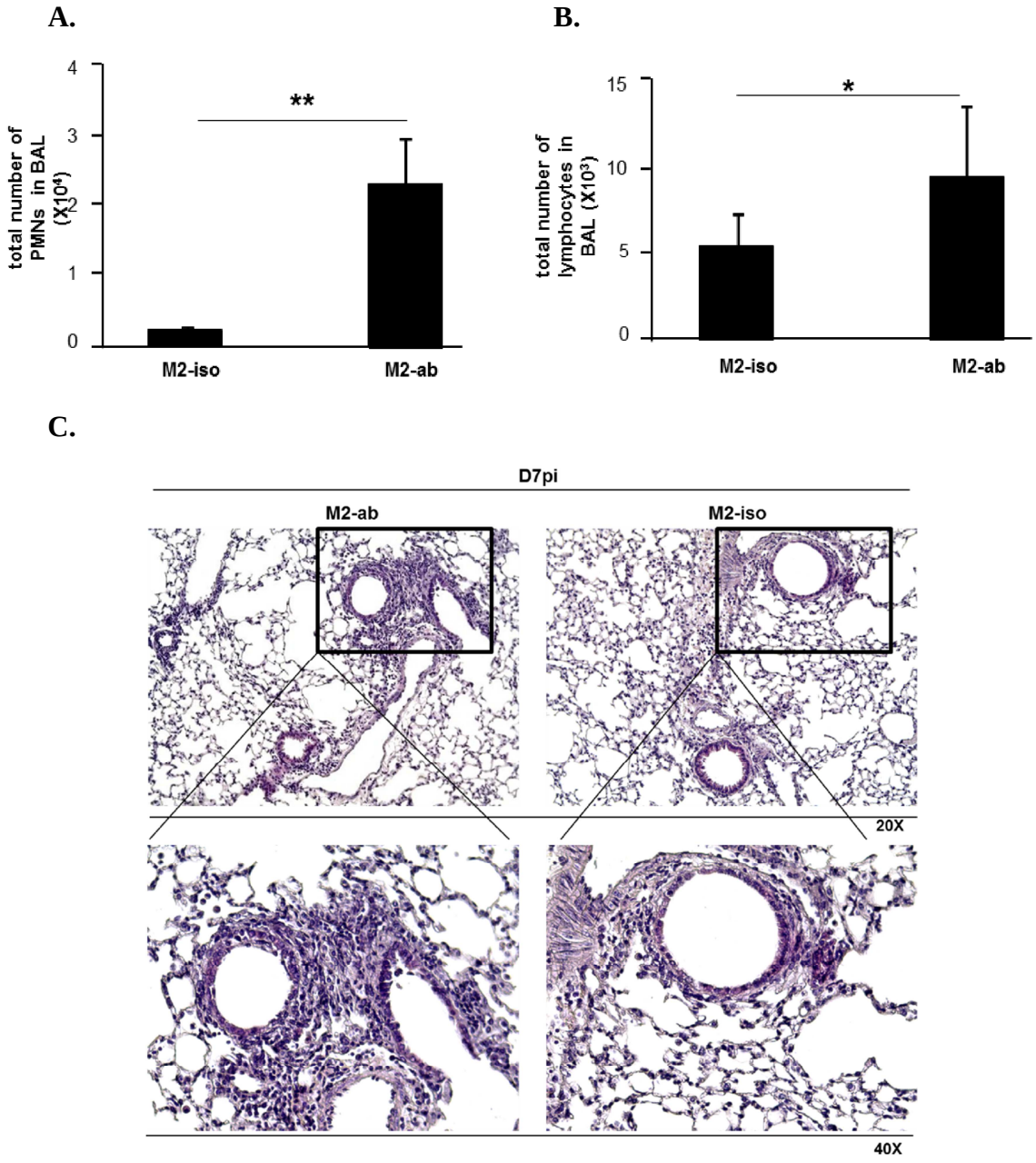

Figure 4-17 Effect of Plet1 inhibition by neutralizing antibody on inflammatory cell infiltration after adoptive transfer of M2ExMa into IAV infected CCR2-/- mice. The bar graphs represent the number of **A.** PMNs and **B.** lymphocytes determined by flow cytometry analysis in bronchoalveolar lavage (BAL) obtained at D7pi from CCR2-/- mice, adoptively transferred with anti-Plet1 antibody+M2ExMa (M2-ab) or IgG-isotype antibody+M2ExMa (M2-iso) at D3pi. Bar graphs show means ± SD of 3n in the M2-iso and M2-ab group. *p<0.05; *p<0.01; *p<0.001. **C.** Representative lung sections from M2-iso and M2-ab groups stained with hematoxylin and eosin (H&E) on D7pi. Boxes represent regions magnified in the lower panel. 3n mice were used in each group.

4.9 Effect of Plet1 on primary mAEC infected with IAV

Plet1 was predicted to be co-expressed and functionally related to TJ proteins (211) that are associated with the alveolar epithelial barrier. In addition, Plet1 was shown to be highly expressed in M2ExMa (Fig. 4-10 F and 4-12), suggesting a role of Plet1 in maintaining the epithelial barrier function in IAV induced ALI. To investigate the effect of Plet1 on trans-epithelial resistance (TER) and TJ proteins, primary murine AEC (mAEC) were isolated from uninfected wt mice, cultured in transwell plates and infected *in vitro* with PR8 (0.5 MOI) or mock infected and treated with recombinant (r)Plet1 (20ng/ml) or control buffer. TER was measured in transwells at different time points post infection (0, 4, 6, 8, 12, 16, 24 and 30hr). TER dropped in mAEC after 4hrs post infection, but addition of rPlet1 to infected mAEC significantly attenuated TER reduction at 6, 8, 12, 16, 24 and 30hr post infection compared to the untreated IAV infected mAEC (Fig. 4-18) indicating a protective effect of Plet1 on epithelial barrier integrity of infected mAEC *in vitro.*

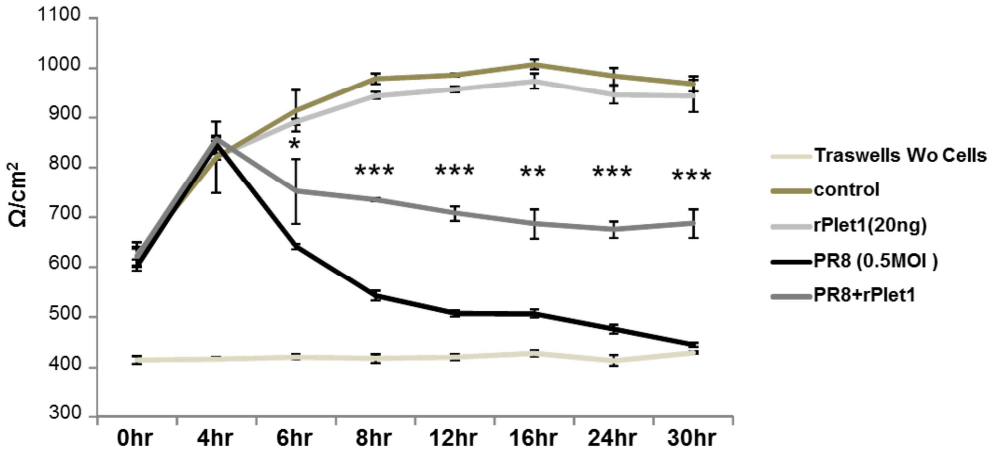

Figure 4-18 rPlet1 improves TER in primary mAEC after IAV infection *in vitro* in a transwell model. Primary murine alveolar epithelial cells (mAEC) were cultured on transwells (0.3×10^5 cells/insert). After 3-5 days, when the trans epithelial resistance (TER) reached a plateau of ≥600Ω /cm^2, confluent mAEC were mock (control) or PR8 infected and left untreated (control, PR8(0.5 MOI) and treated with rPlet1 (20ng/ml) (PR8+rPlet1). TER was measured at different time points post infection (0, 4, 6, 8, 12, 16, 24, 30hrs). Baseline TER is determined in transwells without mAEC (Transwells wo cells). Results are the means ±SD of at least 3 independent experiments. *p<0.05; **p<0.01; ***p<0.001.

To determine whether the protective effect of rPlet1 on TER in IAV infected cells was related to preserved TJ function, we studied the effect of rPlet1 on TJ proteins such as ZO-1, claudin1, occuludin and E-cadherin in IAV infected primary mAEC. Mock or PR8 infected AEC either rPlet1 treated or untreated were collected from transwells at 0, 4 and 12hrs post infection and mRNA was extracted and processed for RT-PCR analysis. rPlet1 treatment significantly increased mRNA expression of ZO-1 and E-cadherin at 12hrs, and of Claudin-1 and Occludin at 4hrs pi compared to untreated IV-infected AEC, suggesting that Plet1 induced the expression of TJ proteins contributes to maintaining TER of primary mAEC after IAV infection *in vitro.*

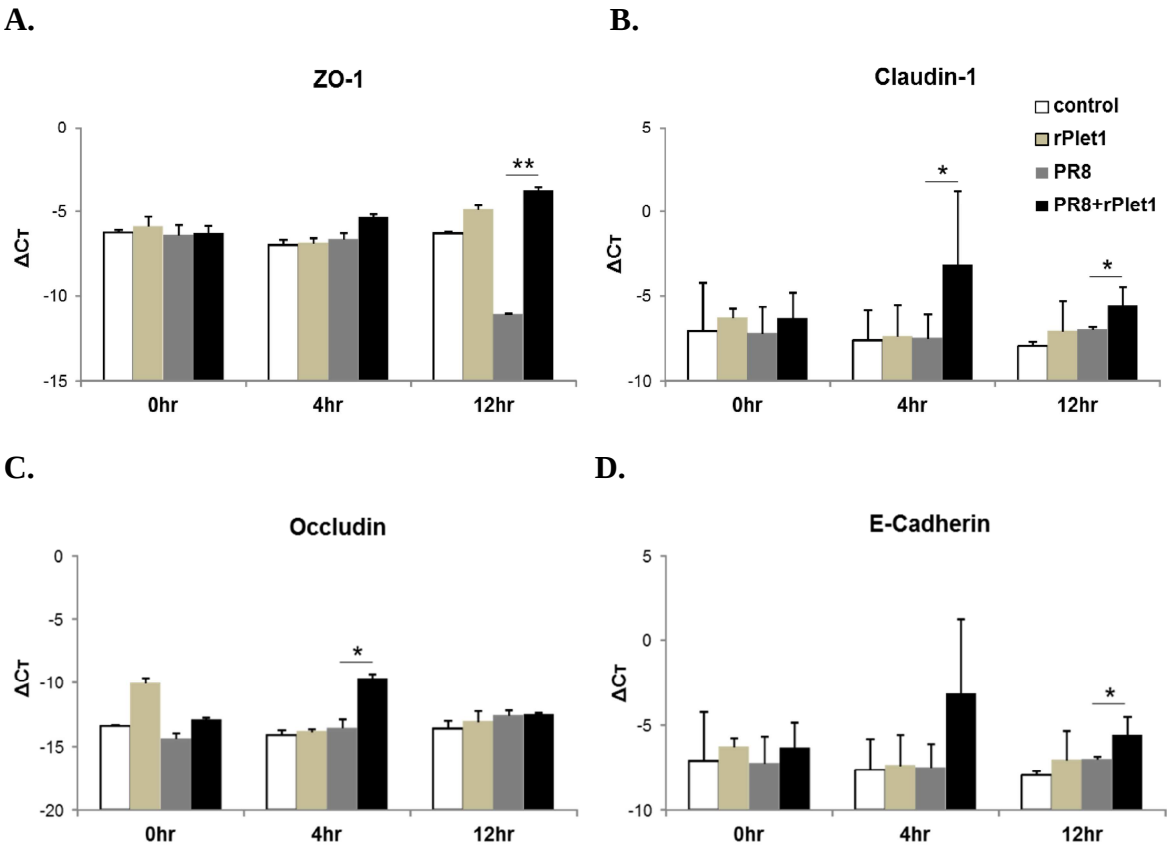

Figure 4-19 rPlet1 upregulated the mRNA expression of TJ proteins in primary mAEC after IAV infection *in vitro*. Bar graphs represents mock infected (control) and treated with rPlet1- 20ng/ml (rPlet1) or PR8 infected (MOI 0.5; PR8) and treated with rPlet1 (PR8+rPlet1) mAEC. mRNA expression of **A.** ZO-1 **B.** Claudin-1 **C.** Occludin **D.** E-Cadherin at different time points post infection (PR8- MOI 0.5). The mRNA analysis on ZO-1, Claudin-1, Occludin and E-cadherin was performed with ΔCT relative expression normalized to β-actin. Results are represented as the mean ±SD of at least 3 independent experiments. *p<0.05; **p<0.01; ***p<0.001.

To investigate the effect of rPlet1 on the membrane expression of TJ protein ZO-1, cultured mAEC were mock infected or infected with PR8 (MOI 0.5) and treated with or without rPlet1 (20ng/ml). Immunofluorescence staining with anti-ZO-1 antibodies showed increased ZO-1 surface expression in mAEC at 12hrs post infection after rPlet1 treatment compared to un-treated infected mAEC.

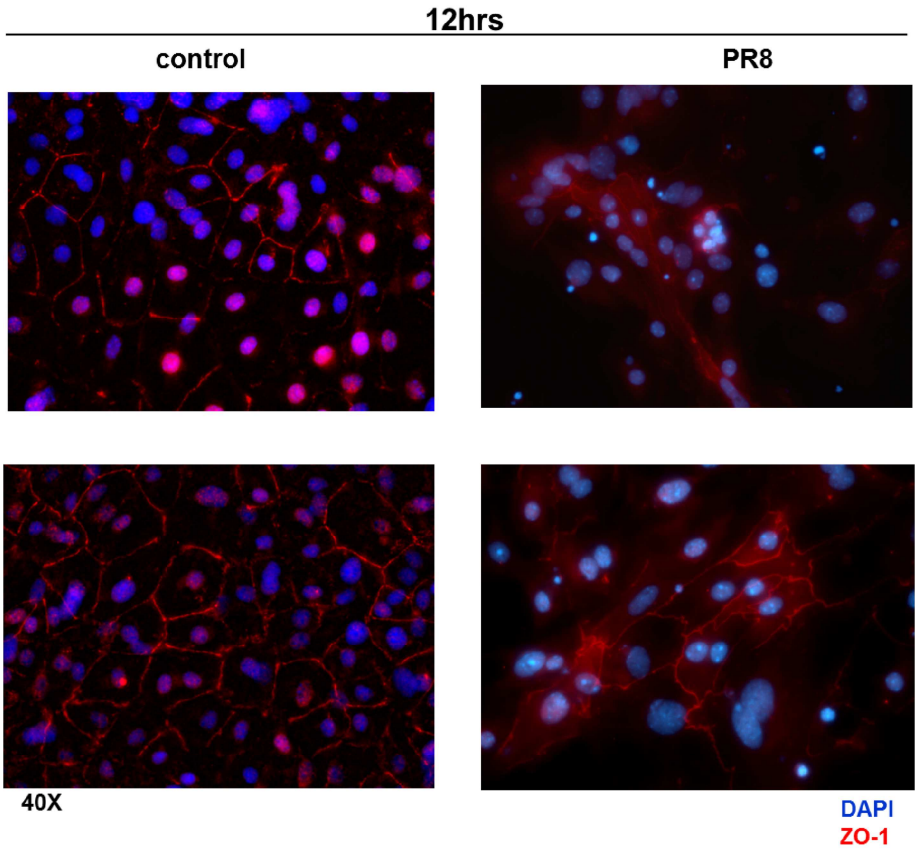

Figure 4-20 rPlet1 increased the expression of TJ protein ZO-1 in primary mAEC after IAV infection *in vitro*. mAEC were mock infected (control) and treated with rPlet1- 20ng/ml (rPlet1) or PR8 infected (MOI 0.5; PR8) and treated with rPlet1 (PR8+rPlet1). The cells were then fixed at 12hrs post infection and stained with ZO-1. The nuclei were stained with DAPI. Images represent 3 independent experiments.

To elucidate the effect of Plet1 on apoptosis and viral replication, caspase 3 activation and expression of IAV nucleoprotein (NP) were analyzed in mock or PR8 (MOI 0.5) infected mAEC treated with rPlet1 (20ng/ml) or left untreated, respectively. The cells were fixed at 6 and 12hrs post infection and analyzed by immunofluroscence for caspase 3 and IAV nucleoprotein (NP). Expression of active caspase 3 (Fig. 4-16 A) and NP (Fig. 4-16 B) was found to be reduced in rPlet1 treated mAEC at 6 and 12hrs post infection indicating an anti-apoptoic effect of Plet1 in IAV infected mAEC associated with reduced IAV replication.

A.

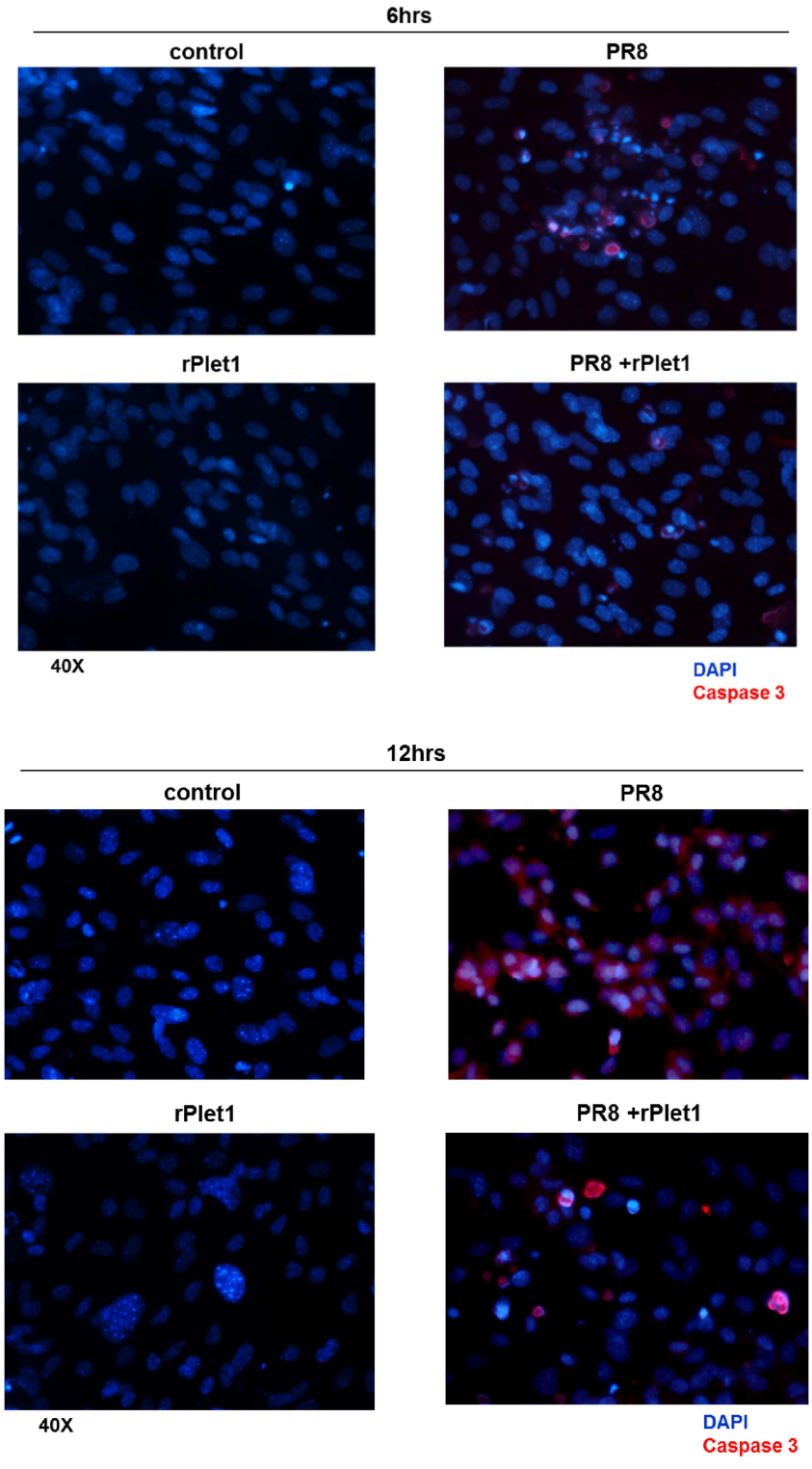
6hrs
control
PR8
rPlet1
PR8 +rPlet1
40X
DAPI
Caspase 3
12hrs
control
PR8
rPlet1
PR8 +rPlet1
40X
DAPI
Caspase 3

B.

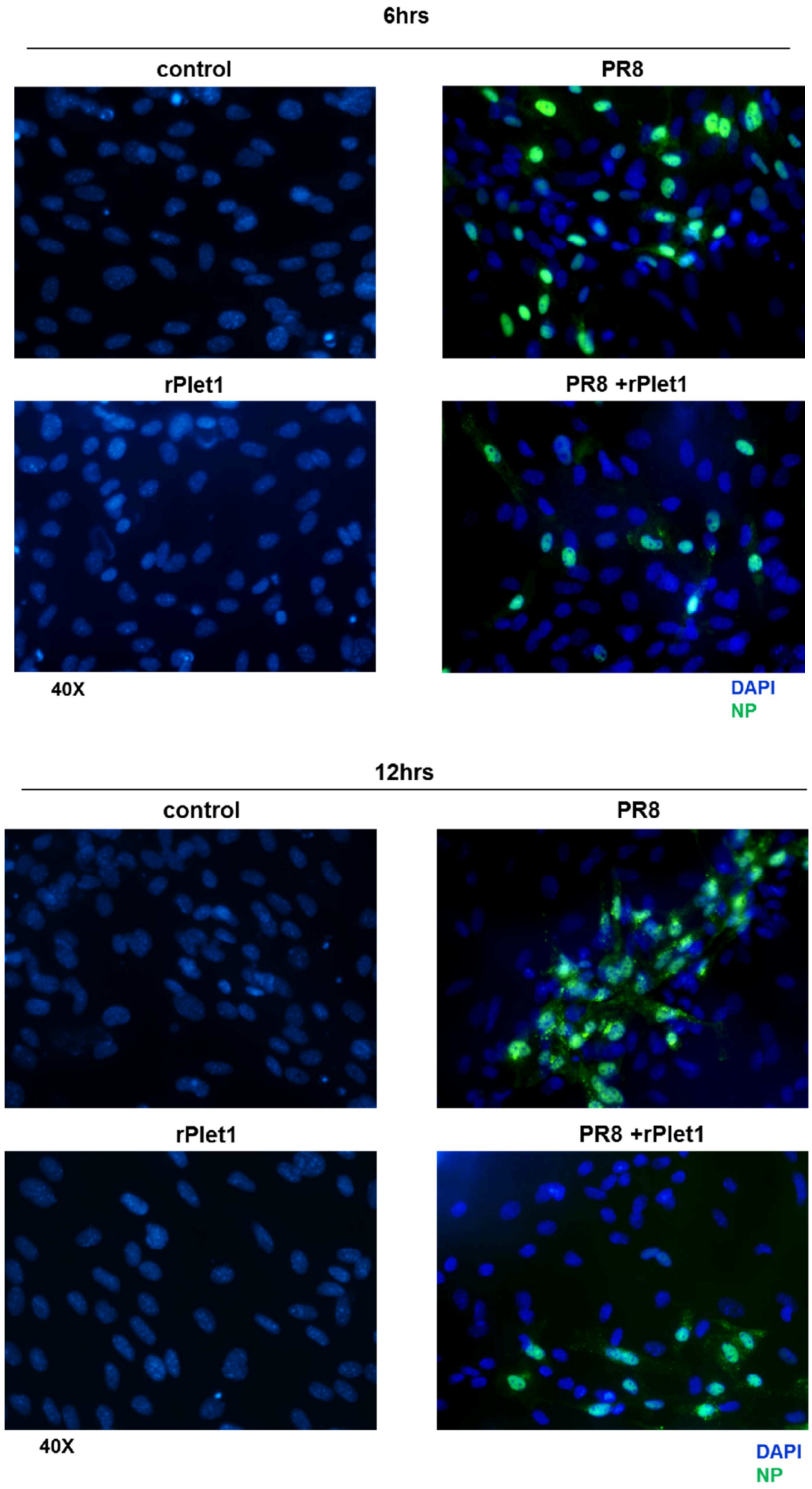

Figure 4-21 rPlet1 treatment reduces apoptosis and viral replication in primary mAEC after IAV infection *in vitro*. Murine alveolar epithelial cells (mAEC) were mock infected without (control) and with addition of rPlet1- 20ng/ml (rPlet1) or PR8 (MOI 0.5) infected without (PR8) and with addition rPlet1 (PR8+rPlet1). Cells were fixed at 6 and 12hrs post infection and stained with **A**. rabbit anti-mouse active caspase3 antibody and phycoerythrin (PE) labelled secondary anti rabbit Ig antibody and **B.** mouse monoclonal anti- NP antibody labelled with Fluorescein isothiocyanate (FITC). The images are representative of 3 independent experiments. IAV NP, influenza A virus nucleo-protein.

4.10 Therapeutic intervention with rPlet1 in IVA induced ALI

The protective effects of M2ExMa (section 4-5) adoptive transfer were largely abolished when the M2ExMa were transferred (orotracheally) along with neutralizing anti-Plet1 antibody *in vivo* (section 4-7). In addition, rPlet1 treatment of PR8 infected mAEC increased the TJ proteins expression, improved TER, and reduced apoptosis and IAV replication *in vitro* (Fig. 4-19, 20, 21). These results identified Plet1 as promising candidate for therapeutic intervention in IAV induced ALI.

To determine the effect of rPlet1 in IAV induced ALI *in vivo,* wt mice were infected with PR8 (250pfu) and PBS or rPlet1 (5µg) in total volume of 60µl were delivered orotracheally on D3pi. The total number of rAM in BAL was analyzed at D7pi of both PBS and rPlet1 treated groups by flow cytometry. The rPlet1 treated group showed a tendency of increase in number of rAM compared to PBS treated group (Fig. 4-22).

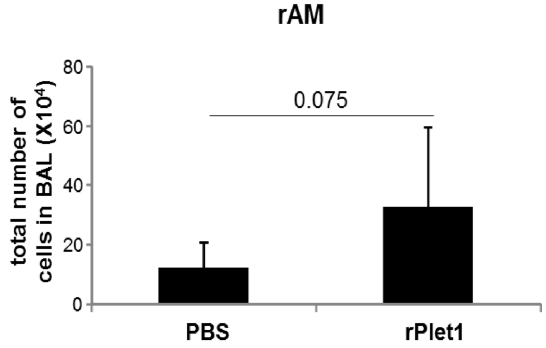

Figure 4-22 rPlet1 showed a trend of increase in total number of rAM in IAV infected mice. A. The bar graph represents the total number of the resident alveolar macrophages (rAM) in bronchoalveolar lavage (BAL) at D7pi of PBS or rPlet1 (5µg) treated groups by flow cytometry analysis. The bar graphs show means ± SD of 8n each in PBS and rPlet1 treated group.

Alveolar albumin leakage analysis of PBS and rPlet1 treated groups at D7pi, showed a significant decrease in albumin leakage in the rPlet1 treated group compared to the PBS treated group (Fig. 4-23)

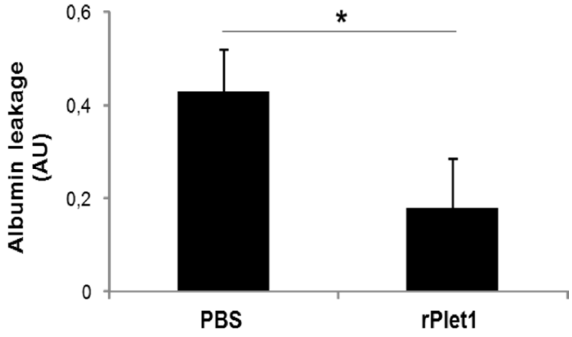

Figure 4-23 rPlet1 treatment reduced alveolar albumin leakage in the IAV infected mice. Alveolar albumin leakage was analyzed in PBS and rPlet1 treated groups at D7pi by intravenous injection of FITC-labeled albumin and is depicted as ratio of serum and BALF FITC- fluorescence in arbitrary units (AU). Bar graphs show means ± SD of minimum 6n each in PBS and rPlet1 treated group.

In addition, AEC proliferation and apoptosis in the lung homogenates of PR8 (250pfu) infected and rPlet1 (5µg) or PBS treated mice was analyzed by flow cytometry. Animals treated with rPlet1animals showed a significantly increased proportion of Ki67 stained $EpCam^{+}$ AEC and a reduced proportion of annexinV stained AEC indicating a pro-proliferative and anti-apoptotic effect of orotracheal Plet1 application on AEC in IAV infected mice.

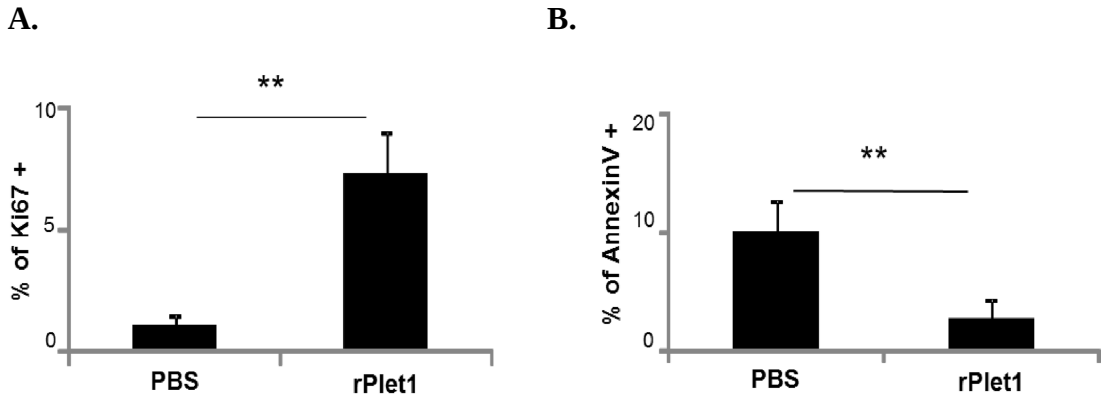

Figure 4-24 rPlet1 increased the proliferation and decreased the apoptosis of AEC in IAV induced ALI. Alveolar epithelial cells (AEC-$EpCam^{+}$) gated by flow cytometry analysis from lung homogenates from PBS and rPlet1 (5µg) treated groups on D7pi were analyzed for **A.** proliferation based on the expression of Ki67 and **B.** apoptosis based on the expression of Annexin V. Bar graph represents the percentage of AEC Bar graphs show means ± SD of minimum 6n each in PBS and rPlet1 treated group.

To evaluate the effect of rPlet1 treatment on TJ proteins of AEC in mice infected with PR8 (250pfu), the superior right lung lobes were harvested from PBS and rPlet1 treated groups and processed for single cell suspension and flow sorting of AEC (Fig. 4-18 A). Flow sorted AEC from PBS and rPlet1 treated groups were then analyzed by RT-PCR for mRNA expression of TJ proteins (Fig. 4-18 B). Levels of ZO-1 and Claudin1 mRNA were found to be significantly increased in the rPlet1 treated group compared to the PBS treated group at D7pi.

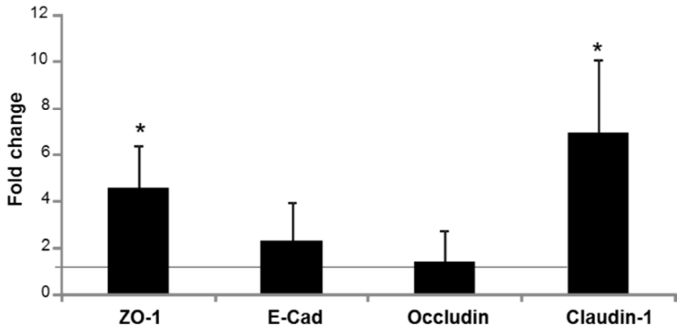

Figure 4-25 rPlet1 treatment increased mRNA expression of TJ proteins on flow sorted AEC from IAV infected mice. Bars represent the mRNA expression of TJ proteins (ZO-1, E-Cadherin (E-Cad), Occludin and Claudin-1) in flow sorted alveolar epithelial cells (AEC) from lung homogenates of PBS and rPlet1 (5µg) treated groups. The mRNA analysis on the genes of TJ proteins was normalized by relative expression normalized to β-actin and is presented as fold change ($2^{\Delta\Delta Ct}$) of the rPlet1 compared to PBS treated group. The Bar graphs represent means ± SD of minimum 6n each in PBS and rPlet1 treated group.

Anti-Plet1 antibody treatment diminished the anti-inflammatory effect of transferred M2ExMa in the adoptive transfer approach (Fig 4-17). Therefore, we investigated the effect of orotrachally delivered rPlet1 on resolving the lung inflammation in after IAV infected mice by analyzing the total number of PMNs and lymphocytes in the BAL by flow cytometry (Fig. 4-25 A, B). In addition, the lungs were harvested from PBS and rPlet1 treated groups and processed for H&E staining. Number of both PMNs and lymphocytes were found to be significant decreased in the rPlet1 treated group compared to the PBS treated group. Accordingly, H&E staining of the lung sections showed reduced cell infiltrations in the peri-bronchiolar space in the rPlet1 treated group compared to the PBS treated group (Fig. 4-25 C). These results demonstrate the anti-inflammatory effect of orotracheal rPlet1 treatment in IAV induced ALI.

A.

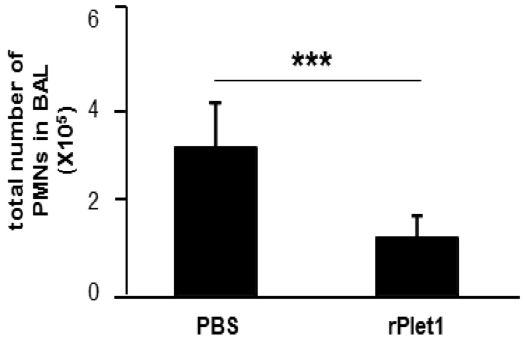

B.

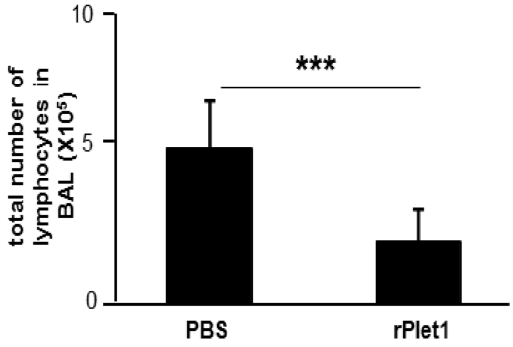

C.

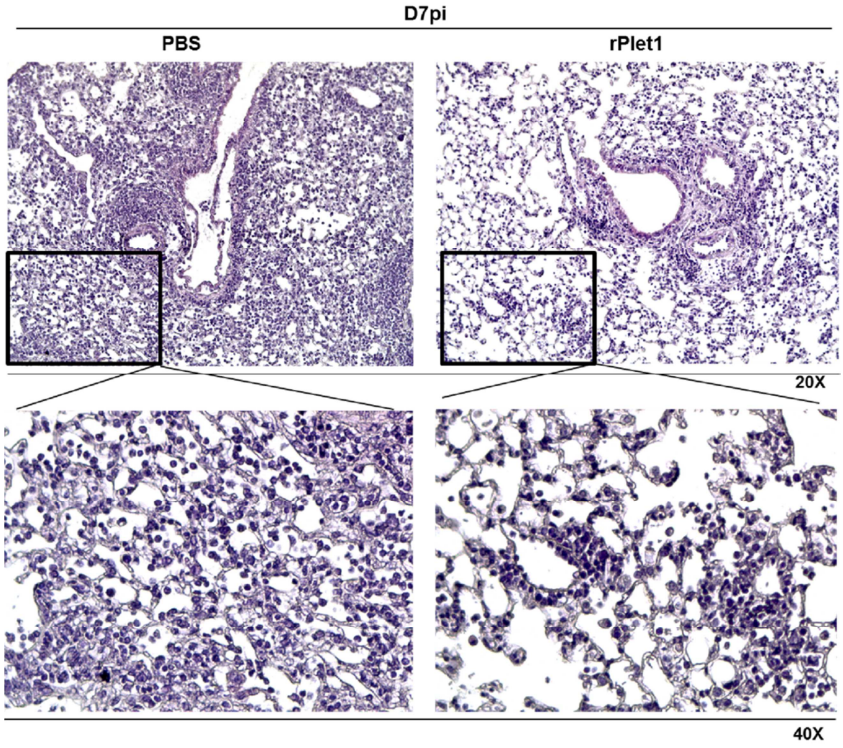

Figure 4-26 rPlet1 attenuate lung inflammation in IAV infected mice. The bar graph represents the number of **A.** PMNs and **B.** lymphocytes in bronchoalveolar lavage (BAL) on D7pi of PBS and rPlet1(5µg) by flow cytometry analysis. Bar graphs show means ± SD of 8n in PBS and rPlet1 treated group. *p<0.05; *p<0.01; *p<0.001. **C.** Lung sections stained with hematoxylin and eosin (H&E) from PBS and rPlet1 treated groups on D7pi. Boxes represent regions magnified in the lower panel. 8n mice were used in each group.

The effect of rPlet1 on the survival rates and their corresponding body weight loss during IVA induced ALI was investigated in the PR8 (500pfu) infected wt mice. The rPlet1 (5µg) or PBS was delivered orotracheally on D3pi and monitored daily twice for their physiological and clinical scores. Accordingly, the mice that received rPlet1 survived better with corresponding increase in the body weight compared to PBS received mice, which indicated that rPlet1 as a potential candidate that can reduce the outcome of mortality during IAV induced ALI (Figure 4-27 A, B)

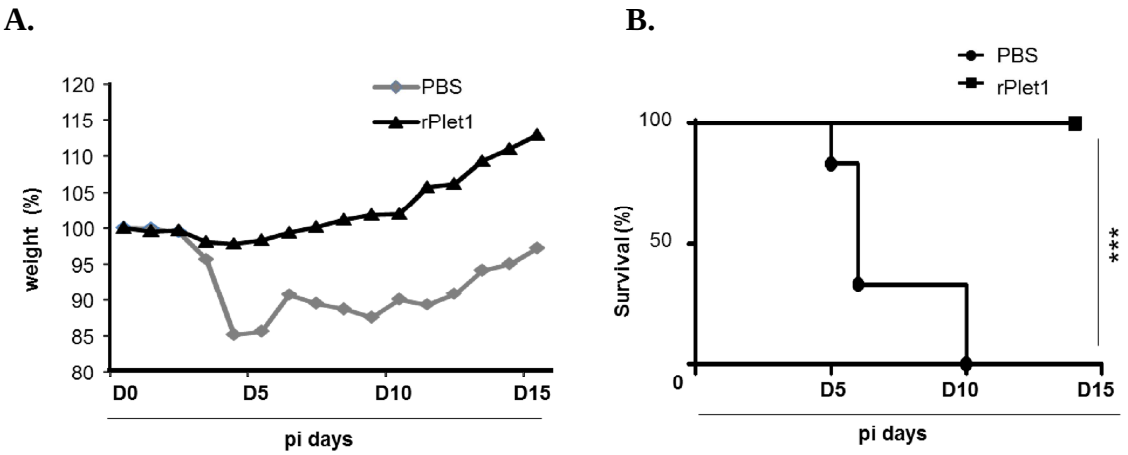

Figure 4-27 rPlet1 improved body weight and survival rate in IAV induced ALI. wt mice were infected with 500pfu PR8 and treated with PBS or rPlet1 (5µg) on D3pi by orotracheal administration. **A.** Body weight (%) of mice in PBS and rPlet1 group (10n in each group). **B.** Represents survival rates (%) of mice in PBS and rPlet1 group (Kaplan-Maier curve; 6n in each group). Mantel-Cox Chi square test was used to calculate the significance for survival rates *$P < 0.05$, ***$P < 0.0001$.

5. Discussion

The pulmonary immune system is constantly responding to pathogenic insult. Adequate immune responses are crucially dependent on distinct discrimination between non-pathogenic and pathogenic antigens in the lung. Pathogen sensing results in the development of acute inflammation which may lead to ALI/ARDS upon severe infection by lung pathogens such as IAV, or when pulmonary inflammation is not adequately controlled by anti-inflammatory and injury-resolving counter-mechanisms. Pulmonary macrophages are known to be crucially involved in balancing pro-inflammatory host defense mechanisms and anti-inflammatory responses with inflammation resolution and repair processes, in a well-coordinated action during the course of pneumonia, and therefore represent key players in orchestrating these processes in the alveolus (12, 13, 24).

Accumulating evidence suggests that, apart from their well-known role in phagocytosis and recognition of foreign antigens, alveolar macrophages are endowed with high functional plasticity allowing them to acquire different pro- or anti-inflammatory as well as tissue-reparative phenotypes during the course of inflammation, dependent on the signals they receive from surrounding cells or from the pathogen itself. The ability to integrate these various signals in the course of inflammation and to mount a differential response empowers the M2 polarized, alternatively activated macrophage to terminate and resolve alveolar inflammation in the later phases of ALI/ARDS and to tightly coordinate parenchymal repair processes that are essential for return to homeostasis (147, 189, 212, 213). Given that the injury specific signals derived from the local alveolar microenvironment are integrated to generate specific macrophage polarization patterns, it is hypothesized that different injuries (eg. pathogenic versus sterile inflammation; viral vs bacterial challenge, etc) generate unique macrophage polarization patterns at defined time points during lung inflammation or infection to serve the particular needs of the infected/inflamed alveolar niche. Previous work from our research group suggested that particularly the ExMa, in contrast to the tissue-resident macrophages revealed a broad functional plasticity (64, 130, 32). A better understanding of these processes would allow to selectively target macrophage pool for better host defense and accelerated lung repair to improve outcome of ALI/ARDS. However, a systemic approach to define these macrophage phenotypes, particularly during pneumonia-induced ALI *in vivo*, has not been established yet. Therefore, the first aim of the presented work was to develop a protocol to

distinguish pulmonary M1- versus M2ExMa in a time course-dependent manner during IAV infection *in vivo*.

5.1 Definition of M1 versus M2 polarization phenotypes of ExMa in IAV-induced ALI/ARDS by FACS reveals distinct gene expression profiles

To estimate M1 and M2 macrophage presence in the BALF of IAV-infected mice, a first approach was to isolate the total alveolar macrophage fraction by positive selection using a MACS technique allowed to isolate these cells to high purity using antibodies against the alveolar macrophage markers CD11c and SiglecF (214). Analysis of well-known M1 versus M2 marker expression by RT-PCR in the course of infection (D0 to D21pi), however, revealed that expression of these markers did not substantially change over time. These data suggested that the macrophage pool was not uniquely polarized towards a defined phenotype, but suggested simultaneous recruitment or presence of M1 and M2 macrophages in the alveolar air space. Also, many studies recently revealed that there is a notable difference between the rAM and the ExMa pool with respect to functional phenotypes and polarization capacity (215-217). Therefore, a multi-colour FACS protocol was used which allowed definition of alveolar (BALF) versus lung-interstitial (lung tissue) ExMa and rAM, respectively, and establishment of a gating strategy to define M1 versus M2 macrophage subsets in lungs of IAV infected mice over time. Established lineage markers for rAM ($CD45^{+}$,$GR\text{-}1^{-}$, $SiglecF^{hi}$, $CD11c^{hi}$, $CD11b^{low}$) and ExMa ($CD45^{+}$, $GR\text{-}1^{-}$, $SiglecF^{low}$, $CD11c^{hi}$, $CD11b^{hi}$) (64, 218) were used to define both alveolar and interstitial ExMa and rAM. To evaluate the efficient markers among different M1 (CD40, CD86, CD80, ICAM-1, iNOS, TNF-α) and M2 (CD71, CD163, CD206) markers, combined 8-colour flow cytometry approach including a dead cell exclusion marker were used (219-224). As a result, two M1 (CD86, CD40) and two M2 (CD71, CD206) markers were found to be differentially expressed particularly on the interstitial and alveolar ExMa population, whereas the rAM populations did not reveal phenotype plasticity, at least not with the markers used. As CD40 (M1) and CD206 (M2) were found to be the most robust antigens differentially expressed on the surface of the respective ExMa phenotype both in the interstitial and alveolar space, they were further used to analyse ExMa polarization profiles after IAV infection in mice over time. Of note, expression of various M1 and M2 phenotype associated genes was analyzed on macrophage phenotypes, flow sorted according to this gating strategy on D10pi, a time point where both M1 and M2ExMa were present in BALF. The data revealed that expression levels of selected M1 markers (iNOS,

IL-1β, TNFα) were significantly higher in $CD40^{hi}$ compared to $CD206^{hi}$ ExMa, and expression of the M2 markers Arg-1, Fizz-1, and TGF-β were significantly increased in $CD206^{hi}$ versus $CD40^{hi}$ ExMa, confirming that the established FACS approach represented a valid strategy to define M1 and M1ExMa.

Application of this multi-color antibody staining method and gating strategy to quantify M1/M2 ExMa and rAM numbers in the course post IAV infection revealed that, during the acute phase of IAV infection (until D7pi), the rAM were depleted and newly recruited M1 polarized ExMa ($CD40^{hi}$) infiltrated the lung, particularly the alveoli, to high numbers. In the early repair phase (until D14pi), both M1 and M2 polarized ExMa were found to be present ($CD40^{hi}$ and $CD206^{hi}$, respectively), whereas exclusively M2ExMa were found at low numbers at D21pi in the late repair phase. These results demonstrate successful establishment of a novel, robust gating strategy to define functional phenotypes of ExMa in murine *in vivo* lung infection model, and reveal substantial plasticity of ExMa in IAV infection. Preliminary data recently showed that this gating strategy is also applicable to mouse pneumonia models induced by *Streptococcus peumoniae* and *Klebsiella pneumoniae* with different kinetics and quantities of M1/M2ExMa accumulation (Selvakumar, B et al, unpublished). This is of particular interest, as none such elaborated FACS strategy has been accessible to date. Plenty of studies have used *in vitro* polarization protocols for ExMa. These protocols usually involve cytokines/PAMPs such as IFN-γ, LPS, and GM-CSF versus IL-4, IL-13, and G-CSF to artificially generate M1 and M2 macrophages, respectively, for further functional studies. As a result, depending on the polarization protocol used, the M1 vs. M2 gene expression profiles vary substantially among each other and do not reflect macrophage M1/M2 programming observed in lung inflammation models *in vivo* (225, 226), as such approaches do not take into account that injury-/pathogen-specific mediators are released from the infected alveolar cells, nor the direct cell-cell interactions occurring during the different stages of infection/inflammation in the alveolus, resulting in an injury and infection specific macrophage polarization pattern in different models of ALI/ARDS (24).

5.2 Functional plasticity of M2-polarized ExMa involves rAM replenishment, protection of the rAM pool and restoration of epithelial barrier function

It has become increasingly evident that, although of different ontogeny, macrophage populations recruited from the bone marrow can replenish an emptied niche of tissue-resident macrophages in different organs, such as the lung and the liver (127).

Therefore, an important task of an ExMa population of high functional plasticity would be to replenish the IAV depleted pool of rAM after recruitment to the alveolar air space. To address this in the current model, bone marrow chimeric mice expressing the CD45.1 alloantigen on tissue-resident leukocytes (such as rAM) and the CD45.2 alloantigen on bone-marrow/ circulating leukocytes (such as blood monocytes, the ExMa precursors) were infected by IAV and the quantity of CD45.2 (donor, circulation-derived) vs. CD45.1 (recipient, tissue-resident) rAM was quantified during the course of infection. The data revealed that indeed, CD45.2 alveolar recruited ExMa had the capacity to differentiate into a macrophage population of rAM phenotype ($CD45.2^{+}$,$GR\text{-}1^{-}$, $SiglecF^{hi}$, $CD11c^{hi}$, $CD11b^{low}$). Although the presented data cannot completely rule out that these cells might still differ from the preexisting, yolk sac-/fetal liver-derived $CD45.1^{+}$ rAM pool (227, 228) with respect to gene expression profiles or epigenetic landscapes (229). They demonstrate that their surface antigen phenotypes are identical, and there is evidence in the literature that they also display a functional profile equal to tissue-resident macrophages in lung and other organs (35, 228, 230). Of interest, the rAM replenishment occurred between D14 to D21pi where primarily M2ExMa are present in the alveoli, suggesting that rAM replenishment is a feature attributed to the M2 rather than the M1ExMa phenotype. Future experiments using orotracheal transfer of flow sorted $CD45.1^{+}$ M1 vs. M2 ExMa into rAM-depleted $CD45.2^{+}$ CCR2-/- (ExMa recruitment–deficient) mice will provide further insight into the properties of ExMa polarization phenotypes with respect to replenishment of an empty rAM niche, and into putative genetic and epigenetic changes associated with this process, in ALI/ARDS models.

Adoptive orotracheal transfer of flow sorted M1 vs. M2ExMa into IAV infected (ExMa recruitment-deficient) CCR2-/- mice furthermore revealed that M2ExMa increased, whereas M1ExMa decreased the numbers of rAM at D7pi. This was not due to early replenishment or induction of proliferation of rAM by M2ExMa resulting in increased rAM numbers, but likely due to release of anti-apoptotic/pro-survival factors promoting survival of rAM. One such factor, TREM-2 was recently identified to maintain the alveolar macrophage pool after sendai virus infection in mice (187, 231). This is of particular importance, as rAM depletion has been described as critical event in driving outgrowth of colonizing bacteria such as *Streptococcus pneumoniae* or *Staphylococcus aureus*, resulting in fatal bacterial super-infection, a frequent event following viral pneumonia (138, 232). Indeed, mRNA expression levels of TREM-2 were strongly increased in M2ExMa as compared to M1ExMa, and alveolarly released TREM-2 protein analyses revealed

corresponding results. Although it is likely that further factors are involved in preventing rAM cell death by M2ExMa, and vice versa in pro-inflammatory/pro-apoptotic depletion of rAM by M1ExMa, it seems that TREM-2 is involved in a protective ExMa-rAM cross-talk (data in progress)

Importantly, flow sorted M2ExMa were found to prevent loss of alveolar epithelial barrier function (alveolar albumin leakage) and to induce proliferation of AEC, whereas M1ExMa increased barrier leak and did not induce AEC proliferation substantially when transferred into IAV infected CCR2-/- mice. These data suggest that M2 in contrast to M1ExMa protected the alveolar barrier by acting in an anti-apoptotic and/or pro-proliferative way on the lung epithelium, to prevent epithelial injury and/or to drive epithelial repair. Furthermore, the data reveal a profound functional difference in the two ExMa polarization phenotypes, which were likely associated with distinct transcriptomic profiles. Moreover, DNA microarray analyses comparing the transcriptomes of M1 vs. M2ExMa flow sorted from BALF of IAV infected mice, revealed striking differences between the two macrophage phenotypes. First of all, heat map clustering of known M1 and M2 marker genes confirmed the distinct phenotypes of M1 versus M2ExMa and provided further evidence that the established FACS gating strategy defining the two polarization subsets was highly valid. Furthermore, genes preferentially expressed in M2ExMa were particularly associated with termination of inflammation (steroid biosynthesis), with epithelial repair and tight junction formation, and with cellular growth and survival. RT-PCR confirmation of some of the highly regulated genes confirmed increased expression of the growth factors PDGFα/β (platelet-derived growth factor alpha/beta), IGF-1 (insulin-like growth factor-1), EGF (epidermal growth factor), and FGF7/10 (fibroblast growth factor 7/10), and of the pro-survival genes Aven (apoptosis and caspase activation inhibitor), Bcl2 (B cell lymphoma 2), Notch1, Ccnd1 (Cyclin D1), TREM-2 (Triggering receptor expressed on myeloid cells 2) and Vopp1 (Vesicular, overexpressed in cancer, survival protein 1), in M2 compared to M1ExMa. Vice versa, M1ExMa highly expressed genes involved in antigen processing, pattern recognition pathways (e.g., IRF7, Interferon regulated factor 7), and inflammation (e.g., CXCL10, CXC chemokine ligand 10/IP-10) (heat maps not shown). One particular gene highly expressed in M1 compared to M2 ExMa was the pro-apoptotic TRAIL (TNF-related apoptosis-inducing ligand), which is directly inducing alveolar epithelial cell apoptosis, inflammatory injury and loss of barrier function in IAV pneumonia (Fig. 4-11 A) (64, 101, 233). Importantly, a substantial number of the highly differentially regulated genes was associated with tissue development and repair, and expressed in M2ExMa, such as Sort1 (Sortilin1, involved in neuronal

development) or Kazald1/IGFBP (insulin-like growth factor binding protein). Among these, Placenta-expressed transcript 1 (Plet1) was the most differentially expressed gene (+7.0380 Log FC). In summary, these results indicate that the functionally different M1 vs. M2 phenotypes have distinct gene expression profiles, with the M1ExMa upregulating inflammatory/pro-apoptotic and host defense pathways, whereas the M2ExMa expressing anti-inflammatory, pro-survival and repair pathways.

5.3 Epithelial barrier-protective properties of M2ExMa are widely mediated by Placenta-expressed transcript 1 (Plet1)

Plet1 *(RIKEN cDNA 1600029D21)* also known as C11orf34 is a glycosylphosphatidylinositol (GPI)-anchored glycoprotein with N-linked carbohydrates in addition to other post-translational modifications (234, 235). Mature mouse Plet1 shares less than 60% amino acid (aa) sequence identity with the most closely related rat or human equivalent. A potential 194 aa mouse splice variant diverges after aa 149 but still contains a hydrophobic sequence at the C-terminus. Placenta expressed transcript 1, opposite strand (Plet1os) exist with 2 transcripts (splice variants). This protein is usually translated from the Plet1 opposite reading frame. Plet1 was found to be localized at the leading edge of epidermal wounds, and modulates keratinocyte migration and cellular adhesion to matrix proteins during wound-healing responses and thereby promotes wound repair (236, 237). Plet1 is known to be a specific marker of early thymic epithelial progenitor cells and is highly expressed in placenta of mouse and pig (234, 235). It is also found to be expressed during embryogenesis, specifically in the distal part of the extraembryonic ectoderm, adjacent to the epiblast, and is therefore a potential candidate for regulating early patterning events (238). The tissue distribution in healthy adult mice showes a widespread and unique expression in proliferating epithelia, such as the hair follicle cell, sebaceous gland of skin, ciliated epithelial cells of trachea and bronchial tube, striated portion of sub-mandibular gland, distal convoluted tubule cells of kidney, ciliated epithelial cells of oviduct, medulla of adrenal gland and anterior lobe of the pituitary gland (236).

Table- 5 Predicted functional partners of Plet1 in mouse

Co-expression with Plet1and the score represent the bits score of co expression (211)

Gene	Protein and known function	Co-expression	Score
Pqlc1	PQ loop repeat containing 1		0.73
Cntd1	cyclin N-terminal domain containing 1		0.632
Tmed5	transmembrane emp24 protein transport domain containing 5		0.551
Wdnm1-like	RIKEN cDNA 1100001G20 gene		0.567
Wdr81	WD repeat domain 81		0.595
Cldn	claudin; major role in tight junction formation	yes	0.506
Esrp1	epithelial splicing regulatory protein 1	yes	0.475
Cdh1	cadherin 1; establishment and maintenance of epithelial cell morphology	yes	0.468
Epcam	epithelial cell adhesion molecule; epithelial cell-cell adhesion	yes	0.456

Of note, the mammary epithelial transcriptome in mastitis-resistant and -susceptible sheep showed that Plet1 was one of the 20 genes that are highly expressed in *Staphylococcus spp*-induced mastitis-resistant animals (239). This suggests a role of Plet1 in host defense mechanisms. Interestingly, Plet1 has been shown to be specifically expressed in an intestinal dendritic cell subset that is in close contact with Rorγt-expressing innate lymphoid cells (ILCs) and seems to be involved in both positive and negative regulation of IL-22 derived mucosal innate immunity (240), suggesting that immune cell-expressed Plet1 might involved in epithelial repair processes mediated by ILCs and IL-22 (241, 242). The database of the human protein atlas shows that Plet1 is expressed in both respiratory epithelial cells and in lung macrophages (243). Plet1 was also predicted to functionally interact with proteins like claudin, cadherin-1, epithelial splicing regulatory protein 1, and epithelial cell adhesion molecule (EpCam) in mouse (Table-5) and with the unc-93 homologue A and ferritin in humans (211). The Plet1 receptor, however, is currently unknown. These data suggest that Plet1, which was most highly upregulated in M2 vs. M1ExMa in the current work, is similarly involved in repair and restoration of the alveolar epithelium after severe insult, particularly after IAV infection, and therefore represented a highly interesting candidate for further investigation.

Therefore, to confirm the inflammation resolving and epithelium repairing effects of M2 ExMa derived Plet1, flow sorted M2ExMa from BALF of IAV infected wt mice, were adoptively transferred along with a neutralizing anti-Plet1 antibody or IgG isotype control antibody into IAV infected CCR2-/- mice at D3pi. The results showed that the rAM-preserving effects of M2ExMa were related to Plet1 expression, and Plet1 mediated the beneficial effects of M2ExMa with regard to protection of epithelial barrier function (alveolar albumin leakage). However, it is speculated that the rAM-preserving effect might be a secondary event associated with reduction of injury-associated inflammation and its putative anti-viral activity, the epithelial-protective effect observed was likely due to its pro-proliferative and anti-apoptotic action towards AEC, known to be endogenous epithelial progenitor cells of the alveoli (244), and associated to upregulation of a variety of tight junctional proteins in flow sorted AECs of the recipient CCR2-/- mice. Noteworthy, the *in vivo* data were confirmed by an *in vitro* approach where isolated murine AECs in culture were IAV infected in presence or absence of Plet1. The results demonstrate that Plet1 indeed prevents IAV induced apoptosis (shown by inhibition of caspase 3 activation), and upregulates TJ gene and protein expression, resulting in significantly increased TER in transwell-cultured AEC monolayers. This is of particular interest in the context of IAV infection, as it was recently demonstrated that IAV disrupts epithelial TJ by direct virus-host interaction at the epithelial interface in the absence of inflammatory leukocytes (245). The Plet1 regulated TJ proteins have been recently associated with both tightness of epithelial layers and barrier properties, but also with proper polarization of the epithelium (246- 249). Such processes are of utmost importance once new epithelial cells are emerging from the proliferating stem cell niche, to build up a tight and functional epithelial barrier.

Interestingly, the presented data also demonstrated that Plet1 treatment of AEC *in vitro* resulted in impairment of viral replication, as demonstrated by immunofluorescence staining for the IAV NP. This is likely due to modulation of various cellular signaling pathways by Plet1, such as pro-proliferative, anti-apoptotic or pro-survival pathways, or due to its effects on cellular polarization processes, all known to be centrally involved in proper propagation of IAV during the viral life cycle. In this respect, it has been recently demonstrated that apoptotic caspase activation is indespensable for IAV replication, as it mediates nuclear export of the viral ribonucleoproteins (250, 251).

These data suggest that Plet1 represents a therapeutic tool to attenuate epithelial injury in pneumonia induced by IAV or other pathogens. To verify a putative therapeutic effect of Plet1 in IAV-induced ALI/ARDS, infected wt mice were orotracheally treated with recombinant Plet1 at D3pi. Plet1 treatment resulted in improved lung barrier function, associated with increased expression of TJ proteins (particularly Claudin 1, ZO-1 and, to lesser extent, E-Cadherin), and induction of AEC proliferation as part of the epithelial repair response. Of note, Plet1 treatment resulted in significantly reduced lung inflammation, as demonstrated by the numbers of PMNs and lymphocytes in the BALF and by histology assessment. It remains currently unclear, whether Plet1 exerts a direct anti-inflammatory action towards the epithelium resulting in down regulation of chemokine and cytokine expression. More likely, the barrier-protective/-regenerative effects of Plet1 would result in earlier termination of inflammation due to i) closure of the epithelial barrier with impaired trans-epithelial migration, and due to ii) faster repair of injured epithelial cells with less release of danger-associated molecular patterns (DAMPs) such as HMGB1, IL-1α, and others, which are ligands for PRRs amplifying inflammation (252). Interestingly, Plet1 also increased the number of rAM in the BALF at D7pi, which is likely not due to a direct pro-survival effect (as Plet1 has been shown to exclusively target the epithelial compartment of various organs both during embryogenesis and organ repair), but might rather be related to earlier resolution of inflammation and the anti-viral properties of Plet1, which would protect the rAM pool. Nonetheless, the presented data cannot fully exclude that rAM are a direct Plet1 target, particularly as the Plet1 receptor has not been defined yet. Finally, orotracheal Plet1 treatment resulted in improved outcome after IAV induced lung injury in terms of morbidity (body weight) and, most importantly, mortality. These data clearly indicate that alveolar Plet1 deposition might represent a therapeutic strategy to attenuate ALI/ARDS induced by IAV or even by other pathogens or insults.

In conclusion, the work presented provides evidence that, during IAV induced lung injury, different polarization phenotypes of ExMa with distinct gene expression and functional properties, defined by a newly established FACS gating strategy, are present in the lung during the course of infection. M2 polarized ExMa are endowed with the ability to preserve and replenish the rAM pool which was depleted upon IAV infection. Most importantly, M2ExMa act in an anti-inflammatory way and protect and regenerate the alveolar epithelial cell barrier, a function which is dependent on the epithelial growth factor Plet1. Orotracheal treatment of IAV infected mice with recombinant Plet1

significantly attenuates inflammation and improves alveolar barrier function and outcome, suggesting that Plet1 might represent a putative therapeutic option to treat humans with ALI/ARDS.

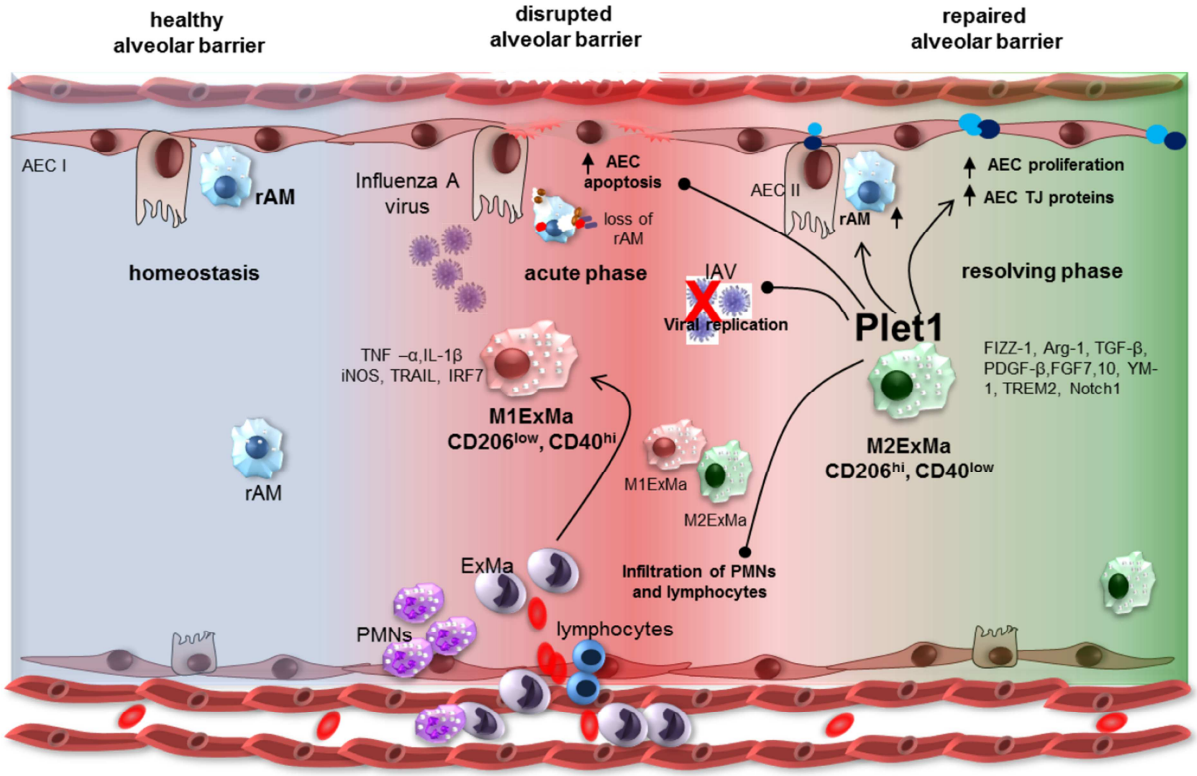

Figure 5-1 Schematic overview of IAV induced alveolar barrier damage and M2ExMa derived Plet1 in attenuating the IAV induced ALI. The left side shows the alveolus during homeostasis with healthy epithelial, endothelial barrier and resident alveolar macrophages (rAM). The center part of the figure shows the acute phase of influenza A virus infection (IAV) demonstrated by disrupted epithelial, endothelial barriers, influx of polymorpho nuclear leukocytes (PMNs), inflammatory monocytes, apoptotic rAM and presence of M1 exudate macrophages (M1ExMa- $CD206^{low}CD40^{hi}$) that releases huge pro-inflammatory cytokines like TNF-α, IFN-γ, iNOS associated with high expression of TRAIL and IRF7. The right side shows the resolving phase characterized by repaired epithelial barrier with increased tight junction (TJ) proteins on alveolar epithelial cells (AEC), presence of M2ExMa- $CD206^{hi}CD40^{low}$ that releases several growth factors (GFs) (PDGF- β, FGF7,10) associated with increased levels of Notch1 and TREM2. Anti-inflammatory cytokines (TGF-β, IL1ra, FIZZ-1, and YM-1) were also found increased in M2ExMa. The M2ExMa also expressed placenta expressed transcript 1 protein (Plet1) that accelerated the barrier repair by increasing the proliferation, TJ proteins and reducing the apoptosis on AEC. Plet1 also showed antiviral effects, reduced the infiltration of polymorpho nuclear leukocytes (PMNs) leukocytes and improved outcome in IAV induced ALI. The round head arrow (↾) denotes the inhibition effects; the up arrow (↑) denotes the increased effects.

6. Summary

Influenza A Virus (IAV)-induced acute lung injury/acute respiratory distress syndrome (ALI/ARDS) is a severe complication of IAV infection in humans with often fatal outcome due to lack of effective therapeutic options. It is characterized by severe inflammation in the alveolar compartment of the lung, associated with apoptotic injury of the alveolar epithelium, resulting in loss of barrier function, edema formation and impaired gas exchange capacity with respiratory failure. Alveolar exudate macrophages (ExMa) have been shown to be key players in both driving inflammatory injury to the alveolar epithelium, but also in promoting resolution of inflammation and driving tissue repair processes, and these different functions have been suggested to be associated with the M1 versus M2 polarization phenotype of macrophages, respectively. However, to date, methods to define these phenotypes in pneumonia models *in vivo* have not been established, nor have the functional properties of M1 and M2ExMa and the signaling pathways or mediators associated with these functions been elucidated, particularly in the context of IAV infection.

The presented data provide evidence that ExMa reveal high functional plasticity during IAV-induced ALI/ARDS. Different polarization phenotypes, M1 and M2ExMa, can be defined and separated by a newly established FACS gating strategy, allowing analyses of their gene expression profiles and correlation to their functional properties in IAV-induced lung injury. Quantitative analyses revealed that in the early, acute phase of IAV infection (D7pi), large numbers of M1ExMa infiltrate the alveolar and, to lesser extent, the interstitial space of the lung. Later on, ExMa numbers decline and increasing proportions of M2ExMa are present. By D21pi, low numbers of ExMa are present which are completely polarized towards an M2 phenotype. Of note, bone marrow chimeric mouse models and adoptive ExMa transfer studies into ExMa recruitment-deficient CCR2-/- mice demonstrated that the functional phenotype of M2ExMa is associated with both preservation and replenishment of the rAM pool depleted upon IAV infection, and with regeneration of the alveolar epithelium and improved epithelial barrier function in IAV-induced ALI/ARDS. Transcriptomic profiling of M1 versus M2ExMa revealed highly distinct gene expression profiles, with M1ExMa expressing pro-inflammatory/pro-apoptotic and host defense-associated genes, whereas M2ExMa upregulating anti-inflammatory/anti-apoptotic genes and a high number of epithelial growth factors. The most highly regulated gene in M2 versus M1ExMa was found to be Placenta-expressed transcript 1 (Plet1), a growth factor previously associated with development of epithelial layers, epithelial cell proliferation and formation of epithelial tight junctions. *In vitro*

infection experiments using primary murine alveolar epithelial cells (mAEC) demonstrated that recombinant Plet1 prevented AEC apoptosis and IAV replication, upregulated tight junction-associated proteins and increased tightness of the AEC monolayer. Blockade of Plet1 in M2ExMa by neutralizing antibodies abolished the epithelial-protective properties of M2ExMa in IAV infection *in vivo*. Orotracheal treatment of IAV infected mice with recombinant Plet1 attenuated inflammation, induced AEC repair, improved alveolar barrier function and increased survival of IAV-induced ALI/ARDS. Together, these data indicate that M1 and M2ExMa are functionally distinct phenotypes evolving during IAV infection, and that M2 programming of ExMa *in vivo* is protective with respect to alveolar barrier function due to expression of Plet1. Moreover, therapeutic intervention using alveolar deposition of Plet1 might be a useful strategy to improve outcome after ALI/ARDS in humans.

7. Zusammenfassung

Das Influenza A Virus (IAV) induzierte akute Lungenversagen/´Acute Respiratory Distress Syndrome` (ARDS) ist eine schwere Komplikation der humanen IAV Infektion mit häufig tödlichem Ausgang aufgrund fehlender effektiver therapeutischer Optionen. Es ist charakterisiert durch eine schwere Entzündung des alveolären Lungenkompartimentes mit apoptotischer Schädigung des Alveolarepithels, was zum Verlust der pulmonalen Schrankenfunktion mit Lungenödem und schwerer Gasaustauschstörung führt. Alveolär rekrutierte (Exudate) Makrophagen (ExMa) sind zentral sowohl an der inflammatorischen Gewebsschädigung des Alveolarepithels als auch an der Entzündungsauflösung und Gewebereparatur beteiligt und diese differenten Prozesse wurden jeweils einer M1 bzw. M2 Polarisation der beteiligten ExMa zugeschrieben. Bisher wurden jedoch weder Methoden etabliert, die es erlauben, diese Polarisationsphänotypen in Pneumonie Modellen in vivo zu unterscheiden, noch wurden bislang insbesondere im Kontext der IAV Infektion das funktionelle Repertoire von M1 vs. M2 polarisierten ExMa und die daran beteiligten Signalwege und Mediatoren aufgeklärt.

Die in dieser Arbeit präsentierten Daten geben Hinweise darauf, dass ExMa im Verlauf des IAV-induzierten Lungenversagens/ARDS eine hohe funktionelle Plastizität aufweisen. Mit Hilfe einer neu etablierten ´FACS- Gating´ Strategie ließen sich M1 und M2 ExMa als distinkte Polarisationsphänotypen identifizieren, durchflusszytometrisch separieren und hinsichtlich ihres Genexpressionsprofils sowie ihrer Funktion im IAV-induzierten Lungenversagen charakterisieren. Quantitative Analysen zeigten, dass in der frühen akuten Phase der IAV Infektion (Tag 7 nach Infektion) M1 ExMa in großer Zahl den Alveolarraum und in geringerem Ausmaß das Lungeninterstitium infiltrieren. Später im Infektionsverlauf sinkt die Zahl der ExMa während der Anteil der ExMa mit M2 Polarisierung zunimmt. An Tag 21 nach Infektion sind nur noch wenige ExMa nachweisbar, die alle einen M2 Phänotyp aufweisen. Durch Untersuchungen in Knochenmarks-chimären Mausmodellen und adoptiven Transfer von ExMa in CCR2-/- Mäuse mit einem endogenen ExMa Rekrutierungsdefekt ließ sich zeigen, dass der funktionelle Phänotyp von M2ExMa zur Erhaltung und Regenerierung des durch die IAV Infektion depletierten Zellpools residenter Alveolarmakrophagen (rAM) beiträgt, was zur Regeneration des Alveolarepithels und verbesserter epithelialer Barrierefunktion im IAV induzierten Lungenversagen/ARDS führte. Transkriptomanalysen von M1 vs M2ExMa zeigten distinkte Genexpressionsprofile, wobei M1ExMa pro-inflammatorische/pro-apoptotische und Wirtsabwehr-assoziierte Gene exprimierten, während in M2 ExMa anti-inflammatorische/anti-apoptotische Gene sowie eine hohe Anzahl von Genen, die

epitheliale Wachstumsfaktoren kodieren, hochreguliert waren. Das am stärksten in M2 versus M1ExMa hochregulierte Gen war ´Placenta-expressed transcript 1´ (Plet1), ein Wachstumsfaktor, dem bereits eine Rolle bei der Entwicklung von Epithelzellschichten, bei der Epithelzellproliferation und der Formierung von epithelialen ´Tight Junctions´ zugeschrieben worden war. In in vitro Infektionsexperimenten an primären murinen Alveolarepithelzellen (AEC) ließ sich zeigen, dass rekombinantes Plet1 die AEC Apoptose und IAV Replikation verhindert, ´Tight Junction` assoziierte Proteine hochreguliert und die Dichtigkeit von AEC Monolayern erhöht. Blockade von Plet1 in M2ExMa durch neutralisierende Antikörper führte zum Verlust der Epithel-protektiven Eigenschaften von M2ExMa im Rahmen der IAV Infektion in vivo. Intratracheale Behandlung von IAV infizierten Mäusen mit rekombinantem Plet1 attenuierte die Inflammation, induzierte AEC Reparatur, verbesserte die alveoläre Barrierefunktion und erhöhte die Überlebensrate von Tieren mit IAV-induziertem ALI/ARDS. Insgesamt zeigen diese Ergebnisse, dass M1 und M2 ExMa funktionell distinkte Phänotypen im Verlauf der IAV darstellen und dass eine M2 Programmierung von ExMa durch die Expression von Plet1 in vivo protektiv für die alveoläre Barrierefunktion ist. Die alveoläre Deposition von Plet1 als therapeutische Intervention könnte deshalb eine nützliche Strategie sein, um das Behandlungsergebnis bei Patienten mit ALI/ARDS zu verbessern.

8. References

1. Brune K, Frank JA, Schwingshackl A, Finigan JH, Sidhaye VK.. Pulmonary epithelial barrier function- some new players and mechanisms. *Am J Physiol Lung Cell Mol Physiol 2015.*
2. Martin TR, Frevert CW. Innate immunity in the lungs. *Proc Am Thorac Soc 2005*.
3. Takemura, R., and Z. Werb. Secretory products of macrophages and their physiological functions. *Am J Physiol 1984.*
4. Weibel ER. Gas exchange: large surface and thin barrier determine pulmonary diffusing capacity. *Minerva Anestesiol 1999.*
5. Mason RJ. Biology of alveolar type II cells. *Respirology 2006.*
6. Brune K, Frank J, Schwingshackl A, Finigan J, Sidhaye VK. Pulmonary epithelial barrier function: some new players and mechanisms. *Am J Physiol Lung Cell Mol Physiol. 2015.*
7. Castranova V, Rabovsky J, Tucker JH, Miles PR. The alveolar type II epithelial cell: A multifunctional pneumocyte. *Toxicol Appl Pharmacol 1988.*
8. Meng W, Takeichi M. Adherens junction: molecular architecture and regulation. *Cold Spring Harb Perspect Biol 2009.*
9. Danjo Y, Gipson I. Actin “purse string” filaments are anchored by E-cadherin-mediated adherens junctions at the leading edge of the epithelial wound, providing coordinated cell movement. *J Cell Sci 1998.*
10. Knust E, Bossinger O. Composition and formation of intercellular junctions in epithelial cells. *Science 2002.*
11. Guilliams M, De Kleer I, Henri S, Post S, Vanhoutte L, De Prijck S, Deswarte K, Malissen B, Hammad H, Lambrecht BN. Alveolar macrophages develop from fetal monocytes that differentiate into long-lived cells in the first week of life via GM-CSF. *J Exp Med 2013.*
12. Davies LC, Jenkins SJ, Allen JE, Taylor PR. Tissue-resident macrophages. *Nat Immunol 2013.*
13. Yona S, Kim K-W, Wolf Y, Mildner A, Varol D, Breker M, Strauss-Ayali D, Viukov S, Guilliams M, Misharin A, Hume DA, Perlman H, Malissen B, Zelzer E, Jung S. Fate mapping reveals origins and dynamics of monocytes and tissue macrophages under homeostasis. *Immunity 2013.*
14. Schlitzer A, McGovern N, Teo P, Zelante T, Atarashi K, Low D, Ho AWS, See P, Shin A, Wasan PS, Hoeffel G, Malleret B, Heiseke A, Chew S, Jardine L, Purvis HA, Hilkens CMU, Tam J, Poidinger M, Stanley ER, Krug AB, Renia L, Sivasankar B, Ng LG, Collin M, Ricciardi-Castagnoli P, Honda K, Haniffa M, Ginhoux F. IRF4 transcription factor-dependent CD11b+ dendritic cells in human and mouse control mucosal IL-17 cytokine responses. *Immunity 2013.*
15. Lambrecht BN. Alveolar macrophage in the driver’s seat. *Immunity 2006.*
16. Westphalen K, Gusarova GA, Islam MN, Subramanian M, Cohen TS, Prince AS, Bhattacharya J. Sessile alveolar macrophages communicate with alveolar epithelium to modulate immunity. *Nature 2014.*
17. Hussell T, Bell TJ. Alveolar macrophages: plasticity in a tissue-specific context. *Nat Rev Immunol 2014.*
18. Watford WT, Wright JR, Hester CG, Jiang H, Frank MM. Surfactant protein A regulates complement activation. *J Immunol 2001*.
19. Haczku A. Protective role of the lung collectins surfactant protein A and surfactant protein D in airway inflammation. *J Allergy Clin Immunol 2008.*

20. Morris DG, Huang X, Kaminski N, Wang Y, Shapiro SD, Dolganov G, Glick A, Sheppard D. Loss of integrin alpha(v)beta6-mediated TGF-beta activation causes Mmp12-dependent emphysema. *Nature 2003.*
21. Murray PJ. The primary mechanism of the IL-10-regulated antiinflammatory response is to selectively inhibit transcription. *Proc Natl Acad Sci U S A 2005.*
22. Snelgrove RJ, Goulding J, Didierlaurent AM, Lyonga D, Vekaria S, Edwards L, Gwyer E, Sedgwick JD, Barclay AN, Hussell T. A critical function for CD200 in lung immune homeostasis and the severity of influenza infection. *Nat Immunol 2008.*
23. Shultz LD, Rajan T V, Greiner DL. Severe defects in immunity and hematopoiesis caused by SHP-1 protein-tyrosine-phosphatase deficiency. *Trends Biotechnol 1997.*
24. Herold S, Mayer K, Lohmeyer J. Acute lung injury: how macrophages orchestrate resolution of inflammation and tissue repair. *Front Immunol 2011*.
25. Taylor PR, Martinez-Pomares L, Stacey M, Lin H-H, Brown GD, Gordon S. Macrophage receptors and immune recognition. *Annu Rev Immunol 2005.*
26. Maris NA, Dessing MC, de Vos AF, Bresser P, van der Zee JS, Jansen HM, Spek CA, van der Poll T. Toll-like receptor mRNA levels in alveolar macrophages after inhalation of endotoxin. *Eur Respir J 2006.*
27. Beutler BA. TLRs and innate immunity. *Blood 2009.*
28. Opitz B, Püschel A, Schmeck B, Hocke AC, Rosseau S, Hammerschmidt S, Schumann RR, Suttorp N, Hippenstiel S. Nucleotide-binding oligomerization domain proteins are innate immune receptors for internalized Streptococcus pneumoniae. *J Biol Chem 2004*.
29. Byrne BG, Dubuisson J-F, Joshi AD, Persson JJ, Swanson MS. Inflammasome components coordinate autophagy and pyroptosis as macrophage responses to infection. *MBio 2013*.
30. Opitz B, Rejaibi A, Dauber B, Eckhard J, Vinzing M, Schmeck B, Hippenstiel S, Suttorp N, Wolff T. IFNbeta induction by influenza A virus is mediated by RIG-I which is regulated by the viral NS1 protein. *Cell Microbiol 2007*.
31. Yoneyama M, Kikuchi M, Natsukawa T, Shinobu N, Imaizumi T, Miyagishi M, Taira K, Akira S, Fujita T. The RNA helicase RIG-I has an essential function in double-stranded RNA-induced innate antiviral responses. *Nat Immunol 2004.*
32. Cabanski M, Steinmüller M, Marsh LM, Surdziel E, Seeger W, Lohmeyer J. PKR regulates TLR2/TLR4-dependent signaling in murine alveolar macrophages. *Am J Respir Cell Mol Biol 2008.*
33. García MA, Gil J, Ventoso I, Guerra S, Domingo E, Rivas C, Esteban M. Impact of protein kinase PKR in cell biology: from antiviral to antiproliferative action. *Microbiol Mol Biol Rev 2006.*
34. Strieter RM, Belperio JA, Keane MP. Host innate defenses in the lung: the role of cytokines. *Curr Opin Infect Dis 2003.*
35. Maus UA, Wellmann S, Hampl C, Kuziel W a, Srivastava M, Mack M, Everhart MB, Blackwell TS, Christman JW, Schlöndorff D, Bohle RM, Seeger W, Lohmeyer J. CCR2-positive monocytes recruited to inflamed lungs downregulate local CCL2 chemokine levels. *Am J Physiol Lung Cell Mol Physiol 2005.*
36. Rubenfeld GD, Caldwell E, Peabody E, Weaver J, Martin DP, Neff M, Stern EJ, and Hudson LD: Incidence and outcomes of acute lung injury. *N Engl J Med. 2005*.
37. Dowdy DW, Eid MP, Dennison CR, Mendez-Tellez PA, Herridge MS, Guallar E, Pronovost PJ, and Needham DM: Quality of life after acute respiratory distress syndrome: a meta-analysis. *Intensive Care Med. 2006*.
38. Ashbaugh DG, Bigelow DB, Petty TL, and Levine BE: Acute respiratory distress in adults. *Lancet. 1967.*

39. Bernard GR, Artigas A, Brigham KL, Carlet J, Falke K, Hudson L, Lamy M, LeGall JR, Morris A, and Spragg R: Report of the American-European Consensus conference on acute respiratory distress syndrome: definitions, mechanisms, relevant outcomes, and clinical trial coordination. Consensus Committee. *J Crit Care. 1994.*
40. Esteban A, Fernandez-Segoviano P, Frutos-Vivar F, AramburuJA, Najera L, Ferguson ND, Alia I, Gordo F, and Rios F: Comparison of clinical criteria for the acute respiratory distress syndrome with autopsy findings. *Ann Intern Med. 2004*.
41. Ferguson ND, Meade MO, Hallett DC and Stewart TE: High values of the pulmonary artery wedge pressure in patients with acute lung injury and acute respiratory distress syndrome. *Intensive Care Med. 2002.*
42. Rubenfeld GD, Caldwell E, Granton J, Hudson LD, and Matthay MA: Interobserver variability in applying a adiographic definition for ARDS. *Chest. 1999.*
43. Meade MO, Cook RJ, Guyatt GH, Groll R, Kachura JR, Bedard M, Cook DJ, Slutsky AS, and Stewart TE: nterobserver variation in interpreting chest radiographs for the diagnosis of acute respiratory distress syndrome. *Am J Respir Crit Care Med. 2000.*
44. Ranieri VM, Rubenfeld GD, Thompson BT, Ferguson ND, Caldwell E, Fan E, Camporota L, Slutsky AS. Acute respiratory distress syndrome: the Berlin Definition. *JAMA 2012.*
45. Ware LB, Matthay MA. The acute respiratory distress syndrome. *N Engl J Med. 2000.*
46. Lipes J, Bojmehrani A, Lellouche F. Low Tidal Volume Ventilation in Patients without Acute Respiratory Distress Syndrome: A Paradigm Shift in Mechanical Ventilation. *Crit Care Res Pract. 2012.*
47. Eisner MD, Thompson T, Hudson LD, Luce JM, Hayden D, Schoenfeld D, Matthay MA; Acute Respiratory Distress Syndrome Network. Efficacy of low tidal volume ventilation in patients with different clinical risk factors for acute lung injury and the acute respiratory distress syndrome. *Am J Respir Crit Care Med.2001.*
48. Johnson ER, Matthay MA. Acute lung injury: epidemiology, pathogenesis, and treatment. *J Aerosol Med Pulm Drug Deliv. 2010.*
49. Pugin J, Verghese G, Widmer MC and Matthay MA: The alveolar space is the site of intense inflammatory and profibrotic reactions in the early phase of acute respiratory distress syndrome. *Crit Care Med. 1999.*
50. Matthay MA, and Zimmerman GA: Acute lung injury and the acute respiratory distress syndrome: four decades of inquiry into pathogenesis and rational management. *Am J Respir Cell Mol Biol. 2005.*
51. Meduri GU, Kohler G, Headley S, Tolley E, Stentz F, and Postlethwaite A: Inflammatory cytokines in the BAL of patients with ARDS. Persistent elevation over time predicts poor outcome. *Chest. 1995.*
52. Parsons PE, Eisner MD, Thompson BT, Matthay MA, Ancukiewicz M, Bernard GR, Wheeler AP, and Network NARDSCT: Lower tidal volume ventilation and plasma cytokine markers of inflammation in patients with acute lung injury. *Crit Care Med. 2005.*
53. Ware LB, Matthay MA, Parsons PE, Thompson BT, Januzzi JL, Eisner MD, National Heart, Lung, and Blood Institute, and Acute Respiratory Distress Syndrome Clinical Trials Network: Pathogenetic and prognostic significance of altered coagulation and fibrinolysis in acute lung injury- acute respiratory distress syndrome. *Crit Care Med. 2007.*
54. Ginzberg HH, Cherapanov V, Dong Q, Cantin A, McCulloch CA, Shannon PT, and Downey GP: Neutrophil-mediated epithelial injury during transmigration: role of elastase. *Am J Physiol Gastrointest Liver Physiol. 2001.*

55. Ginzberg HH, Shannon PT, Suzuki T, Hong O, Vachon E, Moraes T, Abreu MT, Cherepanov V, Wang X, Chow CW, and Downey GP: Leukocyte elastase induces epithelial apoptosis: role of mitochondial permeability changes and Akt. *Am J Physiol Gastrointest Liver Physiol. 2004.*
56. Martin TR, Hagimoto N, Nakamura M, and Matute-Bello G: Apoptosis and epithelial injury in the lungs. *Proc Am Thorac Soc. 2005*.
57. Matute-Bello G, Frevert CW, Liles WC, Nakamura M, Ruzinski JT, Ballman K, Wong VA, Vathanaprida C, and Martin TR: Fas=Fas ligand system mediates epithelial injury, but not pulmonary host defenses, in response to inhaled bacteria. *Infect Immun. 2001*.
58. Matute-Bello G, and Martin TR: Science review: apoptosis in acute lung injury. *Crit Care. 2003.*
59. Zemans RL, Colgan SP, and Downey GP: Transepithelial migration of neutrophils: mechanisms and implications for acute lung injury. *Am J Respir Cell Mol Biol. 2009.*
60. Shasby DM, Fox RB, Harada RN, and Repine JE: Reduction of the edema of acute hyperoxic lung injury by granulocyte depletion. *J Appl Physiol. 1982*.
61. Shasby DM, Vanbenthuysen KM, Tate RM, Shasby SS, McMurtry I, and Repine JE: Granulocytes mediate acute edematous lung injury in rabbits and in isolated rabbit lungs perfused with phorbol myristate acetate: role of oxygen radicals. *Am Rev Respir Dis. 1982*.
62. Abraham E, Carmody A, Shenkar R, and Arcaroli J: Neutrophils as early immunologic effectors in hemorrhage- or endotoxemia-induced acute lung injury. *Am J Physiol Lung Cell Mol Physiol. 2000.*
63. Martin TR, Pistorese BP, Chi EY, Goodman RB, and Matthay MA: Effects of leukotriene B4 in the human lung. Recruitment of neutrophils into the alveolar spaces without a change in protein permeability. *J Clin Invest. 1989.*
64. Herold S, Steinmueller M, von Wulffen W, Cakarova L, Pinto R, Pleschka S, Mack M, Kuziel WA, Corazza N, Brunner T, Seeger W, Lohmeyer J. Lung epithelial apoptosis in influenza virus pneumonia: the role of macrophage-expressed TNF-related apoptosis-inducing ligand. *J Exp Med. 2008*.
65. Lee JW, Fang X, Dolganov G, Fremont RD, Bastarache JA, Ware LB, and Matthay MA: Acute lung injury edema fluid decreases net fluid transport across human alveolar epithelial type II cells. *J Biol Chem. 2007*.
66. Geiser T. Mechanisms of alveolar epithelial repair in acute lung injury—a translational approach. *Swiss Med Wkly. 2003.*
67. Marshall R, Bellingan G, Laurent G. The acute respiratory distress syndrome: fibrosis in the fast lane. *Thorax. 1998*.
68. Ware LB. Pathophysiology of acute lung injury and the acute respiratory distress syndrome. *Semin Respir Crit Care Med. 2006.*
69. Lamb R, Krug R, Knipe D. Orthomyxoviridae: The Viruses and Their Replication. In: Bernard N. Fields, David Mahan Knipe PMH, editor. *Fields Virol Lippincott Williams & Wilkins; 2001*.
70. Fouchier RAM, Munster V, Wallensten A, Bestebroer TM, Herfst S, Smith D, Rimmelzwaan GF, Olsen B, Osterhaus ADME. Characterization of a novel influenza A virus hemagglutinin subtype (H16) obtained from black-headed gulls. *J Virol 2005.*
71. Tong S, Li Y, Rivailler P, Conrardy C, Castillo DAA, Chen L-M, Recuenco S, Ellison JA, Davis CT, York IA, Turmelle AS, Moran D, Rogers S, Shi M, Tao Y, Weil MR, Tang K, Rowe LA, Sammons S, Xu X, Frace M, Lindblade KA, Cox NJ, Anderson LJ, Rupprecht CE, Donis RO. A distinct lineage of influenza A virus from bats. *Proc Natl Acad Sci 2012.*

72. Lamb RA, Choppin PW. The gene structure and replication of influenza virus. *Annu Rev Biochem 1983.*
73. Lamb RA, Lai CJ, Choppin PW. Sequences of mRNAs derived from genome RNA segment 7 of influenza virus: colinear and interrupted mRNAs code for overlapping proteins. *Proc Natl Acad Sci U S A 1981*.
74. Inglis SC, Almond JW. An Influenza Virus Gene Encoding Two Different Proteins. *Philos Trans R Soc B Biol Sci 1980*.
75. Chen W, Calvo PA, Malide D, Gibbs J, Schubert U, Bacik I, Basta S, O'Neill R, Schickli J, Palese P, Henklein P, Bennink JR, Yewdell JW. A novel influenza A virus mitochondrial protein that induces cell death. *Nat Med 2001*.
76. Karlsson Hedestam GB, Fouchier RA, Phogat S, Burton DR, Sodroski J, Wyatt RT. The challenges of eliciting neutralizing antibodies to HIV-1 and to influenza virus. *Nat Rev Microbiol. 2008*
77. Vlahos R, Stambas J, Selemidis S. Suppressing production of reactive oxygen species (ROS) for influenza A virus therapy. *Trends Pharmacol Sci. 2012.*
78. Ramsey CD, Kumar A. Influenza and endemic viral pneumonia. *Crit Care Clin.2013*.
79. De Jong MD, Simmons CP, Thanh TT, Hien VM, Smith GJD, Chau TNB, Hoang DM, Chau NVV, Khanh TH, Dong VC, Qui PT, Cam B Van, Ha DQ, Guan Y, Peiris JSM, Chinh NT, Hien TT, Farrar J. Fatal outcome of human influenza A (H5N1) is associated with high viral load and hypercytokinemia. *Nat Med 2006*.
80. Jain S, Kamimoto L, Bramley AM, Schmitz AM, Benoit SR, Louie J, Sugerman DE, Druckenmiller JK, Ritger KA, Chugh R, Jasuja S, Deutscher M, Chen S, Walker JD, Duchin JS, Lett S, Soliva S, Wells E V, Swerdlow D, Uyeki TM, Fiore AE, Olsen SJ, Fry AM, Bridges CB, Finelli L. Hospitalized patients with 2009 H1N1 influenza in the United States, April-June 2009. *N Engl J Med 2009*.
81. Short KR, Kroeze EJBV, Fouchier R a M, Kuiken T. Pathogenesis of influenza-induced acute respiratory distress syndrome. *Lancet Infect Dis 2014.*
82. Ballinger MN, Standiford TJ. Postinfluenza bacterial pneumonia: host defenses gone awry. *J Interferon Cytokine Res 2010.*
83. Morens DM, Taubenberger JK, Fauci AS. Predominant role of bacterial pneumonia as a cause of death in pandemic influenza: implications for pandemic influenza preparedness. *J Infect Dis 2008.*
84. Golebiewski L, Liu H, Javier RT, Rice AP. The avian influenza virus NS1 ESEV PDZ binding motif associates with Dlg1 and Scribble to disrupt cellular tight junctions. *J Virol 2011*.
85. Lazrak A, Iles KE, Liu G, Noah DL, Noah JW, Matalon S. Influenza virus M2 protein inhibits epithelial sodium channels by increasing reactive oxygen species. *FASEB J 2009*.
86. Gack MU, Shin YC, Joo C-H, Urano T, Liang C, Sun L, Takeuchi O, Akira S, Chen Z, Inoue S, Jung JU. TRIM25 RING-finger E3 ubiquitin ligase is essential for RIG-I-mediated antiviral activity. *Nature 2007*.
87. Clemens MJ, Elia A. The Double-Stranded RNA-Dependent Protein Kinase PKR: Structure and Function. *J Interferon Cytokine Res 2009.*
88. Kumar A, Haque J, Lacoste J, Hiscott J, Williams BR. Double-stranded RNA-dependent protein kinase activates transcription factor NF-kappa B by phosphorylating I kappa B. *Proc Natl Acad Sci U S A 1994*.
89. Gil J, Esteban M. Induction of apoptosis by the dsRNA-dependent protein kinase (PKR): Mechanism of action. *Apoptosis 2000.*

90. Barchet W, Krug A, Cella M, Newby C, Fischer JAA, Dzionek A, Pekosz A, Colonna M. Dendritic cells respond to influenza virus through TLR7- and PKR-independent pathways. *Eur J Immunol 2005.*
91. Le Goffic R, Balloy V, Lagranderie M, Alexopoulou L, Escriou N, Flavell R, Chignard M, Si-Tahar M. Detrimental contribution of the Toll-like receptor (TLR)3 to influenza A virus-induced acute pneumonia. *PLoS Pathog 2006.*
92. Allen IC, Scull MA, Moore CB, Holl EK, McElvania-TeKippe E, Taxman DJ, Guthrie EH, Pickles RJ, Ting JP-Y. The NLRP3 inflammasome mediates in vivo innate immunity to influenza A virus through recognition of viral RNA. *Immunity 2009.*
93. Thomas PG, Dash P, Aldridge JR, Ellebedy AH, Reynolds C, Funk AJ, Martin WJ, Lamkanfi M, Webby RJ, Boyd KL, Doherty PC, Kanneganti T-D. The intracellular sensor NLRP3 mediates key innate and healing responses to influenza A virus via the regulation of caspase-1. *Immunity 2009.*
94. Ludwig S, Pleschka S, Planz O, Wolff T. Ringing the alarm bells: signalling and apoptosis in influenza virus infected cells. *Cell Microbiol 2006.*
95. Chan M, Cheung C, Chui W, Tsao S, Nicholls J, Chan Y, Chan R, Long H, Poon L, Guan Y, others. Proinflammatory cytokine responses induced by influenza A (H5N1) viruses in primary human alveolar and bronchial epithelial cells. *Respir Res 2005*.
96. Tumpey TM, García-Sastre A, Taubenberger JK, Palese P, Swayne DE, Pantin-Jackwood MJ, Schultz-Cherry S, Solórzano A, Van Rooijen N, Katz JM, Basler CF. Pathogenicity of influenza viruses with genes from the 1918 pandemic virus: functional roles of alveolar macrophages and neutrophils in limiting virus replication and mortality in mice. *J Virol 2005.*
97. Lin KL, Suzuki Y, Nakano H, Ramsburg E, Gunn MD. CCR2+ monocyte-derived dendritic cells and exudate macrophages produce influenza-induced pulmonary immune pathology and mortality. *J Immunol 2008.*
98. Szretter KJ, Gangappa S, Lu X, Smith C, Shieh W-J, Zaki SR, Sambhara S, Tumpey TM, Katz JM. Role of host cytokine responses in the pathogenesis of avian H5N1 influenza viruses in mice. *J Virol 2007*.
99. Van Reeth K. Cytokines in the pathogenesis of influenza. *Vet Microbiol 2000.*
100. Baskin CR, Bielefeldt-Ohmann H, Tumpey TM, Sabourin PJ, Long JP, García-Sastre A, Tolnay A-E, Albrecht R, Pyles JA, Olson PH, Aicher LD, Rosenzweig ER, Murali-Krishna K, Clark EA, Kotur MS, Fornek JL, Proll S, Palermo RE, Sabourin CL, Katze MG. Early and sustained innate immune response defines pathology and death in nonhuman primates infected by highly pathogenic influenza virus. *Proc Natl Acad Sci U S A 2009*.
101. Högner K, Wolff T, Pleschka S, Plog S, Gruber AD, Kalinke U, Walmrath H-D, Bodner J, Gattenlöhner S, Lewe-Schlosser P, Matrosovich M, Seeger W, Lohmeyer J, Herold S. Macrophage-expressed IFN-β contributes to apoptotic alveolar epithelial cell injury in severe influenza virus pneumonia. *PLoS Pathog 2013.*
102. Girard TD, Bernard GR. Mechanical ventilation in ARDS: a state-of-the-art review. *Chest. 2007*.
103. England TN: Ventilation with lower tidal volumes as compared with traditional tidal volumes for acute lung injury and the acute respiratory distress syndrome. The Acute Respiratory Distress Syndrome Network. *N Engl J Med* 2000.
104. Hayes M, Curley G, Ansari B, Laffey JG. Clinical review: Stem cell therapies for acute lung injury/acute respiratory distress syndrome - hope or hype? *Crit Care. 2012*.
105. Bernard GR, Luce JM, Sprung CL, et al. High-dose corticosteroids in patients with the adult respiratory distress syndrome. *N Engl J Med.1987*.

106. Suter PM, Domenighetti G, Schaller MD, Laverriere MC, Ritz R, Perret C: N-acetylcysteine enhances recovery from acute lung injury in man. A randomized, double-blind, placebo-controlled clinical study. *Chest 1994*.
107. Bernard GR, Wheeler AP, Arons MM, et al. A trial of antioxidants N-acetylcysteine and procysteine in ARDS. The Antioxidant in ARDS Study Group. *Chest. 1997*.
108. Presneill JJ, Harris T, Stewart AG, Cade JF, Wilson JW: A randomized phase II trial of granulocyte-macrophage colony-stimulating factor therapy in severe sepsis with respiratory dysfunction. *Am J Resp Crit Care Med 2002*.
109. Taylor RW, Zimmerman JL, Dellinger RP, Straube RC, Criner GJ, Davis K Jr, Kelly KM, Smith TC, Small RJ: Low-dose inhaled nitric oxide in patients with acute lung injury: a randomized controlled trial. *JAMA 2004*.
110. Taut FJ, Rippin G, Schenk P, Findlay G, Wurst W, Hafner D, Lewis JF, Seeger W, Gunther A, Spragg RG: A Search for subgroups of patients with ARDS who may benefit from surfactant replacement therapy: a pooled analysis of five studies with recombinant surfactant protein-C surfactant (Venticute). *Chest 2008*.
111. Montravers P, Fagon JY, Gilbert C, et al. Pilot study of cardiopulmonary risk from pentoxifylline in adult respiratory distress syndrome. *Chest. 1993*.
112. Bernard GR, Vincent JL, Laterre PF, et al. Efficacy and safety of recombinant human activated protein C for severe sepsis. *N Engl J Med. 2001*.
113. Almog Y, Shefer A, Novack V, Maimon N, Barski L, Eizinger M, Friger M, Zeller L, and Danon A: Prior statin therapy is associated with a decreased rate of severe sepsis. *Circulation. 2004*.
114. Kruger P, Fitzsimmons K, Cook D, Jones M, and Nimmo G: Statin therapy is associated with fewer deaths in patients with bacteraemia. *Intensive Care Med. 2006*.
115. Thomsen RW, Riis A, Kornum JB, Christensen S, Johnsen SP, and Sorensen HT: Preadmission use of statins and outcomes after hospitalization with pneumonia: population-based cohort study of 29,900 patients. *Arch Intern Med. 2008*.
116. Kor DJ, Iscimen R, Yilmaz M, Brown MJ, Brown DR, and Gajic O: Statin administration did not influence the progression of lung injury or associated organ failures in a cohort of patients with acute lung injury. *Intensive Care Med. 2009*.
117. Rojas M, Xu J, Woods CR, Mora AL, Spears W, Roman J, and Brigham KL: Bone marrow-derived mesenchymal stem cells in repair of the injured lung. *Am J Respir Cell Mol Biol. 2005*.
118. Hayes M, Curley G, Ansari B, Laffey JG. Clinical review: Stem cell therapies for acute lung injury/acute respiratory distress syndrome - hope or hype? *Crit Care. 2012*.
119. McNulty K, Scotton C J, Sage E K, Chambers R C, Janes S M. S73 Macrophages as vehicles for delivering cell therapy to injured lung. *Thorax 2011*.
120. Pollard JW. Trophic macrophages in development and disease. *Nat Rev Immunol. 2009*.
121. Arango Duque G, Descoteaux A. Macrophage cytokines: involvement in immunity and infectious diseases. *Front Immunol. 2014.*
122. Takemura, R., and Z. Werb. Secretory products of macrophages and their physiological functions. *Am J Physiol 1984*.
123. Murray PJ, Wynn TA. Protective and pathogenic functions of macrophage subsets. *Nat Rev Immunol. 2011*.
124. Ginhoux F, Merad M. Ontogeny and homeostasis of Langerhans cells. *Immunol Cell Biol. 2010*
125. Schulz C, Perdiguero EG, Chorro L, Szabo-Rogers H, Cagnard N, Kierdorf K, Prinz M, Wu B, Jacobsen SEW, Pollard JW, Frampton J, Liu KJ, Geissmann F. A lineage of myeloid cells independent of Myb and hematopoietic stem cells. *Science 2012.*

126. Epelman S, Lavine KJ, Randolph GJ. Origin and functions of tissue macrophages. *Immunity. 2014.*
127. Ginhoux F, Jung S. Monocytes and macrophages: developmental pathways and tissue homeostasis. *Nat Rev Immunol. 2014*
128. Liddiard K, Taylor PR. Understanding local macrophage phenotypes in disease: shape-shifting macrophages. *Nat Med. 2015*
129. Serbina NV, and Pamer EG. Monocyte emigration from bone marrow during bacterial infection requires signals mediated by chemokine receptor CCR2. *Nature immunology 2006.*
130. Herold S, Tabar TS, Janssen H, Hoegner K, Cabanski M, Lewe-Schlosser P, Albrecht J, Driever F, Vadasz I, Seeger W, Steinmueller M, Lohmeyer J. Exudate macrophages attenuate lung injury by the release of IL-1 receptor antagonist in gram-negative pneumonia. *Am J Respir Crit Care Med. 2011.*
131. Hoeffel G, Ginhoux F. Ontogeny of Tissue-Resident Macrophages. *Front Immunol. 2015*
132. Geissmann F, Jung S, and Littman DR. Blood monocytes consist of two principal subsets with distinct migratory properties. *Immunity 2003.*
133. Dunay IR., Damatta RA, Fux B, Presti R, Greco S, Colonna M, and Sibley LD. Gr1 (+) inflammatory monocytes are required for mucosal resistance to the pathogen Toxoplasma gondii. *Immunity 2008.*
134. Getts DR, Terry RL, Getts MT, Muller M, Rana S, Shrestha B, Radford J, Van Rooijen N, Campbell IL, and King NJ. Ly6c+ "inflammatory monocytes" are microglial precursors recruited in a pathogenic manner in West Nile virus encephalitis. *The Journal of experimental medicine 2008.*
135. Geissmann F, Manz MG, Jung S, Sieweke MH, Merad M, Ley K. Development of monocytes, macrophages, and dendritic cells. *Science. 2010*
136. Yona S, Kim KW, Wolf Y, Mildner A, Varol D, Breker M, Strauss-Ayali D, Viukov S, Guilliams M, Misharin A, Hume DA, Perlman H, Malissen B, Zelzer E, Jung S. Fate mapping reveals origins and dynamics of monocytes and tissue macrophages under homeostasis. *Immunity. 2013.*
137. Hashimoto D, Chow A, Noizat C, Teo P, Beasley MB, Leboeuf M, Becker CD, See P, Price J, Lucas D, Greter M, Mortha A, Boyer SW, Forsberg EC, Tanaka M, van Rooijen N, García-Sastre A, Stanley ER, Ginhoux F, Frenette PS, Merad M. Tissue-resident macrophages self-maintain locally throughout adult life with minimal contribution from circulating monocytes. *Immunity 2013.*
138. Ghoneim HE, Thomas PG, McCullers JA. Depletion of alveolar macrophages during influenza infection facilitates bacterial superinfections. *J Immunol. 2013.*
139. Zigmond E, Varol C, Farache J, Elmaliah E, Satpathy AT, Friedlander G, Mack M, Shpigel N, Boneca IG, Murphy KM, Shakhar G, Halpern Z, Jung S. Ly6C hi monocytes in the inflamed colon give rise to proinflammatory effector cells and migratory antigen-presenting cells. *Immunity 2012*.
140. Murray PJ, Allen JE, Biswas SK, Fisher EA, Gilroy DW, Goerdt S, Gordon S, Hamilton JA, Ivashkiv LB, Lawrence T, Locati M, Mantovani A, Martinez FO, Mege JL, Mosser DM, Natoli G, Saeij JP, Schultze JL, Shirey KA, Sica A, Suttles J, Udalova I, van Ginderachter JA, Vogel SN, Wynn TA. Macrophage activation and polarization: nomenclature and experimental guidelines. *Immunity. 2014*
141. Martinez FO, Gordon S. The M1 and M2 paradigm of macrophage activation: time for reassessment. *F1000Prime Rep. 2014.*
142. Stein M, Keshav S, Harris N, Gordon S. Interleukin 4 potently enhances murine macrophage mannose receptor activity: a marker of alternative immunologic macrophage activation. *J Exp Med. 1992*

143. Mills CD, Kincaid K, Alt JM, Heilman MJ, Hill AM. M-1/M-2 macrophages and the Th1/Th2 paradigm. *J Immunol. 2000.*
144. Mills CD. M1 and M2 Macrophages: Oracles of Health and Disease. *Crit Rev Immunol. 2012*
145. Biswas SK, Mantovani A. Macrophage plasticity and interaction with lymphocyte subsets: cancer as a paradigm. *Nat Immunol. 2010*
146. Edwards JP, Zhang X, Frauwirth KA, Mosser DM. Biochemical and functional characterization of three activated macrophage populations. *J Leukoc Biol. 2006*
147. Mantovani A, Sica A, Locati M. Macrophage polarization comes of age. *Immunity.2005*
148. Stout RD, Jiang C, Matta B, Tietzel I, Watkins SK, Suttles J. Macrophages sequentially change their functional phenotype in response to changes in microenvironmental influences. *J Immunol. 2005*
149. Stout RD, Suttles J. Functional plasticity of macrophages: reversible adaptation to changing microenvironments. *J Leukoc Biol. 2004*
150. Joshi S, Singh AR, Zulcic M, Bao L, Messer K, Ideker T, Dutkowski J, Durden DL. Rac2 controls tumor growth, metastasis and M1-M2 macrophage differentiation in vivo. *PLoS One. 2014*
151. Fleetwood AJ, Dinh H, Cook AD, Hertzog PJ, Hamilton JA. GM-CSF- and M-CSF-dependent macrophage phenotypes display differential dependence on type I interferon signaling. *J Leukoc Biol. 2009*
152. Dalton DK, Pitts-Meek S, Keshav S, Figari IS, Bradley A, Stewart TA. Multiple defects of immune cell function in mice with disrupted interferon-gamma genes. *Science. 1993*.
153. Huang S, Hendriks W, Althage A, Hemmi S, Bluethmann H, Kamijo R, Vilcek J, Zinkernagel RM, Aguet M. Immune response in mice that lack the interferon-gamma receptor. *Science. 1993.*
154. Krausgruber Blazek TK, Smallie T, Alzabin S, Lockstone H, Sahgal N, Hussell T, Feldmann M, and Udalova IA. IRF5 promotes inflammatory macrophage polarization and TH1-TH17 responses. *Nature immunology 2011*.
155. Meraz MA, White JM, Sheehan KC, Bach EA, Rodig SJ, Dighe AS, Kaplan DH, Riley JK, Greenlund AC, Campbell D, Carver-Moore K, DuBois R.N, Clark R, Aguet M, and Schreiber RD. Targeted disruption of the Stat1 gene in mice reveals unexpected physiologic specificity in the JAK-STAT signaling pathway. *Cell 1996.*
156. Mosser DM, and Edwards JP. Exploring the full spectrum of macrophage activation. *Nature reviews 2008.*
157. Duffield JS. The inflammatory macrophage: a story of Jekyll and Hyde. *Clin Sci (Lond). 2003.*
158. Gordon S. Alternative activation of macrophages. *Nat Rev Immunol 2003*.
159. Ma J, Chen T, Mandelin J, Ceponis A, Miller NE, Hukkanen M, Ma GF, Konttinen YT. Regulation of macrophage activation. *Cell Mol Life Sci. 2003*.
160. Mosser DM. The many faces of macrophage activation. *J Leukoc Biol. 2003*.
161. Luster AD. The role of chemokines in linking innate and adaptive immunity. *Curr Opin Immunol. 2002.*
162. Adams LB, Dinauer MC, Morgenstern DE, and Krahenbuhl JL. Comparison of the roles of reactive oxygen and nitrogen intermediates in the host response to Mycobacterium tuberculosis using transgenic mice. *Tuber Lung Dis 1997.*
163. Khan N, Gowthaman U, Pahari S, Agrewala JN. Manipulation of costimulatory molecules by intracellular pathogens: veni, vidi, vici!! *PLoS Pathog. 2012*.
164. Gibbs DF, Shanley TP, Warner RL, Murphy HS, Varani J, Johnson KJ. Role of matrix metalloproteinases in models of macrophage-dependent acute lung

injury.Evidence for alveolar macrophage as source of proteinases. *Am J Respir Cell Mol Biol. 1999.*
165. Chizzolini C, Rezzonico R, De Luca C, Burger D, Dayer JM. Th2 cell membrane factors in association with IL-4 enhance matrix metalloproteinase-1 (MMP-1) while decreasing MMP-9 production by granulocyte-macrophage colony-stimulating factor-differentiated human monocytes. *J Immunol. 2000.*
166. Boyle JJ, Weissberg PL, Bennett MR. Tumor necrosis factor-alpha promotes macrophage-induced vascular smooth muscle cell apoptosis by direct and autocrine mechanisms. *Arterioscler Thromb Vasc Biol. 2003.*
167. Duffield JS, Ware CF, Ryffel B, Savill J. Suppression by apoptotic cells defines tumor necrosis factor-mediated induction of glomerular mesangial cell apoptosis by activated macrophages. *Am J Pathol. 2001*.
168. Satoh T, Takeuchi O, Vandenbon A, Yasuda K, Tanaka Y, Kumagai Y, Miyake T, Matsushita K., Okazaki T, Saitoh T, Honma K, Matsuyama T, Yui K, Tsujimura T, Standley DM, Nakanishi K, Nakai K, and Akira S. The Jmjd3- Irf4 axis regulates M2 macrophage polarization and host responses against helminth infection. *Nature immunology 2010.*
169. Ohmori Y, and Hamilton TA. IL-4-induced STAT6 suppresses IFNgamma-stimulated STAT1-dependent transcription in mouse macrophages. *J Immunol 1997*.
170. Watanabe K, Jose PJ, and Rankin SM. Eotaxin-2 generation is differentially regulated by lipopolysaccharide and IL-4 in monocytes and macrophages. *J Immunol 2002*.
171. Bonecchi RS. Sozzani JT. Stine W, Luini G, D'Amico P, Allavena D, Chantry and Mantovani A. Divergent effects of interleukin-4 and interferongamma on macrophage-derived chemokine production: an amplification circuit of polarized T helper 2 responses. *Blood 1998.*
172. Katakura T, Miyazaki M, Kobayashi M, Herndon DN, and Suzuki F. CCL17 and IL-10 as effectors that enable alternatively activated macrophages to inhibit the generation of classically activated macrophages. *J Immunol* 2004.
173. Loke P, Nair MG, Parkinson J, Guiliano D, Blaxter M, Allen JE. IL-4 dependent alternatively-activated macrophages have a distinctive in vivo gene expression phenotype. *BMC Immunol 2002.*
174. Lin EY, Li JF, Gnatovskiy L, Deng Y, Zhu L, Grzesik DA, Qian H, Xue XN, and Pollard JW. Macrophages regulate the angiogenic switch in a mouse model of breast cancer. *Cancer Res 2006.*
175. Roberts AB, Sporn MB, Assoian RK, Smith JM, Roche NS, Wakefield LM, Heine UI, Liotta LA, Falanga V, Kehrl JH, and et al.. Transforming growth factor type beta: rapid induction of fibrosis and angiogenesis in vivo and stimulation of collagen formation in vitro. *Proc Natl Acad Sci U S A 1986.*
176. Shimokado K, Raines EW, Madtes DK, Barrett TB, Benditt EP, and Ross R. A significant part of macrophage-derived growth factor consists of at least two forms of PDGF. *Cell 1985.*
177. Jenkins SJ, Ruckerl D, Cook PC, Jones LH, Finkelman FD, Van Rooijen N, MacDonald AS, and Allen JE. Local macrophage proliferation, rather than recruitment from the blood, is a signature of TH2 inflammation. *Science 2011.*
178. Lauzon-Joset JF, Marsolais D, Langlois A, Bissonnette EY. Dysregulation of alveolar macrophages unleashes dendritic cell-mediated mechanisms of allergic airway inflammation. *Mucosal Immunol. 2014.*
179. O'Reilly M, Newcomb DE, Remick D. Endotoxin, sepsis, and the primrose path. *Shock 1999.*

180. Wermuth PJ, Jimenez SA. The significance of macrophage polarization subtypes for animal models of tissue fibrosis and human fibrotic diseases. *Clin Transl Med. 2015.*
181. Hassoun PM, Mouthon L, Barberà JA, Eddahibi S, Flores SC, Grimminger F, Jones PL, Maitland ML, Michelakis ED, Morrell NW, Newman JH, Rabinovitch M, Schermuly R, Stenmark KR, Voelkel NF, Yuan JX, Humbert M. Inflammation, growth factors, and pulmonary vascular remodeling. *J Am Coll Cardiol. 2009.*
182. O'Neill LA, and Bowie AG. The family of five: TIR-domain-containing adaptors in Toll-like receptor signalling. *Nature reviews 2007.*
183. Burns K, Janssens S, Brissoni B, Olivos N, Beyaert R and Tschopp J. Inhibition of interleukin 1 receptor/Toll-like receptor signaling through the alternatively spliced, short form of MyD88 is due to its failure to recruit IRAK-4. *The J. Exp. Med. 2003.*
184. Kobayashi K, Hernandez LD, Galan JE, Janeway CA, Medzhitov R and Flavell RA. IRAK-M is a negative regulator of Toll-like receptor signaling. *Cell 2002*.
185. Ravetch JV and Lanier LL. Immune inhibitory receptors. *Science 2000.*
186. Bouchon A, Dietrich J and Colonna M. Cutting edge: inflammatory responses can be triggered by TREM-1, a novel receptor expressed on neutrophils and monocytes. *J Immunol 2000.*
187. Turnbull IR, Gilfillan S, Cella M, Aoshi T, Miller M, Piccio L, Hernandez M, and Colonna M. Cutting edge: TREM-2 attenuates macrophage activation. *J Immunol 2006.*
188. Hochreiter-Hufford A, Ravichandran KS. Clearing the dead: apoptotic cell sensing, recognition, engulfment, and digestion. *Cold Spring Harb Perspect Biol. 2013*
189. Hume DA. The Many Alternative Faces of Macrophage Activation. *Front Immunol. 2015*.
190. Taylor PR, Martinez-Pomares L, Stacey M, Lin HH, Brown GD, Gordon S. Macrophage receptors and immune recognition. *Annu Rev Immunol. 2005*.
191. Peiser L, Gordon S. The function of scavenger receptors expressed by macrophages and their role in the regulation of inflammation. *Microbes Infect. 2001*.
192. Wang J, Nikrad MP, Travanty EA, Zhou B, Phang T, Gao B, Alford T, Ito Y, Nahreini P, Hartshorn K, Wentworth D, Dinarello CA, Mason RJ. Innate immune response of human alveolar macrophages during influenza A infection. *PLoS One. 2012.*
193. Kumagai Y, Takeuchi O, Kato H, Kumar H, Matsui K, Morii E, Aozasa K, Kawai T, Akira S. Alveolar macrophages are the primary interferon-alpha producer in pulmonary infection with RNA viruses. *Immunity. 2007.*
194. Hillaire ML, Haagsman HP, Osterhaus AD, Rimmelzwaan GF, van Eijk M. Pulmonary surfactant protein D in first-line innate defence against influenza A virus infections. J Innate Immun. 2013
195. Hashimoto Y, Moki T, Takizawa T, Shiratsuchi A, Nakanishi Y. Evidence for phagocytosis of influenza virus-infected, apoptotic cells by neutrophils and macrophages in mice. *J Immunol. 2007.*
196. Chen XJ, Seth S, Yue G, Kamat P, Compans RW, Guidot D, Brown LA, Eaton DC, Jain L. Influenza virus inhibits ENaC and lung fluid clearance. *Am J Physiol Lung Cell Mol Physiol. 2004.*
197. Herold S, Wulffen W Von, Steinmueller M, Pleschka S, Kuziel WA, Mack M, Srivastava M, Seeger W, Maus UA, Lohmeyer J. Alveolar epithelial cells direct monocyte transepithelial migration upon influenza virus infection: impact of chemokines and adhesion molecules. *J Immunol 2006.*
198. Landsman I, Varol C, Jung S. Distinct differentiation potential of blood monocyte subsets in the lung. *J. Immunol. 2007.*

199. Rosseau S, Hammer P, Maus U, Harodt J, Temmesfeld B, Seeger W, Lohmeyer J. Phenotypic characterization of alveolar monocyte recruitment in adult respiratory distress syndrome. *Am. J. Physiol. Lung. Cell. Mol. Physiol. 2000.*
200. Cabanski M, Wilhelm J, Steinmüller M, Fink L, Seeger W, Lohmeyer J. Genome-wide transcriptional profiling of mononuclear phagocytes recruited to mouse lungs in response to alveolar challenge with the TLR2-agonist Pam3CSK4. *Am. J. Physiol. Lung Cell. Mol Physiol. 2009.*
201. Martinez FO. Macrophage activation and polarization. *Front Biosci 2008*.
202. Auffray C, Fogg D, Garfa M, Elain G, Join-Lambert O, et al. Monitoring of blood vessels and tissues by a population of monocytes with patrolling behaviour. *Science 2007.*
203. Seo SU, Kwon HJ, Ko HJ, Byun YH, Seong BL, Uematsu S, Akira S, Kweon MN. Type I interferon signaling regulates Ly6C (hi) monocytes and neutrophils during acute viral pneumonia in mice. *PLoS Pathog. 2011.*
204. Kuziel WA, Morgan SJ, Dawson TC, Griffin S, Smithies O, Ley K, Maeda N. Severe reduction in leukocyte adhesion and monocyte extravasation in mice deficient in CC chemokine receptor 2. *Proc Natl Acad Sci U S A. 1997*
205. Corti M, Brody AR, Harrison JH. Isolation and primary culture of murine alveolar type II cells. *Am J Respir Cell Mol Biol. 1996*
206. Cakarova L, Marsh LM, Wilhelm J, Mayer K, Grimminger F, Seeger W, Lohmeyer J, Herold S. Macrophage tumor necrosis factor-alpha induces epithelial expression of granulocyte-macrophage colony-stimulating factor: impact on alveolar epithelial repair. *Am J Respir Crit Care Med. 2009*
207. R Core Team. R: A language and environment for statistical computing. R Foundation for Statistical Computing, Vienna, Austria. *URL https://www.R-project.org/ 2015.*
208. Smyth, G. K. Linear models and empirical Bayes methods for assessing differential expression in microarray experiments. *Statistical Applications in Genetics and Molecular Biology, 2004.*
209. Kanehisa M, Goto S, Sato Y, Kawashima, M, Furumichi M, and Tanabe M. Data, information, knowledge and principle: back to metabolism in KEGG. *Nucleic Acids Res. 2014.*
210. Kanehisa M. and Goto, S. KEGG: Kyoto Encyclopedia of Genes and Genomes. *Nucleic Acids Res. 2000.*
211. String Protein DATABASE: http://string-db.org/newstring_cgi/show_network_section.pl.
212. Guth AM, Janssen WJ, Bosio CM, Crouch EC, Henson PM, Dow SW. Lung environment determines unique phenotype of alveolar macrophages. *Am J Physiol Lung Cell Mol Physiol 2009.*
213. Gordon S, Plüddemann A, Estrada FM. Macrophage heterogeneity in tissues: phenotypic diversity and functions. *Immunol Rev. 2014.*
214. Misharin AV, Morales-Nebreda L, Mutlu GM, Budinger GR, Perlman H. Flow cytometric analysis of macrophages and dendritic cell subsets in the mouse lung. *Am J Respir Cell Mol Biol. 2013.*
215. Dalrymple H, Barna BP, Malur A, Malur AG, Kavuru MS, Thomassen MJ. Alveolar macrophages of GM-CSF knockout mice exhibit mixed M1 and M2 phenotypes. *BMC. Immunol. 2013.*
216. Holt PG. Inhibitory activity of unstimulated alveolar macrophages on T- lymphocyte blastogenic response. *Am. Rev. Respir. Dis. 1978.*

217. Holt PG, Oliver J, Bilyk N, McMenamin C, McMenamin PG, Kraal G, Thepen T. Downregulation of the antigen presenting cell function(s) of pulmonary dendritic cells in vivo by resident alveolar macrophages. *J. Exp. Med.1993.*
218. Unkel B, Hoegner K, Clausen BE, Lewe-Schlosser P, Bodner J, Gattenloehner S, Janßen H, Seeger W, Lohmeyer J, Herold S. Alveolar epithelial cells orchestrate DC function in murine viral pneumonia. *J Clin Invest. 2012.*
219. Johnston LK, Rims CR, Gill SE, McGuire JK, Manicone AM. Pulmonary macrophage subpopulations in the induction and resolution of acute lung injury. *Am J Respir Cell Mol Biol. 2012*
220. Davis MJ, Tsang TM, Qiu Y, Dayrit JK, Freij JB, Huffnagle GB, Olszewski MA. Macrophage M1/M2 polarization dynamically adapts to changes in cytokine microenvironments in Cryptococcus neoformans infection. *MBio. 2013*
221. Antonios JK, Yao Z, Li C, Rao AJ, Goodman SB. Macrophage polarization in response to wear particles in vitro. *Cell Mol Immunol. 2013*
222. Liu C, Li Y, Yu J, Feng L, Hou S, Liu Y, Guo M, Xie Y, Meng J, Zhang H, Xiao B, Ma C. Targeting the shift from M1 to M2 macrophages in experimental autoimmune encephalomyelitis mice treated with fasudil. *PLoS One. 2013*
223. Zhang Y, Choksi S, Chen K, Pobezinskaya Y, Linnoila I, Liu ZG. ROS play a critical role in the differentiation of alternatively activated macrophages and the occurrence of tumor-associated macrophages. *Cell Res. 2013*
224. Yang M, Liu J, Piao C, Shao J, Du J. ICAM-1 suppresses tumor metastasis by inhibiting macrophage M2 polarization through blockade of efferocytosis. *Cell Death Dis. 2015*
225. Davidson S, Crotta S, McCabe TM, Wack A. Pathogenic potential of interferon αβ in acute influenza infection. *Nat Commun. 2014.*
226. Pajarinen J, Tamaki Y, Antonios JK, Lin TH, Sato T, Yao Z, Takagi M, Konttinen YT, Goodman SB. Modulation of mouse macrophage polarization in vitro using IL-4 delivery by osmotic pumps. *J Biomed Mater Res A. 2015.*
227. Gomez Perdiguero E, Klapproth K, Schulz C, Busch K, Azzoni E, Crozet L, Garner H, Trouillet C, de Bruijn MF, Geissmann F, Rodewald HR. Tissue-resident macrophages originate from yolk-sac-derived erythro-myeloid progenitors. *Nature. 2015.*
228. Guilliams M, De Kleer I, Henri S, Post S, Vanhoutte L, De Prijck S, Deswarte K, Malissen B, Hammad H, Lambrecht BN. Alveolar macrophages develop from fetal monocytes that differentiate into long-lived cells in the first week of life via GM-CSF. *J Exp Med. 2013.*
229. Lavin Y, Winter D, Blecher-Gonen R, David E, Keren-Shaul H, Merad M, Jung S, Amit I. Tissue-resident macrophage enhancer landscapes are shaped by the local microenvironment. *Cell. 2014.*
230. Maus U, Herold S, Muth H, Maus R, Ermert L, Ermert M, Weissmann N, Rosseau S, Seeger W, Grimminger F, Lohmeyer J. Monocytes recruited into the alveolar air space of mice show a monocytic phenotype but upregulate CD14. *Am J Physiol Lung Cell Mol Physiol. 2001.*
231. Wu K, Byers DE, Jin X, Agapov E, Alexander-Brett J, Patel AC, Cella M, Gilfilan S, Colonna M, Kober DL, Brett TJ, Holtzman MJ. TREM-2 promotes macrophage survival and lung disease after respiratory viral infection. *J Exp Med. 2015*.
232. McCullers JA. The co-pathogenesis of influenza viruses with bacteria in the lung. *Nat Rev Microbiol. 2014.*
233. Davidson S, Crotta S, McCabe TM, Wack A. Pathogenic potential of interferon αβ in acute influenza infection. *Nat Commun. 2014.*

234. Raymond K, Richter A, Kreft M, Frijns E, Janssen H, Slijper M, Praetzel-Wunder S, Langbein L, Sonnenberg A. Expression of the orphan protein Plet-1 during trichilemmal differentiation of anagen hair follicles. *J Invest Dermatol. 2010*.
235. Depreter MG, Blair NF, Gaskell TL, Nowell CS, Davern K, Pagliocca A, Stenhouse FH, Farley AM, Fraser A, Vrana J, Robertson K, Morahan G, Tomlinson SR, Blackburn CC. Identification of Plet-1 as a specific marker of early thymic epithelial progenitor cells. *Proc Natl Acad Sci U S A. 2008.*
236. Tatefuji T, Arai C, Mori T, Okuda Y, Kayano T, Mizote A, Okura T, Takeuchi M, Ohta T, Kurimoto M. The effect of AgK114 on wound healing. *Biol Pharm Bull. 2006*.
237. Takeuchi M, Tatefuji T, Kayano T, Okura T, Mori T, Ohta T, Kurimoto M. Distribution of a novel protein AgK114 expression in the normal tissues of adult mice: dual expression of AgK114 and growth hormone in anterior pituitary cells. *Zoolog Sci. 2005*.
238. Zhao SH, Simmons DG, Cross JC, Scheetz TE, Casavant TL, Soares MB, Tuggle CK. PLET1 (C11orf34), a highly expressed and processed novel gene in pig and mouse placenta, is transcribed but poorly spliced in human. *Genomics. 2004*.
239. Bonnefont CM, Rainard P, Cunha P, Gilbert FB, Toufeer M, Aurel MR, Rupp R, Foucras G. Genetic susceptibility to S. aureus mastitis in sheep: differential expression of mammary epithelial cells in response to live bacteria or supernatant. *Physiol Genomics. 2012.*
240. Karrich J, Comelissen F, Spierenburg-Papazian N, Kwedkkeboom J, Lindenbergh-Kortleve D, Blackbum C, Samsom J, Cupedo T. Characterizationn of Plet1 expressing Dcs in the intestine and their putative role in controlling IL-22 driven mucosal innate Immunity. *Dutch Society of Immunology, 2013.*
241. Artis D, Spits H. The biology of innate lymphoid cells. *Nature. 2015*
242. Pociask DA, Scheller EV, Mandalapu S, McHugh KJ, Enelow RI, Fattman CL, Kolls JK, Alcorn JF. IL-22 is essential for lung epithelial repair following influenza infection. *Am J Pathol. 2013*
243. Plet1 human protein atlas database: http://www.proteinatlas.org/ENSG00000188771-LET1/tissue/staining+overview.
244. Barkauskas CE, Noble PW. Cellular mechanisms of tissue fibrosis. 7. New insights into the cellular mechanisms of pulmonary fibrosis. *Am J Physiol Cell Physiol. 2014*
245. Short KR, Kasper J, van der Aa S, Andeweg AC, Zaaraoui-Boutahar F, goeijenbier M, Richard M, Herold S, Becker C, Scott DP, Limpens RWAL, Barcena M, Fouchier RAM, Kirkpatrick CJ, Kuiken T. Influenza Virus damages the alveolar barrier by disrupting epithelial tight junctions. *Eur Resp Journal, in press, 2015*
246. Overgaard CE, Daugherty BL, Mitchell LA, Koval M. Claudins: control of barrier function and regulation in response to oxidant stress. *Antioxid Redox Signal. 2011*
247. Cummins PM. Occludin: one protein, many forms. *Mol Cell Biol. 2012*
248. Van Itallie CM, Anderson JM. Claudin interactions in and out of the tight junction. *Tissue Barriers. 2013*
249. Torres-Flores JM, Arias CF. Tight Junctions Go Viral! *Viruses. 2015*
250. Wurzer WJ, Ehrhardt C, Pleschka S, Berberich-Siebelt F, Wolff T, Walczak H, Planz O, Ludwig S. NF-kappaB-dependent induction of tumor necrosis factor-related apoptosis-inducing ligand (TRAIL) and Fas/FasL is crucial for efficient influenza virus propagation. *J Biol Chem. 2004*

251. Mühlbauer D, Dzieciolowski J, Hardt M, Hocke A, Schierhorn KL, Mostafa A, Müller C, Wisskirchen C, Herold S, Wolff T, Ziebuhr J, Pleschka S. Influenza virus-induced caspase-dependent enlargement of nuclear pores promotes nuclear export of viral ribonucleoprotein complexes. *J Virol. 2015*
252. Tolle LB, Standiford TJ. Danger-associated molecular patterns (DAMPs) in acute lung injury. *J Pathol. 2013*

9. Supplements

9.1 List of figures

9.2 List of tables

Pages

9.3 Abbreviations

AEC- alveolar epithelial cells
ALI acute lung injury
AM- alveolar macrophage
APC- allophycocyanin
ARDS- adult respiratory distress syndrome
BALF- bronchoalveolar lavage fluid
BSA- bovine serum albumin
°C- Celsius
CCR2- chemokine receptor 2
CCL2- chemokine ligand 2
CD- cluster of differentiation
cDNA- complementary DNA
Cl- chloride
DC dendritic cells
dH_2O- deionisized water
DMEM- dulbecco's modified Eagle's medium
DNA- desoxyribonucleic Acid
dNTP- desoxynucleosidtriphosphate
DTT- dithiotreitol
Dpi- days post infection
ExMa- exudate macrophages
EDTA- ethylendinitrilotetraacetic acid
ELISA- enzyme Linked Immunosorbent Assay
EpCAM-epithelial cell adhesion molecule
FasL Fas ligand
FACS- fluorescence activated cell sorting, flow cytometry
FCS- fetal calf serum
FP- forward primer
FSC- forward scatter
g- grams
GFP- green fluorescent protein
GM-CSF- granulocyte macrophage colony-stimulating factor
h- Hours
HA- hemagglutinin
HCl- hydrochloric acid
HRP- horseradish peroxidase
HPAIV highly pathogenic avian influenza virus
HRP horse radish peroxidase
IFN- type I interferon
IFNα- interferon alpha
IFNβ- interferon beta
IFNAR- interferon-alpha/beta receptor
IL-1α- interleukin 1 alpha
Ig- immunglobuline
IAV- influenza A virus
IVC- individually ventilated cages, conventional
L- litter
Min- minute

mAb- monoclonal antibody
MACS- magnetic assisted cell separation
Mn- mononuclear
MOI- multiplicity of infection
M1ExMa- M1 exudate macrophage
M2ExMa- M2 exudate macrophage
mRNA- messenger RNA
M- micro
n- nano
NA- neuraminidase
NP- nucleoprotein
Nt- nucleotide
PB-Mo peripheral blood monocyte
PFU plaque forming units
PR/8 A/PR/8/34
PR8- influenza virus A/Puerto Rico/8/34 (H1N1)
PB1- polymeraseprotein basic 1
PB2- polymeraseprotein basic 2
PBS- phosphate buffered saline
PCR- polymerase chain reaction
PE- phycoerythrin
PFA- paraformaldehyde
pi- post infection
Pfu- plaque forming units
pH - potentia hydrogenii
PKC- protein kinase C
Plet1- placenta expressed transcript 1 protein
RT-PCR- real time polymerase chain reaction
rAM- resident alveolar macrophage
RANTES- regulated on activation, normal T cell expressed and secreted
RP- reverse primer
Rpm- rounds per minute
RNA- ribonucleic acid
s- seconds
RT- room temperature
TNF-α- tumor necrosis factor-alpha
TRAIL-TNF-related apoptosis-inducing ligand
TGF-β- transforming growth factor beta
TNF-α- tumour necrosis factor alpha
SSC- side scatter
SA- sialic acid
SPF- specific pathogen-free
Wt- wildtype

Der Lebenslauf wurde aus der elektronischen Version der Arbeit entfernt.

The curriculum vitae was removed from the electronic version of the paper.

11. Acknowledgements

First and foremost, I would like to thank Prof. Werner Seeger for providing me an opportunity to perform my doctoral thesis at the Medical Clinic II, Department of Internal Medicine, Justus Liebig University Giessen.

I would also like to thank Prof. Jürgen Lohmeyer and Prof. Susanne Herold for guiding my doctoral thesis in all the possible scientific aspects. I would like to specially thank Prof. Susanne Herold, for observing my PhD project with a closer view and constantly guiding me, by her valuable suggestions throughout my PhD project. My PhD project was funded by the DFG within the SFB-TR84 "Innate Immunity of the Lung" (Project B3 "Development and function of respiratory macrophages and dendritic cell subsets during bacterial pneumonia")

I like to thank the members of international PhD programs (GGL and MBML) especially Dr. Lorna Lueck and Dr. Rory Morty for their valuable support and suggestions. I also would like to thank Dr. Jochen Wilhelm for helping me in generating genome array data for this study.
I also would like to thank my past colleagues Dr. Katrin Högner, Dr. Oana Gottschald for helping me to learn the flow cytometry and sorting techniques which helped me throughout the period of my PhD project. I wish to thank, Ms. Margret Lohmeyer for a constant moral support with carrying suggestions from the beginning of my PhD, which always helped me to re-boost myself. I like to thank all my past and present colleagues Gudrun Biemer-Mansouri, Rebecca Winkler, Elena Roth, Julia Rupp, Julia Bespalowa, Maria Koch, Jennifer Quantius, Barbara Unkel, Christin Becker, Lina Jankauskaite, Ivonne Vasquez Amendariz, Monika Heiner and Carole Schmoldt for their help and support whenever required. I like to specially thank Julia Bespalowa not only for her technical support but also for personal support which greatly helped me to pass thorough language barriers at many times.

I have to thank my master thesis supervisor Dr. Arjun Ram (senior scientist, IGIG, Delhi, India) for his constant support, encouraging words and scientific training to acquire the deep knowledge in science and research. I also have to thank Prof. Dr. Vasanthi Nachiyappan, Dr. Anusuyadevi Jayachandran, Dr. Ravi kumar for their highly supportive reference letters.

I also like to thank all my friends with beautiful hearts who always gave me a special support and memorable moments in Gießen. I would like to specially thank Ranjith Kumar, Gopala Krishna, and the precious MBML mates.

Finally, I would like to thank all my family members for constant support and encouraging words without which, it would have been difficult to pass through several hard times during the period of my stay in Germany. A special thanks to my parents who understands my situations and supporting me from India

Thank you very much to all of you!

12. Declaration

Hereby I Declare:

All the experimental data contained in this thesis is the result of my independent work without any unauthorized foreign authorities. The theoretical aspects in the thesis are obtained literally or analogously from published and unpublished scientific literatures that are coated with their references respectively. No part of this thesis has been previously submitted for any other degree at any other institution. I have the principles of good scientific practice according to the regulations of the University of Giessen.

Gießen, on 16. Mai 2016

Balachandar Selvakumar